Underwater concrete floors: improving design efficiency

A parametric approach to studying the impact of design parameters and the benefits of fibre reinforcement

---

Master thesis

Pim van Starrenburg

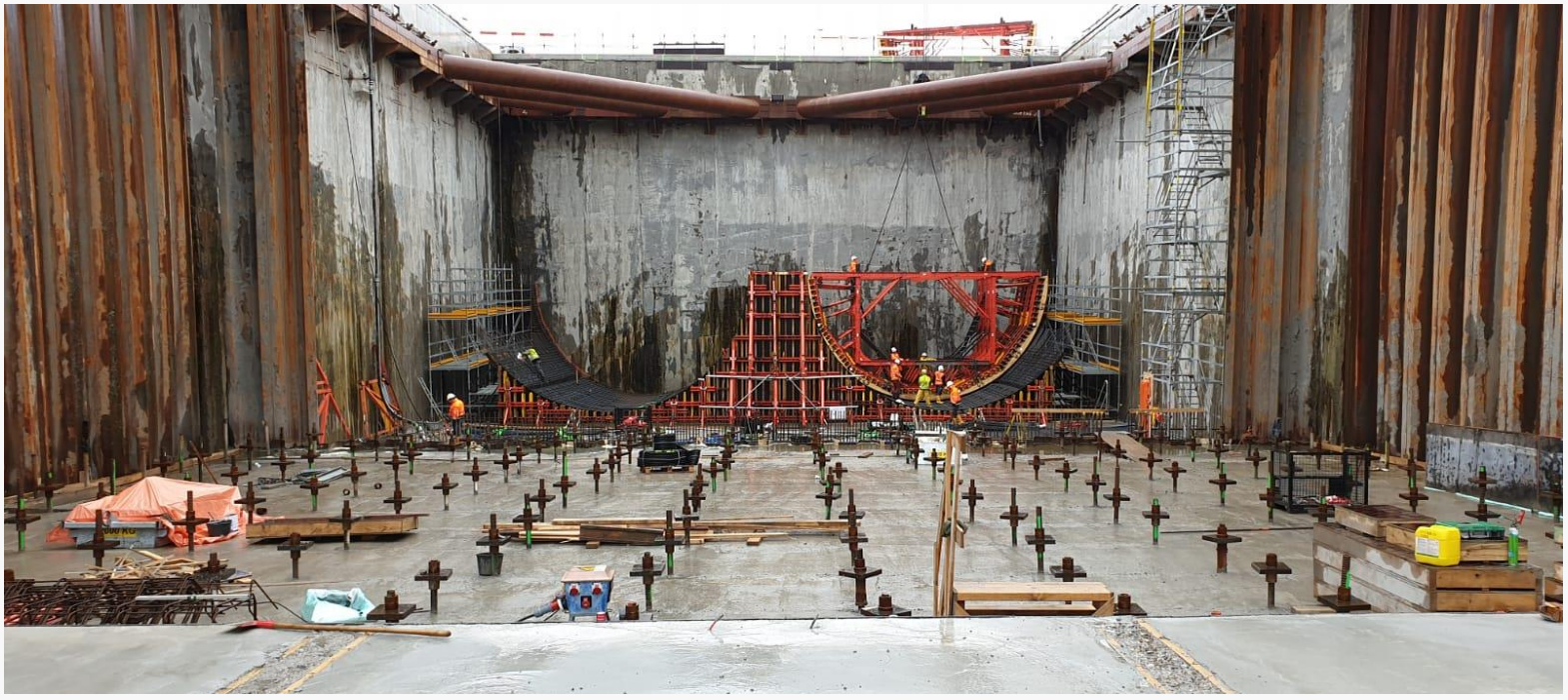

Graduation committee:

Prof.dr.ir. M.A.N. Hendriks	(TU Delft/committee chair)
Dr.ir C.B.M. Blom	(TU Delft/supervisor)
Ir. H. Ramler	(TU Delft/supervisor)
Ir. J. Tuls	(BAM Infra/supervisor)

Colophon

Author:	Pim van Starrenburg
Student number:	5185963
Date:	1 March 2023
Faculty:	Civil Engineering and Geosciences (CiTG)
Master:	Structural Engineering
Section:	Concrete Structures
Subject:	The impact of design parameters and the benefits of fibre reinforcement on the design of underwater concrete floors.

Technische Universiteit Delft
Faculty of Civil Engineering and Geosciences
Stevinweg 1
2628 CN Delft

BAM Infraconsult bv
H.J. Nederhorststraat 1
2801 SC Gouda

Graduation committee:

Chair:
Prof.dr.ir. M.A.N. Hendriks
TU Delft – section Concrete Structures

Supervisor:
Dr.ir C.B.M. Blom
TU Delft – section Concrete Structures

Supervisor:
Ir. H. Ramler
TU Delft – CiTG

Supervisor:
Ir. J. Tuls
BAM Infraconsult

Preface

After two and a half years of following the Structural Engineering program at TU Delft, this thesis marks the end of my academic journey in Delft. Working in collaboration with BAM Infraconsult bv, a parametric model was built to examine the impact of parameters on the design of underwater concrete floors. The study also assesses the potential for material savings through the incorporation of fibre reinforcement. The developed model provided an opportunity to contribute to the advancements within BAM Infraconsult in regard to parametric design. By further refining the model, a design tool was created that can be used in future projects to determine economically optimized designs for underwater concrete floors.

My first hands-on experience with an underwater concrete floor was on a tunnelling project where I did a practical internship for my bachelor studies. On the first day, I was tasked with measuring how far cuts of tensile elements were outside the execution tolerance. During my internship I witnessed the entire execution process from casting underwater concrete floors to constructing tunnel elements in the building pit. Ever since, I have been fascinated and eager to learn more about this subject. When Johan Tuls approached me with this thesis opportunity, I was excited to take it on. It was a great chance to delve into a topic I have been interested in for years and learn about a new parametric design approach that will be important for the future of a structural engineer. I can say without a doubt that this experience has taught me a lot and expanded my knowledge on multiple fronts.

I would like to express my gratitude to the graduation committee, Max Hendriks, Cees Blom, and Hans Ramler, for their insightful advice and constructive feedback during my thesis period. Their support elevated the quality of my work and provided me with a new perspective on the topic at times that it was needed. A special thanks goes to Johan Tuls, who gave me the opportunity to work on this thesis project that I truly enjoyed over the last nine months. Introducing me to the parametric design approach has given me a more comprehensive skill set and I am confident that it will serve me well as I embark on my career.

Pim van Starrenburg
Delft, March 2023

Summary

In the construction of subsoil structures, a common challenge is the presence of a high groundwater level in combination with the absence of a naturally impermeable layer or an environment susceptible to settlements due to lowering the groundwater level. To overcome this issue, a building pit with an underwater concrete floor (UCF) can be constructed. The UCF ensures structural rigidity and allows for the building pit to be drained such that a dry and safe subsoil construction site is obtained.

The objective of this thesis is to investigate how design efficiency of underwater concrete floors can be improved. In an effort to reduce material usage and achieve cost-effective structures, the following research question was stated:

"What is the influence of design parameters and how can parameters be adjusted to improve design efficiency of an underwater concrete floor, and to what extent can the addition of fibre reinforcement contribute to this optimization?"

A parametric model was developed to provide insight to the sensitivity of parameters and their impact on design resistance. Furthermore, the model was utilized to examine under what circumstances potential material savings can be obtained by implementing fibre reinforced concrete in UCF's. This was accomplished through the evaluation and comparison of the minimum required thickness based on bending moment resistance in various scenarios, for both UCF's and steel fibre reinforced UCF's (SFUCF).

Results obtained with the parametric model established that, in order to enhance the bending moment resistance of an uncracked UCF, increasing the nominal thickness becomes relatively more effective compared to increasing the concrete strength class for higher normal forces. When utilizing a compression arch to obtain bending moment resistance, the implementation of ribbed tensile elements or an increase in nominal thickness are found to be the most suitable methods for increasing resistance. For enhanced shear force resistance, increasing the nominal thickness over the concrete class provides relatively more additional resistance for slender UCF's. The results found that through the application of ribbed piles, most punching shear force resistance can be obtained.

Three use cases for a SFUCF were identified using the parametric model. When centre to centre (c.t.c.) distances larger than 4.4m are applied in combination with a substantial normal force, significant material savings of up to 0.3m thickness are possible, which equates to a reduction of material usage by 30%. For situations where the effective height of the compression arch is small, it was also found that material usage could be reduced by 30%. Perhaps the most significant use case for a SFUCF is when the normal force is close to zero, and additional normal force cannot be obtained through membrane action. In these situations, the application of a SFUCF can make an otherwise near impossible project feasible.

As a new design approach, a cost-based optimization tool was developed using the parametric model. An already executed UCF was evaluated using the tool, it was determined that a more cost-effective design could have been achieved, with potential savings of up to 30% in costs.

This thesis has made significant contributions to the field of civil engineering by providing detailed insights into the impact of various parameters on the design of (SF)UCF's, thereby enabling more informed decision-making when utilizing a traditional design approach and improving design efficiency. Moreover, the thesis has advanced decision-making with respect to the incorporation of steel fibre reinforcement in UCF's. The parametric approach used in this thesis facilitates exploration of the application of fibre reinforcement across a wide range of load cases and sets of parameters. This allows more exact insight in scenarios where steel fibres provide additional value as well as the quantification of their added value.

This thesis is also innovative in that it introduces a new design approach for (SF)UCF's. The optimization tool, which was derived from the parametric model, effectively bridges the two disciplines of computer science and civil engineering, enabling the identification of optimal designs for structural elements using computer-based methods.

Table of contents

List of symbols

Symbol	Definition
A_{cc}	Area of compressive zone
A_{dish}	Effective area of dish anchor
a_r	Distance between ribs on ribbed tensile element
a_{rN}	Reduction factor for membrane action
a_v	Distance over which the field with a mechanism comes up as consequence of deformation
d_{min}	Effective floor thickness
f_{cd}	Design strength of concrete
f_{cvd}	Design value of concrete strength under shear and compression
F_{tot}	Increased normal force by membrane action
h_{min}	Minimal floor thickness
h_{nom}	Nominal floor thickness
k_1	Stiffness of retaining wall
k_2	Stiffness of tensile element
k_3	Stiffness of ULS-membrane spring
k_r	Reduction factor for punching force resistance of dish anchor
M_b	Component of plastic moment
M_{cr}	Cracking moment of cross-section
M_d	Component of plastic moment
M_{Ed}	Acting bending moment
$M_{Nb1,2}$	Component of plastic moment
M_{Nt1-3}	Component of plastic moment
M_p	Plastic moment resistance of cross section
M_t	Component of plastic moment
$M_{x=hmin/2}$	Bending moment at a distance of $h_{min}/2$ away from retaining wall
N_b	Internal compressive force
$N_{b1,2}$	Component of internal compressive force
N_{Ed}	Normal force in UCF
N_t	Internal tensile force
N_{t1-3}	Component of internal tensile force
p_{head}	Pressure head with reference to top of UCF
q_{Ed}	Distributed load
q_u	Ultimate distributed load to prevent snap through of mechanism
u_1	Circumference of punching cone projected on bottom of UCF
v_{min}	Shear resistance according to shear bending strength
V_{Rd}	Shear capacity with respect to ULS
$V_{sup,max}$	Maximum shear force at tensile elements
$V_{x=hmin}$	Shear force at a distance of h_{min} away from retaining wall

$V_{x=hmin}$	Shear force at a distance of $h_{min}/2$ away from retaining wall
x_1	Height of yielded compressive zone
x_2	Height of uncracked tensile zone
x_{field}	Height of compressive zone in centre of field
$x_{support}$	Height of compressive zone above support
x_u	Compressive zone height
ε_{bpl}	Yield-strain of concrete
ε_{fbr}	Cracking-strain of concrete
ε_{svu}	Maximum strain of fibre reinforced concrete
ε_{top}	Strain at outer fibre of compressive side
μ_{sv}	Reduction factor for concrete tensile strength before pull-out of fibres
σ_{cp}	Average stress in compressive zone
σ_{Ed}	Tensile stress in outer fibre of UCF
σ_M	Stress at certain height in UCF as consequence of bending moment
$\sigma_{principal}$	Principal stress
σ_x	Stress at certain height in UCF as consequence of bending moment and normal force
τ_{cp}	Maximum shear stress in compressive zone
τ_{xy}	Shear stress
Δu	Compression of ULS-membrane spring
A	Maximum distance between compressive zone above support and middle of field.
B	Width of square tensile element
c	Roughness-coefficient of smooth tensile element
c. t. c.	Centre to centre distance of tensile elements
D	Diameter of circular tensile element
d	Diameter of dish anchor
h	Cross-sectional height when considering membrane action
k	Parameter for determination of v_{min}
K	Curvature of cross-section
L	Length of field
O	Circumference of cross section for smooth tensile element
p	Distance from top UCF to bottom of dish anchor
S	First moment of area
$tol_{anchorage}$	Tolerance of actual level compared to theoretical (nominal) level of anchorage
tol_{bottom}	Tolerance of actual level compared to theoretical (nominal) level of top UCF
tol_{top}	Tolerance of actual level compared to theoretical (nominal) level of bottom UCF
z	Internal lever arm
β	Reduction factor for concrete tensile strength after cracking
μ	Friction coefficient between UCF and retaining wall
$z2$	Internal lever arm for membrane action

1. Introduction

In the construction of subsoil structures, such as parking garages or tunnels, the excavation of the building site is a crucial stage in the execution process. One of the challenges faced in the Netherlands is the presence of a high groundwater level. A method to address this issue is to artificially reduce the groundwater level, which facilitates the excavation process without the need for temporary structures. However, this approach may have adverse effects on nearby buildings, such as a loss of skin friction along pile shafts [1]. To mitigate these issues, building pits are commonly constructed as a safer and more effective method of creating a dry building site. To prevent leakage and upburst, natural watertight layers or soil-injected layers may be used. In cases where these methods are undesirable or not feasible, an underwater concrete floor (UCF) can be cast, which is an expensive but widely applied method. Figure 1.1 depicts a typical cross-section of a building pit with a UCF.

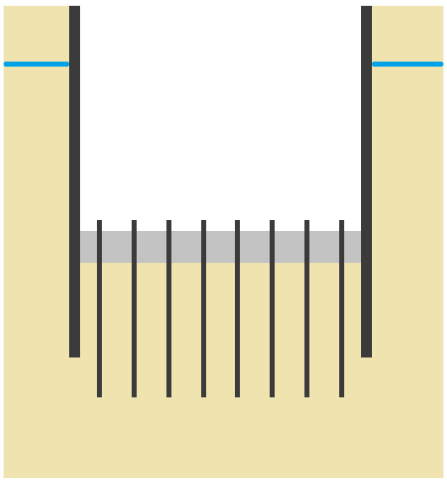

Figure 1.1: cross-section building pit

The structural components of a building pit comprise retaining walls, tensile elements, and a UCF. The UCF serves two functions; it creates a watertight boundary of the building pit and acts as a strut, mitigating deflection of the retaining walls. As a result, large normal forces are introduced into the UCF. To prevent upburst and counteract the vertical loads exerted by the hydrostatic pressure head and heave, tensile elements are used. The UCF is cast after the soil between the retaining walls has been excavated, and the concrete mix contains anti-washout admixtures preventing the mixture from segregating when submerged [2]. Once the concrete has hardened, the water in the building pit can be drained to create a dry building site.

The application of a UCF as a structural element is often temporary due to the absence of reinforcement. Applying conventional reinforcement is a challenge due to the execution method and large tolerances that should be accounted for. In addition, diver safety plays a role in opting not to use a reinforced UCF. As a result, UCF's often require large thicknesses or close centre to centre distances between the tensile elements, which lead to high financial costs and significant material consumption. By providing insight into efficiently altering the design parameters of a UCF, these disadvantages may be mitigated.

An alternative method for reducing material usage and cost of a UCF may be the use of fibre reinforcement. The addition of fibre reinforcement enables equilibrium in the cross-section, even in the post-cracking stage. As a result, more energy can be stored in the system and a more ductile response can be obtained. Unlike conventional reinforcement, fibre reinforcement does not have the same disadvantages concerning execution difficulties.

Recent advancements in hardware and software have provided civil engineers with accessible tools, allowing for development of parametric models. By creating a parametric model for the design of a UCF, a comprehensive understanding of the impact of design parameters can be gained. Furthermore, the potential benefits of incorporating steel fibre reinforcement can be explored through data generated using the parametric model. The design of a UCF is comprised of a set of parameters that define its geometry and therefore, material usage and cost. An optimization tool based on the parametric model can provide an efficient method for comparing design alternatives and finding the optimal set of parameters for a specific project, based on cost. The desire of reducing material consumption and cost, which are related, has resulted in the formulation of the following research question:

"What is the influence of design parameters and how can parameters be adjusted to improve design efficiency of an underwater concrete floor, and to what extent can the addition of fibre reinforcement contribute to this optimization?"

In the following section, the research question will be further elaborated. Furthermore, the main goal, scope and methods of this research will be described.

1.1 Main goal

The research question gives rise to the primary objective of this thesis, which is to:

Create a parametric model of a (fibre-reinforced) underwater concrete floor in a programming language to generate data that can provide insight into the influence of parameters and fibre reinforcement on the design of a UCF, and to develop an optimization tool using the parametric model that can find the optimal set of parameters for a specific case, based on price.

To accomplish the primary objective, the thesis has been divided into four parts. The main goal was broken down into sub-goals expressed as secondary research questions. Each part of this thesis focuses on a specific topic, with corresponding secondary research questions, which facilitates a step-by-step approach to answering the main research question.

Part 1: Literature study & parametric model (chapter 2 & 3)

1. What is a suitable method to model a (fibre reinforced) UCF and how can the force distribution be found in a parametric manner?
2. What failure mechanisms should be considered when verifying the resistance of a UCF and what calculation procedure can be used?

Part 2: Parameter influence on design efficiency (chapter 4)

3. What parameters influence the resistance of the failure mechanisms to be considered in the design of a UCF and how can these parameters be altered to improve design efficiency in a traditional design approach?

Part 3: Fibre-reinforced UCF (chapter 5)

4. How does the addition of fibre reinforcement influence the behaviour of a UCF and in what scenarios can the addition of fibres be beneficial in terms of material savings or resistance gain?

Part 4: Optimization tool (chapter 6 & 7)

5. How can a user-friendly tool be developed that chooses a set of parameters from a large pool, based on cost, leading to the optimal design for a specific case?
6. How do the results of this new design approach, through the use of an optimization tool, compare to an engineer-optimized design of an already executed UCF?

1.2 Relevance

The execution of numerous projects with UCF's by BAM Infra highlights the significance of understanding the impact of design parameters on the efficiency of a UCF design. Having a tool that can determine the optimal set of parameters for a UCF design can aid in cost-effectively executing projects and may accelerate the overall design process.

The parametric design of UCF's can be the foundation for automating design calculations of larger structures or even entire projects. By parametrizing the design calculations of various structural elements in a building pit, they can be coupled. For instance, if tools are created to find the optimal design for retaining walls and tension piles, they could be combined to find the optimal design for an entire building pit.

Finally, it is important to note that concrete is a significant contributor to carbon dioxide emissions [3], making it crucial to minimize its use and reduce its impact on the environment. By exploring ways to optimize the design of UCF's and reduce material consumption, this research can contribute to a more sustainable future.

1.3 Scope

The scope of this study is limited to conventional UCF's as defined in [4]. This means that UCF's with a minimum thickness of 800mm, that are confined by retaining walls and connected to tensile elements spaced in a regular grid, are considered. The UCF's analysed in this thesis will be modelled using a one-dimensional beam approach and are intended for temporary use. Only the connection strength between the UCF and tensile elements will be evaluated, not the tensile element's bearing capacity.

A specific concrete mix design will be used to determine the resistance of a fibre reinforced UCF. Mix designs with other material properties are not taken into account. The optimization tool will only find the optimal parameters based on cost, not other factors.

1.4 Methodology

The thesis is divided into four parts to address the main research question, as outlined in paragraph 1.1. To answer the secondary research questions in parts 2-4, a parametric model for UCF design will be developed which is based on information and calculation methods obtained through literature study. The model will be verified.

The parametric model will be used to generate data, with which a sensitivity analysis will be performed to examine the impact of various parameters on the design of a UCF. The parametric model is also used to evaluate the benefits of fibre reinforcement. For a large number of load cases, a minimum required thickness for both a conventional and fibre reinforced UCF will be calculated. Comparing the required thicknesses leads to results regarding potential material savings that can be obtained by using fibre-reinforcement. Chapters 4 and 5 present the results obtained from data generated though the parametric model, which can assist an engineer who adheres to a traditional design approach for a UCF by providing insights that can aid in making efficient design choices.

For part 4, an optimization tool will be developed using the parametric model. The tool can be used to find an optimal set of parameters for the design of a UCF in a given case, based on cost. A distinction is made between case-specific parameters and variable parameters. Iteration through a large pool of variable parameters will be performed such that the optimal set of parameters is found for the specific case. A calculation report will be automatically generated for the optimal set of parameters. Chapter 6 describes the iteration process and contains a manual for using the optimization tool. The optimization tool provides the engineer with an additional and new design approach for a UCF that can aid in cost-effectively executing projects and may accelerate the overall design process.

2. Literature study

The literature study is divided into two sections. Section 1 covers general information on underwater concrete floors, modelling of a UCF, and force distribution analysis. It also outlines the failure modes that must be evaluated to ensure adequate resistance. Section 2 focuses on the use of fibre reinforcement in UCF's. Various types of fibres and the corresponding material properties are discussed. Additionally, reference projects are analysed and a calculation method for a fibre reinforced UCF is set up.

2.1 Conventional UCF

2.1.1 Introduction

When constructing an underground structure, the most desirable method for creating a safe and dry building site is through the reduction of the groundwater table and the use of sloped excavation. Vertical retaining walls can be applied in case there is limited available space, such as sheet piled walls, combi-walls, or diaphragm-walls. However, it is important to note that reducing the groundwater table may have negative impacts on the surrounding environment and may not always be permitted.

A preferred solution for this problem is to place the retaining walls within a watertight soil layer. After excavating the soil between the retaining walls, the water can be removed from the building pit and the watertight layer will ensure a dry building site. In this manner, the surrounding groundwater table is not affected. An obvious condition for this method to be successful is that there should be a watertight soil layer present at the location.

In the absence of a watertight soil layer and if decreasing the water table is not feasible, an artificial watertight layer can be applied. One option is to use an injection layer, however a more traditional and more commonly used method is the implementation of an underwater concrete floor (UCF), of which the modelling and verification of the corresponding failure mechanisms can be performed according to the CUR-77 guideline [4]. Following excavation, a concrete floor with a relatively large thickness (minimum nominal thickness of 800mm) is cast. The large thickness is necessary because of the brittle behaviour of an unreinforced UCF and because of large execution tolerances. Upon hardening of the concrete, the water can be removed from the building pit. As the UCF serves only as a temporary solution due to difficulties with reinforcement, a reinforced construction floor must be cast on top to provide permanent structural support. A distinction is made between 3 types of UCF's:

- Weight based UCF: This type of UCF relies solely on its self-weight to compensate the upward hydrostatic load, including safety factors. However, this typically results in a very thick and cost-inefficient design.
- UCF anchored to retaining walls: In situations where the UCF's weight is insufficient, a mechanical or friction-based connection between the UCF and retaining wall can provide vertical equilibrium. However, this still often results in a thick and costly design for larger spans.

- UCF anchored to retaining walls and tensile elements: The load is compensated by the weight of the UCF, as well as by the ability of retaining walls and tensile elements to transfer the forces to the underlying soil layers through friction. A centre to centre distance of 2 to 3 meters between the tensile elements is used [5]. This type of UCF is most commonly applied, as the other two types are rarely feasible in practice.

Tensile elements

Three types of tensile elements, listed below, are considered in [4]. The type of tensile element used, affects the force distribution in the UCF, and the connection between the tensile element and UCF determines how much force can be transferred. The choice for a specific connection type may depend on the necessity to transfer compression forces in the use-phase of the construction.

- Smooth piles: Steel hollow smooth piles can have a large stiffness depending on their diameter. They are suitable to transfer compression forces in the use phase. The connection between the UCF and pile is often not adequate to transfer large forces.
- Ribbed piles: Concrete or steel ribbed piles have ridges to create a better connection between the UCF and the pile itself, such that large tensile forces can be transferred. This pile type is also suitable to transfer compression forces.
- Anchor rods with dish anchor: This pile type is most commonly applied as it is often found to be the most economical and easiest to execute. The thin shaft of the pile may lead to a reduction of total material usage. The dish anchor creates a good connection between the pile and UCF. However, the pile type is less suitable to transfer compression forces.

Execution methods

The soil between the retaining walls can be excavated using claws attached to a crane or excavator, or a dredging machine. If the bottom of the building pit consists of a sand layer, the surface will be smooth after excavation. This allows direct casting of the UCF. It is crucial to allow for a settling period between excavation and casting, to ensure settling of small particles and sediment at the bottom.

For a soil layer consisting of clay or peat, the excavation surface may be comparatively less smooth. To ensure a smooth surface for casting the UCF, it is necessary to excavate the soil to a deeper level and apply an equalizing layer of sand or gravel. In the case of a peat layer, special care must be taken as it can exhibit instability and is susceptible to heave as a result of excavation [5].

For casting underwater concrete, two methods are used in practice:

- Hop-dobber method
- Contractor and valve method

In the latter, concrete is dispensed through a vertical steel pipe. To prevent the concrete mix from washing out, the end of the pipe must remain within the already cast concrete. This method is not continuous and the tube will recoil when the bottom is opened, increasing the risk of washout. The

diameter of the bottom of the pipe is smaller compared to the Hop-dobber method, making it more appropriate for scenarios with tensile elements that are positioned close to each other.

In the Hop-dobber method, the bottom of the steel tube is fitted with a dish that has a diameter of approximately 1.5m and floats on the surface of the concrete. The flow of concrete is lower for this method, allowing for a continuous casting process, provided that there are no strutting frames or obstructions at the bottom of the building pit.

Tolerances

As a result of execution methods and uncertainties, the actual level of the top and bottom of a UCF may deviate from its intended level. These deviations must be accounted for as tolerances, leading to a nominal and minimum UCF thickness as outlined in [4]. In design calculations for stress and strength, the minimum thickness (h_{min}) should be used, while for stiffness purposes, the nominal thickness (h_{nom}) may be utilized. The tolerances are illustrated in figure 2.1, and the minimum thickness can be calculated as follows:

$$h_{min} = h_{nom} - \left(tol_{top}^2 + tol_{bottom}^2\right)^{1/2}$$

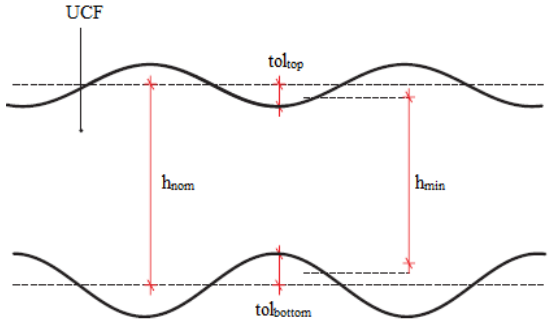

Figure 2.1: Tolerances [4]

If the UCF is connected to tensile elements through dish anchors, an additional tolerance must be considered for the resistance to bending moments and punching shear. The values for all relevant tolerances can be found in table 2.1 and must always be verified during the construction process.

Table 2.1: Tolerances [4]

	tol_{bottom}	tol_{top}	$tol_{anchorage}$
Soil: sand	150 mm	-	-
Soil: clay	350 mm	-	-
Soil: equalizing layer	150 mm	-	-
Execution: Hop-dobber method	-	75 mm	-
Execution: Contractor- en Ventiel method	-	150 mm	-
Connection	-	-	100 mm

Loads

When designing a UCF according to the CUR-77 guideline, four load cases must be considered. These are combined using load combinations, in which the safety factors are determined based on the consequence class of the UCF. The consequence class can be determined using [6]. In the formulas below, $\rho_{concrete}$ and ρ_{water} equal 23 kN/m³ and 10 kN/m³ respectively.

- Load case 1 (LC1): Self-weight of the UCF: $q_{g,k} = h_{nom} * \rho_{concrete}$
- Load case 2 (LC2): Upward water pressure: $q_{w,k} = (p_{head} + h_{nom}) * \rho_{water}$
- Load case 3 (LC3): Horizontal strutting force N_{Ed}, to be determined using a series of computations described in [7].
- Load case 4 (LC4): Heave: $q_{z,k}$

For ultimate limit state (ULS) calculations, the normal force in the UCF should be taken equal to 0.9 * N_{Ed}, while the minimum value of $q_{ULS,1}$ and $q_{ULS,2}$ may be used for the distributed load. However, when checking for punching shear, $q_{ULS,2}$ may not be taken into account. For serviceability limit state (SLS) calculations, q_{SLS} may be used. The safety factors to be considered are listed in table 2.2.

$$q_{ULS,1} = -09 * LC1 + \gamma_w * LC2 + \gamma_h * LC4$$
$$q_{ULS,2} = -09 * LC1 + (\gamma_w - 0.1) * (top_{pit} - top_{UCF} + h_{nom}) * \rho_{water} + \gamma_h * LC4$$
$$q_{SLS} = -1.0 * LC1 + 1.0 * LC2 + 1.0 * LC4$$

Table 2.2: Safety factors

Safety factor	γ_w	γ_h
Consequence class 2	1.2	1.35
Consequence class 3	1.3	1.5

Material properties

When designing a UCF, three concrete strength classes are considered, the properties of which are listed in table 2.3. Higher strength classes are disregarded as they may result in issues with thermal shrinkage [4]. In accordance with [8], an additional reduction factor shall be applied to the tensile and compressive strength of the material due to the lack of reinforcement and therefore reduced ductility properties of the UCF.

Table 2.3: Material properties

Strength class	$f_{ctd,pl}$ [N/mm²]	$f_{cd,pl}$ [N/mm²]	f_{ck} [N/mm²]	E_{cm} [N/mm²]
C20/25	0.80	10.7	20	27500
C25/30	0.96	13.3	25	29000
C30/37	1.07	16.0	30	31000

2.1.2 Modelling a UCF

Following the design approach in [4], a UCF can be modelled as a 1D beam model. Depending on what span of the UCF is considered, as well as whether or not sufficient friction can build up between the UCF and retaining wall, the discretization to a model differs. This paragraph illustrates the different beam models and describes in what situations they should be applied.

Short- and long span

A distinction is made between the short- and long span of a UCF, as illustrated in an arbitrary building pit top view in figure 2.2:

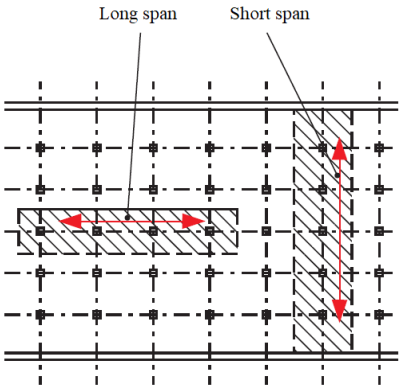

Figure 2.2: Short- and long span of UCF [4]

Short span – uncracked beam model

The UCF is modelled as a continuous, uncracked beam supported by vertical springs that represent the retaining walls and tensile elements. This beam model is utilized to evaluate the UCF's capacity to withstand bending moments, shear forces, and punching shear forces. The minimum of $q_{ULS,1}$ and $q_{ULS,2}$ may be used to calculate the force distribution, however $q_{ULS,1}$ is mandatory to calculate punching shear force. Figure 2.3 depicts a beam model of a UCF with n fields.

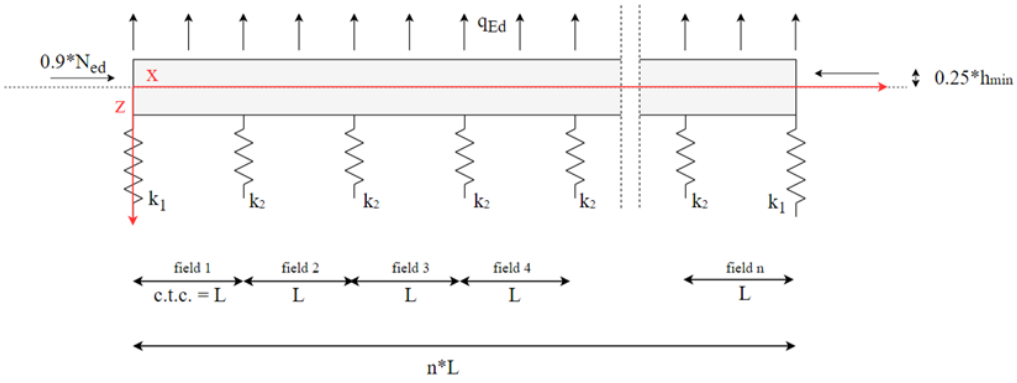

Figure 2.3: Non-slipping beam model

The bending stiffness of the beam is computed using h_{nom}, while the eccentricity of the normal force is calculated using h_{min}. This eccentricity results in a bending moment at the edge of the UCF and replicates the manner in which the deformed retaining wall applies the normal force onto the UCF. The distribution of forces shall be calculated twice, using the method of variation of coefficients. In the

scenario of "high stiffness" the stiffness of the tensile elements remains unchanged, while the stiffness of the retaining walls is multiplied by the square root of 2. Conversely, in the scenario of "low stiffness", the stiffness of the retaining walls remains unchanged, while the stiffness of the tensile elements is divided by the square root of 2.

Boundary disturbance zone

The boundary disturbance effect is a result of stiffness differences between the retaining wall and tensile elements, leading to significant bending moments in the UCF. It takes around 20m for this effect to be dampened [4]. Narrow building pits may experience overlapping boundary disturbance zones, resulting in increased bending moments.

Slipping beam model

In the event that the shear force at the edge of the UCF exceeds the maximum friction force attainable between the retaining wall and UCF, a slipping beam model should be used to recalculate the force distribution. The model should be adjusted to correspond with figure 2.4. All checks related to bending moment, shear force, and punching shear force should still have sufficient resistance after altering the model. It is important to note that in this beam model, the normal force is applied centrically.

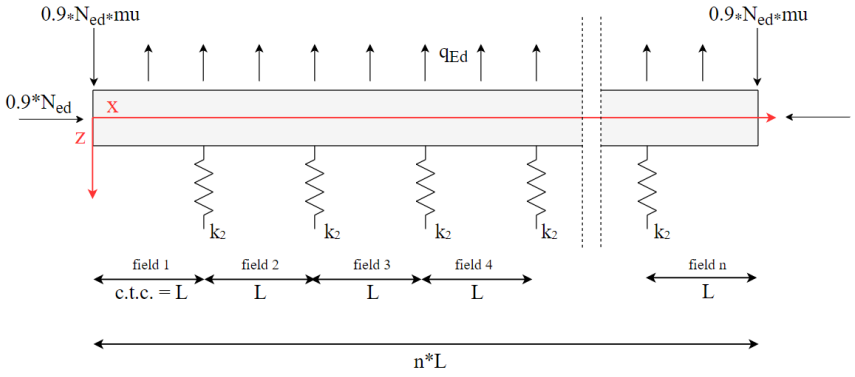

Figure 2.4: Slipping beam model

Short span – cracked beam model

If it is determined that the UCF does not provide sufficient bending moment resistance when calculated with a continuous beam model, the UCF will crack. In this scenario, the UCF may be modelled as a single span where a compression arch can offer additional bending moment resistance. The beam model is illustrated in figure 2.5, it is supported by two simple supports (tensile elements) and is loaded by a centrically applied normal force.

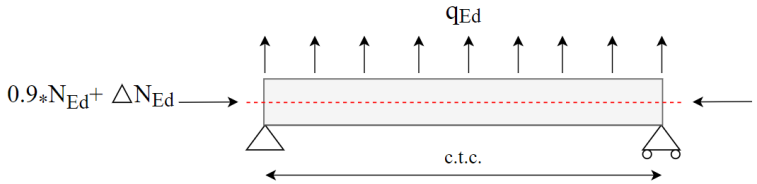

Figure 2.5: cracked beam model

It is possible to account for an increase in normal force due to membrane action (ΔN_{ed}). When cracked segments of the UCF rotate, it causes an increase in the length of the complete span. The retaining wall can be modelled as a spring, causing additional normal force when compressed. In accordance with [4], membrane action may only be considered if the pressure head relative to the top of the UCF is less than 10m, and should be reduced between 5-10m.

Long Span

The long span of a UCF can be modelled as a simply supported beam on two supports, loaded by a distributed load equal to q_{SLS}, provided that the conditions outlined below are satisfied. The conditions depend on the method used to achieve bending moment resistance for the short span, where failure mechanism A represents adequate bending moment resistance to prevent cracking of the continuous beam model, and failure mechanism B represents adequate bending moment resistance through the compression arch.

- If the bending moment resistance of failure mechanism A was found to be sufficient:
  - And: The stiffness of the retaining wall in the long span is smaller or equal to the stiffness of the retaining wall in the short span;
  - And: The normal force in the UCF along the long span is equal to or larger than the normal force along the short span.

- If the bending moment resistance of failure mechanism B was found to be sufficient:
  - And: The centre to centre distances between the tensile elements along the long span are smaller or equal to the centre to centre distances along the short span;
  - And: The normal force in the UCF along the long span is equal or larger to the normal force along the short span.

In case these conditions are not met, the long span should be considered in the same manner as the short span.

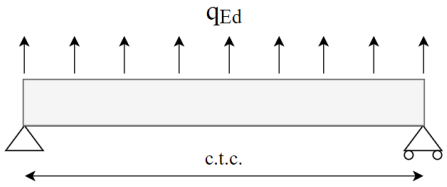

Figure 2.6: Beam model if conditions are met

2.1.3 Force Distribution

Reference [9] and [10] were used to set up a method for finding the force distribution using differential equations according to Euler-Bernoulli beam theory. This paragraph gives a concise overview of how to calculate the force distribution. A more detailed description can be found in annex B.

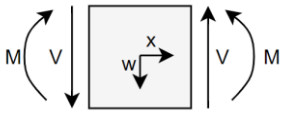

Figure 2.7 Positive directions of moments and shear forces

Positive directions for an arbitrary cross-section are taken according to [10] as in figure 2.7. For the sake of simplicity, the f(x) symbols have been omitted in the relations between displacement, rotation, bending moment and shear force.

$$q_{Ed}(x) = EI * \frac{d^4 w(x)}{dx^4}$$

$$V = -EI * \frac{d^3 w}{dx^3}$$

$$M = -EI * \frac{d^2 w}{dx^2}$$

$$\varphi = -\frac{dw}{dx}$$

Integration of the ODE gives n*4 unknown integration coefficients that must be solved, in which n is the number of fields along the span of the UCF. Using boundary and interface conditions, a system of equations was set up to find the integration coefficients. For the boundary/interface a distinction is made between a slipping beam model and a non-slipping beam model.

Non-slipping beam model

The boundary and interface conditions are derived using figure 2.8. The coordinate of the cross-sections corresponds with the beam model in figure 2.3.

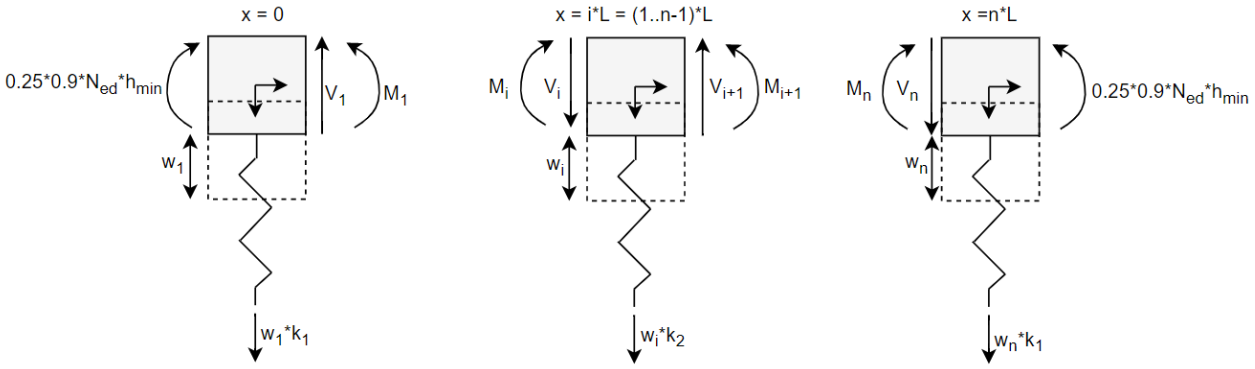

Figure 2.8: Boundary and interface sections for non-slipping beam model.

- BC: $M_{x=0} = 0.9 * N_{ed} * 0.25 * h_{min}$
- BC: $M_{x=n*L} = 0.9 * N_{ed} * 0.25 * h_{min}$
- BC: $V_{x=0} = k_1 * w_1$
- BC: $V_{x=n*L} = -k_1 * w_n$
- IC: $for\ i = 1 \ldots . n-1$: $w_i = w_{i+1}$
- IC: $for\ i = 1 \ldots . n-1$: $\varphi_i = \varphi_{i+1}$
- IC: $for\ i = 1 \ldots . n-1$: $M_i = M_{i+1}$
- IC: $for\ i = 1 \ldots . n-1$: $V_i = V_{i+1} - k_2 * w_i$

The amount of unknowns is equal to the amount of boundary/interface conditions, meaning all unknows can be found.

Slipping beam model

The boundary conditions are derived using figure 2.9, the interface conditions remain unchanged compared to the non-slipping beam model. The coordinate of the cross-sections corresponds with the beam model in figure 2.4.

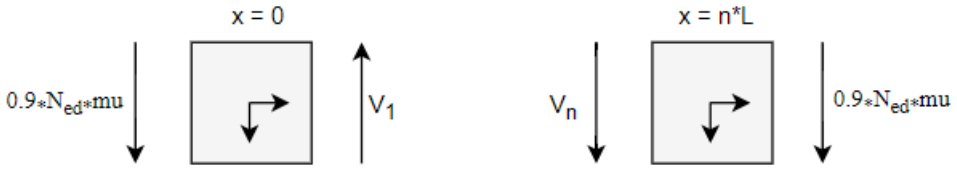

Figure 2.9: Boundary sections for a slipping beam model

- BC: $M_{x=0} = 0$
- BC: $M_{x=n*L} = 0$
- BC: $V_{x=0} = 0.9 * N_{Ed} * \mu$
- BC: $V_{x=n*L} = -0.9 * N_{Ed} * \mu$
- IC: $for\ i = 1 \ldots . n-1$: $w_i = w_{i+1}$
- IC: $for\ i = 1 \ldots . n-1$: $\varphi_i = \varphi_{i+1}$
- IC: $for\ i = 1 \ldots . n-1$: $M_i = M_{i+1}$
- IC: $for\ i = 1 \ldots . n-1$: $V_i = V_{i+1} - k_2 * w_i$

This again results in n*4 boundary/interface conditions, which is sufficient for the determination of all integration coefficient.

2.1.4 Failure mechanisms

A number of design checks should fulfill along both the long- and short span. The beam model from which the force distribution should be obtained to verify the failure mechanism is listed. A complete description of each failure mechanism including formulas can be found in [4].

Checks for the UCF (short span + long span in case conditions are not met):

Failure mechanism B1:	Beam model figure 2.3/2.4,	Tensile resistance of UCF
Failure mechanism B2:	Beam model figure 2.5,	Compression arch resistance
Failure mechanism B3:	Beam model figure 2.5,	Compression arch incl. membrane action
Failure mechanism C1:	Beam model figure 2.3/2.4,	Bending shear fracture resistance
Failure mechanism C2a:	Beam model figure 2.3/2.4,	Tensile resistance of UCF
Failure mechanism C2b:	Beam model figure 2.3/2.4,	Tension shear fracture resistance
Failure mechanism C2c:	Beam model figure 2.3/2.4,	Main tensile stress resistance

Checks for the UCF (long span in case conditions are met):

Failure mechanism A:	Beam model figure 2.6,	Tensile resistance UCF

Checks for the connection between UCF and tensile element

Failure mechanism G1:	Beam model figure 2.3/2.4,	Smooth pile connection
Failure mechanism G2:	Beam model figure 2.3/2.4,	Punching resistance concrete ribbed pile
Failure mechanism G3:	Beam model figure 2.3/2.4,	Punching shear resistance steel ribbed pile
Failure mechanism G4a:	Beam model figure 2.3/2.4,	Punching shear resistance dish anchor
Failure mechanism G4b:	Beam model figure 2.3/2.4,	Concrete compressive stress under dish anchor

2.2 Fibre reinforced UCF

2.2.1 Fibre reinforced concrete

Fibre reinforced concrete (FRC) is a composite material comprised of concrete and fibres that can be produced from various materials. The purpose of adding fibres is to enhance the properties of the composite after cracking. When the material cracks, the fibres are activated, thereby transferring tensile stresses across the crack and providing additional toughness and residual strength. Furthermore, the addition of fibres increases the ductility of the material, allowing for the formation of plastic hinges and the application of plastic theory. This can result in redistribution of bending moments in the UCF and the possibility of increased resistance or material savings. The concept of using fibres to improve the behaviour of materials dates back to ancient times, such as the use of horsehair in mortar and straw in mudbricks. The utilization of fibres in concrete dates back to the 1960's, primarily in elastically supported slabs, but also in several UCF projects [5]. These projects will be further elaborated in section 2.2.3.

Ensuring equal distribution of fibres in the material while maintaining proper workability for execution purposes is crucial for underwater concrete. Fibres can be incorporated into the concrete mix either individually or in bundles, depending on the type of fibre used. Avoiding nesting of fibres is important and is typically a risk when large aggregate sizes or high fibre dosages are used. It also depends on the parameters of the fibre itself. The most essential parameters in characterizing a type of fibre are [5]:

- L(length)/D(diameter) aspect ratio
- Shape (hooked, flat, waved, etc.)
- Material (tensile strength, modulus of elasticity)

It is important to distinguish between the function of fibre reinforcement in concrete on both the macro and micro levels [11]. On the micro level, microcracks within the cement matrix can be mitigated by the fibres. This is particularly relevant during the early stages of concrete, as the cement matrix shrinks during the hydration process, leading to tension and microcracks caused by deformation restrained by the rigid structure of aggregates. Adjacent fibres can prevent the expansion of microcracks by absorbing tension forces around the crack's tip (as depicted in figure 2.10, left). The greater the axial stiffness of the fibre, the more effective it will be in preventing crack formation.

In the event that a fibre spans a crack, it serves as reinforcement (as shown in figure 2.10, right). This applies to both micro and macro levels, with macrolevel referring to larger cracks caused by external forces or bending moments. When functioning as reinforcement, factors such as bond strength, tensile strength, and length-to-diameter ratio have a greater impact than the axial stiffness of the fibre. When a crack occurs, the forces are entirely carried by the fibres spanning the crack and are transferred to the concrete through the end of the fibre. If the fibre does not span the crack perpendicularly, it will experience tension, shear, and bending loads. The extent to which the forces can be transferred to the concrete is determined by the strength of the matrix, the shape of the fibre, and the bonding properties between the concrete and the fibre. To prevent brittle failure of the concrete, the bond strength of the

fibre should be sufficient to allow for slight deformation on both anchoring sides, enabling the fibres to elongate and slip out of the matrix slightly before breaking.

Fibres embedded in the cement matrix have two modes of failure, and the specific mode that occurs depends on the aspect ratio, anchorage, tensile strength, and bond strength of the fibre.

- Failure mechanism 1: pull-out of fibre from cement matrix
- Failure mechanism 2: rupture of fibre

The workability of the underwater concrete mix is critical due to the casting method used for UCF. The addition of fibres increases the surface area of the concrete mix, thereby requiring a higher amount of water. A study to a suitable mix design for a UCF in the Botlekspoortunnel revealed that the use of plasticizers was necessary to preserve the desired workability [12]. The typical dosage of fibres, particularly steel fibres, ranges from 30-35 kg/m³, which is equivalent to 0.39-0.45% of the volume [13]. The use of higher dosages may result in problems with nesting and workability.

When adding fibres to a concrete mix, they are meant to strengthen the concrete such that every random volume-unit of the material has uniform properties. The size of the aggregates in the mix affects the distribution of fibres, with larger aggregate diameters limiting the amount of fibres that can fit in a particular volume unit. It is recommended that the largest aggregate diameter is smaller than half of the fibre length [11]. For underwaterconcrete this leads to a maximum nominal aggregate size of 32mm as fibres are generally not longer than 60mm due to workability reasons.

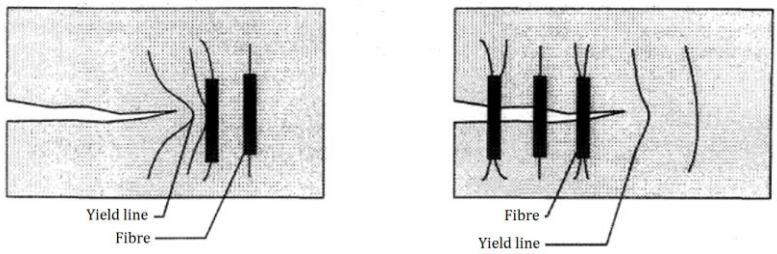

Figure 2.10: Function of fibres on micro- and macro-level [11]

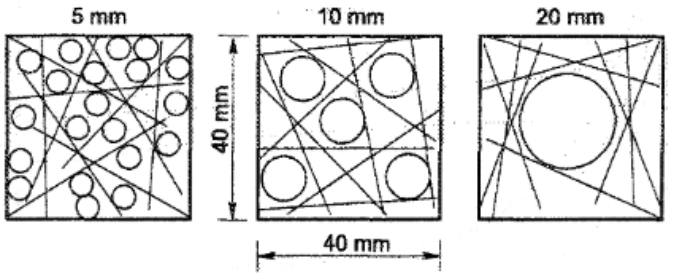

Figure 2.11: Effect of aggregate size on distribution of fibres [11]

2.2.2 Types of fibres

When selecting the type of fibre reinforcement to be used in the design of a concrete structure, several factors must be considered. An evaluation of the properties and behaviour of various fibre materials should be undertaken in order to make an informed decision on the most suitable fibre type for application in a UCF. Some of the most commonly used or previously used fibre types include [14]:

- Steel fibre reinforcement
- Polypropylene fibre reinforcement
- Glass fibre reinforcement
- Asbestos fibre reinforcement

The use of asbestos fibres as an additive in concrete dates back to the early 1900s, however, its utilization has become limited due to health hazards associated with inhaling its microscopic particles [15]. Despite the hazardous nature, research on its influence on concrete continues to be conducted. An experimental analysis on asbestos fibre reinforcement [16] found that it can significantly improve the compression and flexural strength of concrete, with an optimum fibre dosage (based on volume) of 0.66% for flexural strength and 0.33% for compression strength. The use of asbestos in new products in the Netherlands is forbidden by law as of 1993. Besides, the health hazards make it unsuitable for use in UCF's in parts of the world where the application of asbestos is legal.

A type of fibre that is currently widely applied in a number of use cases is polypropylene fibres. One of the advantages of polypropylene fibres is that it increases the fire resistance of concrete by making it less sensitive to spalling. Besides, in projects where aesthetics play an important role, polypropylene fibres can be applied as they are hardly visible. Both of these advantages are of less importance when applied in a UCF. The effect of multifilament polypropylene fibres (micro, length of 1.8mm, aspect ratio of 333), plastic polypropylene fibres (macro, length of 50mm, aspect ratio of 50) and steel hooked fibres (macro, length of 50mm, aspect ratio of 50) on compressive strength, split-tensile strength and workability was studied in [17]. Samples with 1%, 2% and 4% fibre dosage (based on weight) were tested. It was found that for all three types of fibre, the compressive stress was slightly decreased after 28 days compared to regular concrete. The tensile stress of samples with 4% hooked steel fibres almost doubled, while the macro-polypropylene fibres increased by a factor of 1.5. The micro-polypropylene fibres only showed a slight increase. The addition of polypropylene fibres caused problems with workability as they work as a thickening agent.

A fourth type of fibre that can be used to reinforce concrete is glass. An investigation on strength and fire resistance properties of glass fibre reinforced concrete was performed in [18]. It was found that adding 0.5% of volume of the concrete increased the compressive strength by 13% and the flexural strength by 42%. The improved properties were even more noticeable with a higher dose of 1% by volume: the compressive stress improved by 35% whilst the flexural strength improved by 75%. In [19] a literature review was done on steel and glass fibre reinforced concrete. The most important conclusions were that the use of glass and steel fibres increase the fundamental properties of concrete but only showed positive results up to a certain point before the concrete starts to lose strength. Besides, the brittleness of concrete could be improved with the addition of steel fibres, however not so much with glass fibres.

Based on the findings from previous research, it can be concluded that steel fibres exhibit the most significant improvement in the performance of concrete. In a UCF, factors such as aesthetics and fire resistance are of lesser importance, as it is a temporary structure that will eventually be covered by a construction floor. Therefore, steel fibres are deemed the most appropriate choice for reinforcement in a UCF. The following section will outline five reference projects where steel fibre reinforcement was utilized in a UCF.

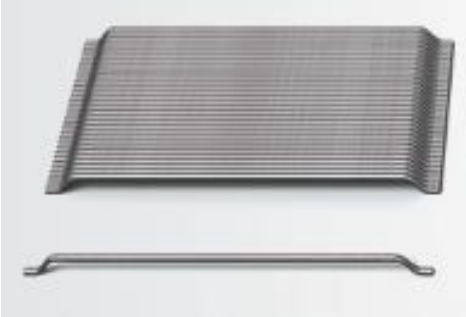

Figure 2.12: Steel fibres with hooked ends [20]

2.2.3 Reference projects

This section outlines 5 examples of reference projects where a steel fibre reinforced underwater concrete floor (SFUCF) was implemented. The purpose behind their use can provide valuable insights for addressing the sub-questions and determining the conditions under which steel fibre reinforcement can be beneficial.

Potsdamer Platz Berlin

In the heart of Berlin lies the Potsdamer Platz, in the 1990's it is being transformed into a multi-functional town centre with shops, high rise buildings and offices. The entire construction is built in a single building pit with a length of 560m and a width of up to 280m, the total area is 70000m². The bottom of the building pit reaches far underground (9-18m), whilst the groundwater-level lies 2-3m below the surface. Lowering the groundwater level was not an option because this could cause disturbances in Berlin's most important drinking water reservoir. For depths of up to 12m it was possible to use a natural or artificial layer to seal the building pit, although for deeper parts a UCF was required.

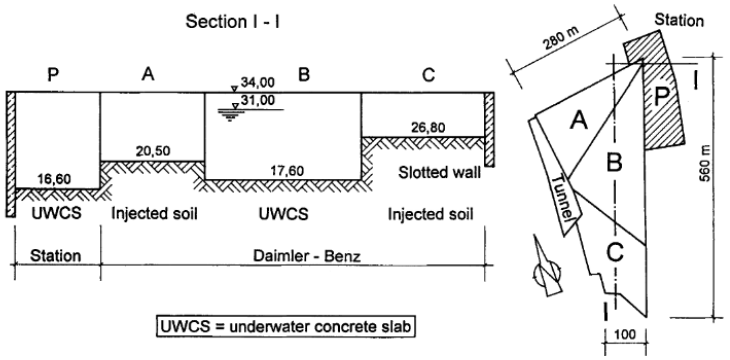

Figure 2.13: Cross-section (left) and top view (right) of building pit Potsdamer Platz [21]

It was shown by calculation that the bending moment capacity was too little to prevent brittle failure of the floor, unless the thickness was increased. Based on experience gained by tests on steel fibre reinforced construction floors [21], it was concluded that a SFUCF would be more suitable to take up the differential displacements of the tensile elements because of its more ductile behaviour. To further test the applicability, scale models of 3mx3mx0.28m with the addition of 60kg/m³ and 40kg/m³ Dramix 3D fibres, as well as unreinforced concrete were tested [21]. The conventional UCF showed a brittle failure while both the SFUCF's showed much more resistance and ductility. Eventually the tests had to be stopped because the hydraulic jacks reached their maximum pressure output. The scale model with a fibre dosage of 40 kg/m³ showed more load carrying capacity than the 60kg/m³ model, hence this dosage was chosen to be applied in the full-scale UCF. The floor could be executed with a thickness of 1.3m instead of 1.5m because of the addition of steel fibres, which saved 4400 m³ of concrete [5].

Underpass Heinesoweg Zwolle

The city of Zwolle is located between a dense network of railway tracks, and in the late 1990s, an effort was made to create safer infrastructure by replacing multiple railway crossings with grade-separated intersections. One of these projects at Heinesoweg was completed under heavy time constraints due to limited train traffic disruption. The construction included a slid-in-place reinforced concrete deck and a SFUCF to meet the tight schedule. [22].

A building pit was necessary for the construction of a sub-surface road and bicycle path. During the execution phase, the railway tracks were temporarily removed, and soil excavation took place. Due to high water levels near the surface and an unsuitable soil type for lowering the groundwater level, a UCF was used to seal the building pit. Given the tight schedule, only a limited amount of piles could be driven. This meant that large centre to centre distances had to be applied in the UCF. A SFUCF was deemed the most cost-effective and best suitable method to address this challenge. Besides being the most cost-effective, the increased ductility was also found to give better resistance to differential settlements and alternating stresses caused by train loads.

Based on positive experiences with the Dramix 3D fibres in Potsdamer Platz, these fibres were also applied at Heinesoweg. The dosage of fibres and workability of the concrete was closely monitored during execution. At the building site, Bekaert also casted beam models to be tested in a laboratory. The desired strength was confirmed to be reached.

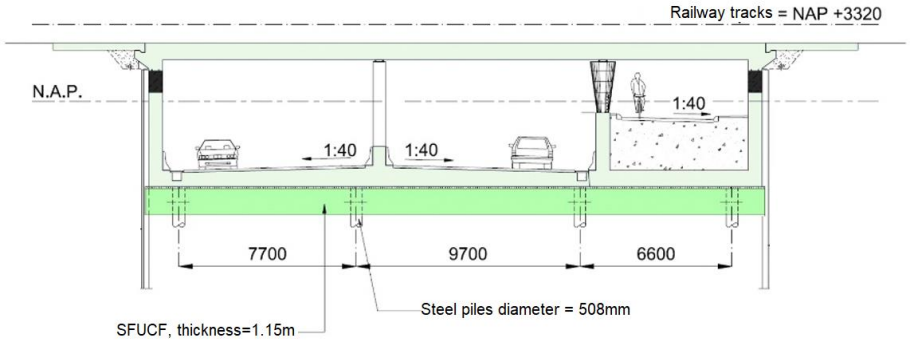

Figure 2.14: Cross-section of building pit Heinesoweg [22]

Mauritshuis

For an expansion of The Mauritshuis in 2012, three sequential building pits were constructed. The guaranteed normal force in the central building pit was close to zero. This was because of the safety factors, deformation requirements and the shallow depth of the building pit [13]. At the time of designing, the old CUR guideline was still applied, thus the positive effects of membrane action were not considered. A minimum floor thickness of 1500mm was calculated, even though the upward pressure was only 30 kN/m². By designing the UCF using a slipping beam model and taking into account the improved material properties by applying steel fibre reinforcement, the floor thickness was optimized to 900mm. An additional advantage was the shallower excavation depth, this meant that deformation in the retaining walls was smaller and that risks of damage to neighbouring buildings was decreased.

Groninger Forum

The Groninger Forum is a 45 metre high building in the centre of the city of Groningen. A 5 layered parking garage is located underneath the building and extends to a depth of 17m beneath the surface. In order to construct the building and parking garage, a building pit of over 80m in length was excavated (figure 2.15). It features a diaphragm wall with a rounded edge on the west-side. The pit is sealed by a UCF which is connected to relatively flexible Gewi-piles and stiff tubex-piles. The latter piles are placed in groups to serve as foundation underneath the stability cores of the building, however in the execution phase they will also act as tensile elements. The UCF is loaded by a pressure head of 10m [23]. Three major problems made it difficult to apply a conventional UCF [13]:

- The normal force in the UCF at the location of the rounded edge is very low because the ground pressure is taken up as a ring force in the diaphragm wall;
- Large stiffness differences between the diaphragm wall, Gewi-piles and tubex-piles cause differential deformations and large bending moments;
- Due to the large span of the building pit, through cracks because of shrinkage can cause leakage.

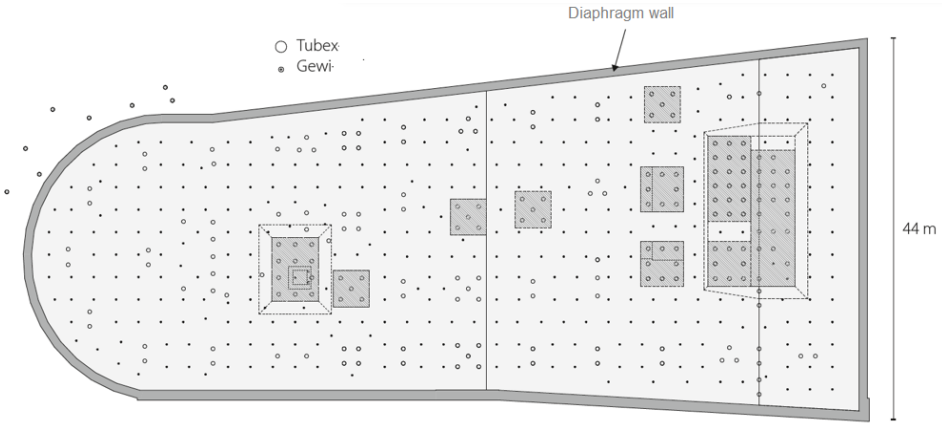

Figure 2.15: Top view of SFUCF Groninger forum [23]

By adding steel fibre reinforcement, the floor was optimized to a thickness of 1000mm. MPZ-HT-50/1.0 fibres with a dosage of 35 kg/m³ were added to the concrete. These fibres are very similar to Dramix 3D fibres with a length of 50mm and an aspect ratio of 50.

In an evaluation of the design of Groninger forum [23] it was found that it would have been practically impossible to apply a conventional UCF when normal forces were completely neglected (conservative approach). If the normal forces were halved, a minimum thickness of 1500mm would be required [24]. Based on calculations performed with the updated CUR-guideline, a conventional UCF would be feasible and a minimum thickness of 1000mm would be required. This difference is explained by the membrane action that could be taken into account.

Botlekspoortunnel

In 1999, the Botlekspoortunnel project involved the construction of a building pit to accommodate the tunnel boring machine. The building pit had a depth of 22 meters and was subjected to an extreme load case, due to a pressure head of 18 meters [25]. The retaining walls were constructed using stiff combi-walls, while the UCF was attached to relatively flexible Gewi piles. The design of the UCF was based on the NS-guideline, which dictated that the tensile stress of the concrete should not be exceeded, a challenging requirement given the significant stiffness difference between the combi-wall and tensile elements. After good experiences at Potsdamer Platz, the feasibility of using a SFUCF was explored for this project.

Prior to execution, a study was set up to the properties of the concrete mix to be used at this project. The results of this study were made available for this thesis and form the basis of design calculations on SFUCF's performed in this thesis. This also means that results of this thesis are only 1:1 applicable to the mix design that was used at Botlekspoortunnel. The mix design used was relatively standard but has the addition of steel fibres and plasticizers. It had the following properties:

- Strength class B25 (C20/25 equivalent)
- 300 kg/m³ CEM III/B
- 70 kg/m³ fly-ash
- 30 kg/m³ hooked steel fibres with aspect ratio 60/0.75
- Water/cement factor 0.58
- Maximum aggregate size of 32mm.
- Plasticizer 0.5%
- Superplasticizer 0.7%
- Air 1%

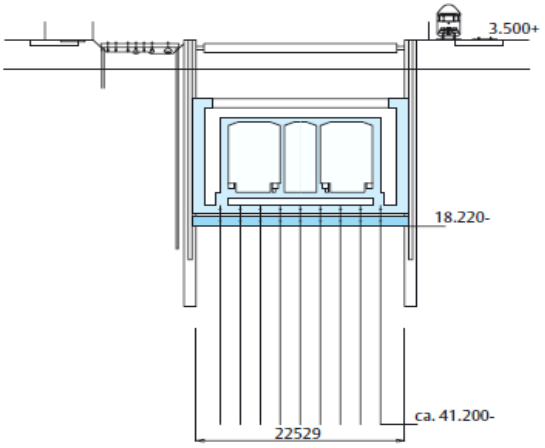

Figure 2.16: Cross-section of building pit Botlekspoortunnel [25]

After research, a successful solution with the addition of steel fibres was found. A maximum dosage of 30 kg/m³ Dramix 3D fibres was used to reinforce the UCF as it was found that higher dosages would have too much influence on the workability. The study existed of laboratory tests on sample beams to find post-cracking material properties and to find workability properties. Besides, a model of the UCF was casted (3x10m) to determine workability and distribution of fibres in practice, sample beams were made from the concrete that was casted and these were also tested for strength values. Results of the tests on workability and post-cracking tensile strength can be found in Annex D. The post-cracking tensile strength values that were used for the design were:

$$f_{ctm,eq300} = 2.7\ N/mm^2$$
$$f_{ctm,eq150} = 2.5\ N/mm^2$$

These values will be applied in the calculation method for bending moment resistance of a SFUCF further described in paragraph 2.2.4.

2.2.4 Behaviour of a SFUCF

Steel fibres are only mobilised when cracking occurs, they serve their function in the post-cracking stage by carrying tensile stresses across a crack, fibres give the concrete extra toughness and residual tensile strength. Figure 2.17 [26] describes the effect of reinforcing concrete with fibres, a distinction is made between "softening behaviour" (row A) and "hardening behaviour" (row B), of which the latter guarantees plastic behaviour [13]. Column I shows an element under uniaxial tension, while column II shows an element under pure bending. A construction element on macro-level is illustrated in column III. In the figure, the arrows show that even though a structure may have softening behaviour under pure tension or bending, it can still obtain hardening behaviour on macro-level, for example under an acting normal force.

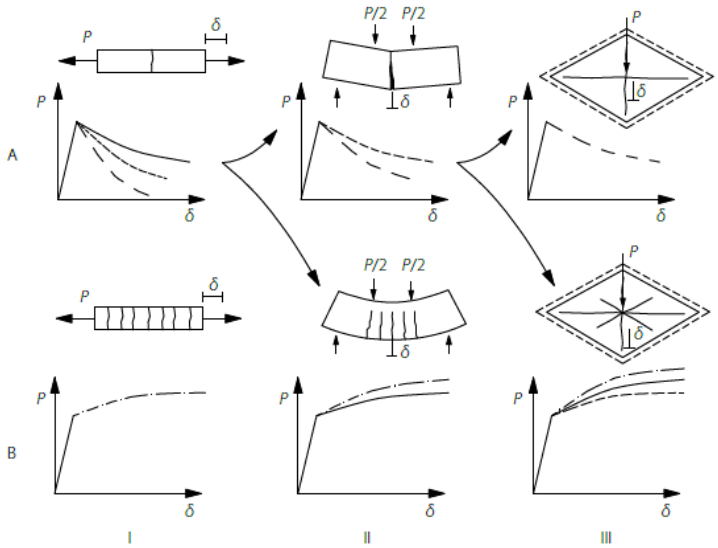

Figure 2.17: softening and hardening behaviour [26]

For a UCF to benefit from the addition of fibre-reinforcement, hardening behaviour should be obtained. This means the plastic moment (M_p) is higher than the cracking moment (M_{cr}) such that an ascending curve is present in the M-N-k diagram. The ratio M_p/M_{cr} can also be defined as the hardening factor. After cracking, a fine pattern of small cracks can be expected above the supports or in the middle of the fields, acting as a hinge. Because of this post-cracking behaviour, moments can be redistributed along the UCF. In theory, a chain reaction could occur where a plastic hinge forms above each support and in the middle of each field. A mechanism with brittle failure will then form, which should be avoided. Figure 2.18 shows hinges along the UCF after complete redistribution of bending moments. If the load is increased and hinges will also form above the supports, brittle failure will occur.

Two important conditions for the situation in figure 2.18 to form are:

1. The curvature in all hinges should remain below the pull-out curvature of the fibres.
2. The hardening factor may not be smaller than 1.0.

To confirm these boundary conditions, tests or extensive calculations have to be performed before applying a SFUCF in a project.

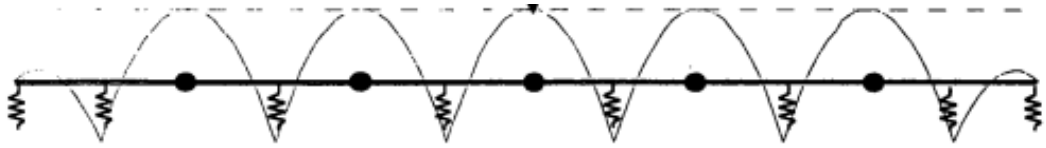

Figure 2.18: Hinges at the locations where M_{cr} was exceeded, reaching M_{cr} above the supports should be avoided to prevent brittle failure. [5]

Stress-strain relationship

For describing the stress-strain relationship of fibre-reinforced concrete, the following diagram is used, which is a simplified version of the stress-strain diagram given in [27]. The tests performed to determine the post-cracking tensile strength for the concrete mix used in Botlekspoortunnel, which are used as reference values in this thesis, were derived with the intent to use in correspondence with this stress-strain diagram.

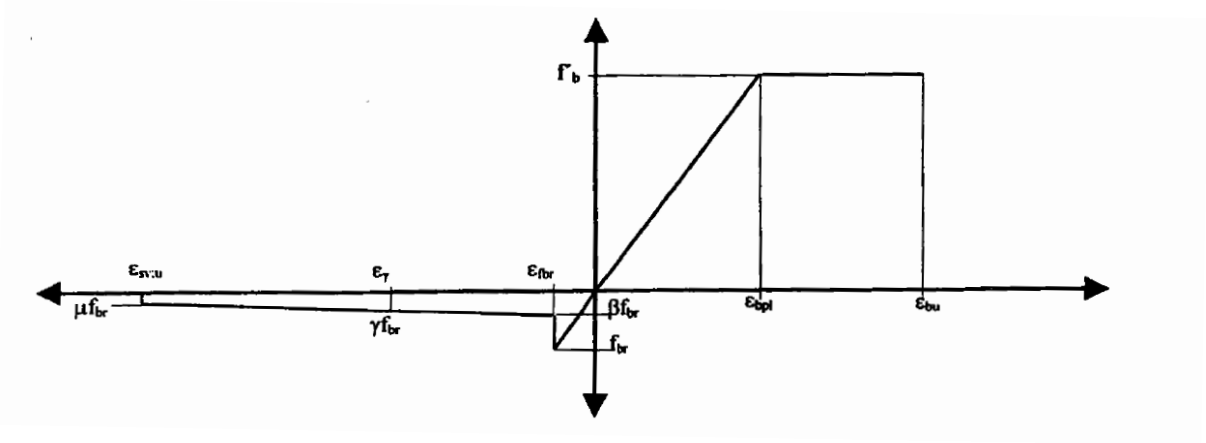

Figure 2.19 Stress-strain diagram [5]

The symbols in the stress-strain diagram have the following definition:

$\varepsilon_{sv,u}$ = ultimate strain of steel fibres = 0.005

ε_{fbr} = strain at cracking of concrete = $f_{ctd,pl}/E_{cm}$

ε_{bpl} = strain at yielding of concrete = f_{ck}/E_{cm}

ε_{bu} = ultimate strain of concrete = 0.0035

f_b = compressive strength concrete, equivalent to f_{ck}

f_{br} = tensile strength concrete, equivalent to $f_{ctd,pl}$

β = reduction factor for tensile strength after cracking = $0.37 * f_{ctm,eq300}/f_{ctm}$

μ = reduction factor for tensile strength at ultimate strain = $0.37 * f_{ctm,eq150}/f_{ctm}$

To obtain the values for $f_{ctm,eq300}$ and $f_{ctm,eq150}$, four-point bending tests were performed on sample beams with a height and width of 150mm and a span of 450mm. An example of a load-deflection

diagram obtained from a four-point bending test is illustrated in figure 2.20. The test results of the reference concrete mix design can be found in Annex D.

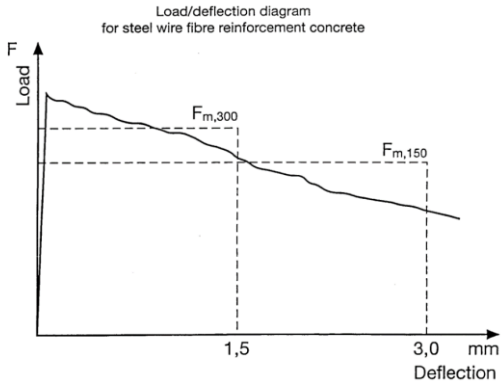

Figure 2.20 : Load deflection diagram

The absorbed energy during the displacement-controlled bending test has to be measured until the beam reaches a displacement of 3mm. The energy is the product of the displacement and average load (F) in the interval until 1.5mm or 3mm. Equivalent values for the post-cracking tensile strength can then be calculated with:

$$f_{ctm,eq300} = F_{m300} * L/bh^2$$
$$f_{ctm,eq150} = F_{m150} * L/bh^2$$

Moment - Normal force - curvature diagram

Using the stress-strain diagram, a M-N-k diagram can be calculated and plotted to find the value of the plastic moment and the maximum allowable curvature in a hinge. An example of a M-N-k diagram is given below. The markings correspond with the stress and strain distribution illustrated in figure 2.22.

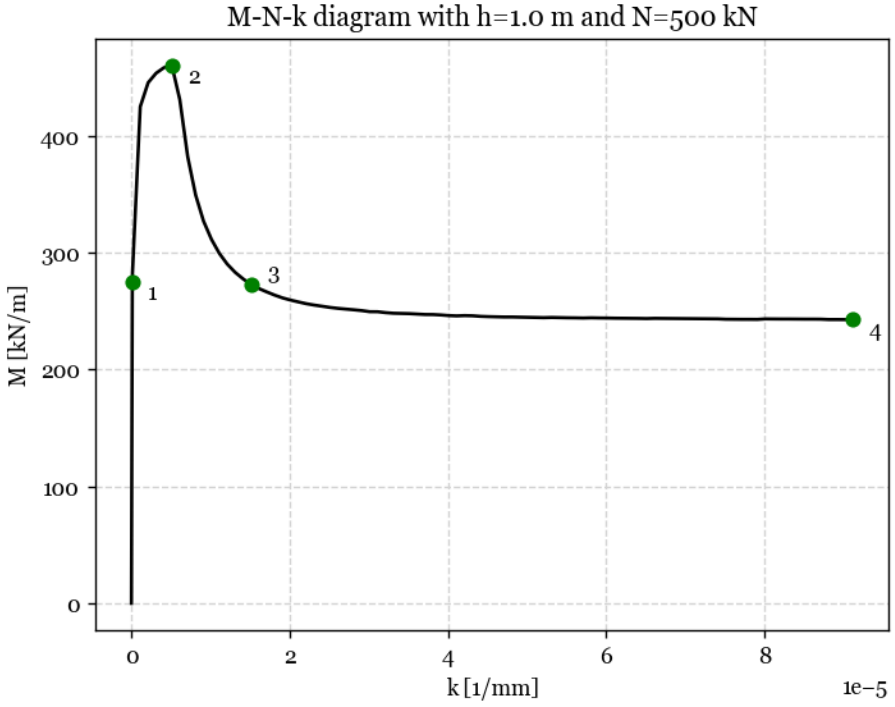

Figure 2.21: example of M-N-k diagram

Point 1 to 4 mark:

- 1: cracking of concrete

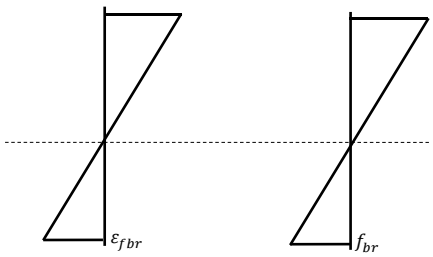

- 2: pull-out of fibres starts.

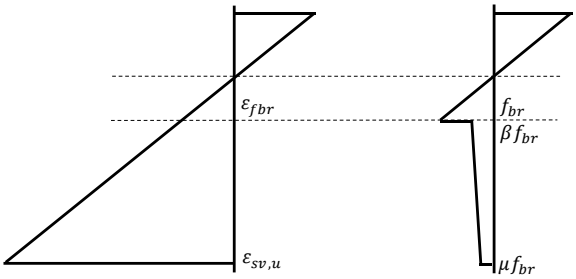

- 3: partial pull-out of fibres

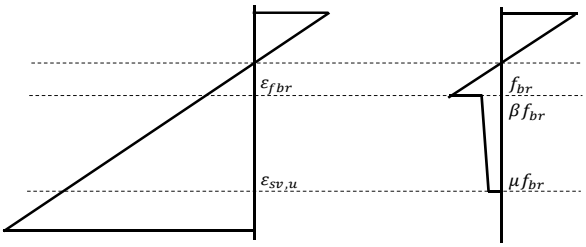

- 4: crushing of concrete

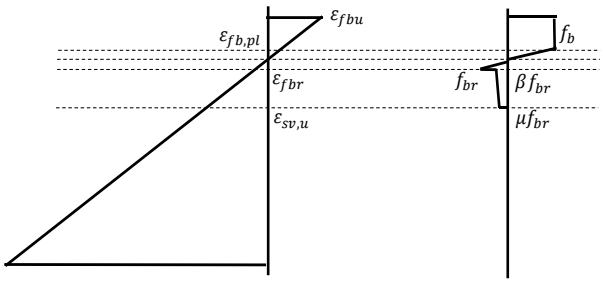

Figure 2.22: Points 1-4 in the M-N-k diagram

The M-N-k diagram shows that the ultimate strain of the fibres is reached earlier than the concrete starts to yield. This means that there is a drop in bending moment resistance of the cross-section, after which it will reach an asymptote equal to $N_{Ed}*h_{min}/2$ until the concrete crushes. To optimally utilize the increased resistance of the steel fibres, pull-out should be prevented. This means that only the ascending curve of the M-N-k diagram will be used and that the maximum allowable curvature of the cross-section is equal to $k_{pullout}$. This also means that all hinges must form before one hinge reaches this

curvature limit. A few examples of M-N-k diagrams with various normal forces and post-cracking tensile strengths are given in figure 2.23, where the maximum curvature is set to $k_{pullout}$.

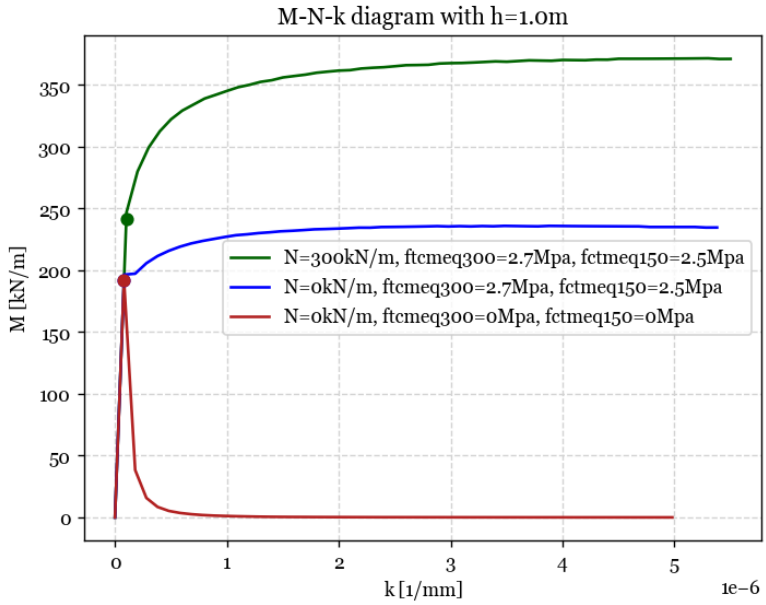

Figure 2.23: M-N-k diagram for different normal forces and post-cracking strength

2.2.5 SFUCF failure mechanisms

This paragraph describes a method to calculate the resistance of a SFUCF.

Bending moment resistance

The formation of plastic hinges above all supports and at all midpoints leads to brittle failure, which should be prevented. The state just before the formation of a mechanism is depicted in figure 2.24 and resembles a beam supported at both ends. In this case, the value of the moments at the supports is M_p. The maximum resistance in terms of loading can be calculated through the formula below [22]. A safety factor of 1.25 is recommended according to [5].

$$q_{Ed,max} = 8 * (M_p + M_{cr}/\gamma)/\ L^2$$

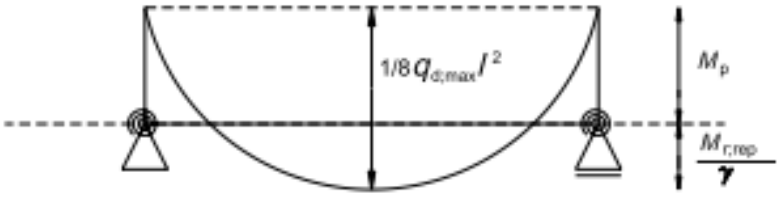

Figure 2.24: Moment line just before brittle failure [22]

(Punching) shear force resistance

The toughening behaviour of a SFUCF has a positive impact on (punching) shear resistance, as explained in [13]. A calculation method for taking into account the effects of steel fibre-reinforcement on the (punching) shear force resistance is described in [23]. This calculation method is based on results

from a three-point bending test, this is not consistent with the reference concrete mix design test results, as these were obtained through a four-point bending test. As a result, there is no appropriate data to take into consideration the improved (punching) shear force resistance. Using the (punching) shear force resistance of a conventional UCF is a safe approach, however, it is recommended to conduct the three-point bending tests on the reference concrete mix design such that the improvements can be taken into account.

2.3 Reflection

The information gathered in the previous two paragraphs of the literature study was used to formulate calculation methods for designing a UCF and a SFUCF. For the design of a conventional UCF, this thesis builds upon previous research outlined in the CUR-77 Guideline [4]. While earlier research has been conducted on the influence of design parameters on the resistance of various failure mechanism of a UCF [29], the relevance of that study to this thesis is limited.

The process of discretizing a UCF into a 1D beam model is detailed in [4], but the method of computing force distribution is not explicitly defined. In order to address this, a parametric calculation method to determine the force distribution in a UCF was established using [9] and [10]. The calculation method uses the Euler-Bernoulli beam theory.

The literature study has explored various types of fibres that can be utilized for reinforcing concrete, and it was determined that the properties of steel fibre reinforcement are best suited for use in UCF's. Several earlier executed UCF projects incorporating steel fibres were reviewed to evaluate the scenarios where fibre reinforcement could offer added value and potential material savings. The Botlekspoortunnel project implemented a specific concrete mix design, for which supplementary data regarding post-cracking tensile strength and workability properties was studied and is available within BAM Infraconsult. This thesis builds upon the findings of that study and uses the concrete mix as a reference for the remainder of the thesis.

All gathered information regarding the calculation method for a (SF)UCF is incorporated into a parametric design model that will be further elaborated in the next chapter and that will serve as a method of answering the main research question.

3. Parametric design model for a (SF)UCF

Given the information that was obtained though literature study, a model was developed to address the main research question and sub-questions outlined in section 1.2. The model allows to quickly perform design calculation on a (SF)UCF and consists of various building blocks that represent the failure modes of a (SF)UCF. These building blocks take input, perform a series of calculations or processes, and produce output. The building blocks can be arranged in a desired sequence to generate the data required to answer the research question. This chapter visualizes the process within these building blocks and states the formulas used. The model's output was verified, of which a summary is provided in this chapter. The complete verification can be found in Annex A. The model consists of the following building blocks:

- Force distribution
- Force distribution with slip
- FM B1: Tensile resistance
- FM B2: Compression arch
- FM B3: Compression arch with membrane action
- FM C1: Bending shear fracture
- FM C2: Additional shear resistance
- FM G: Punching shear resistance
- FM BF: Bending resistance SFUCF

3.1 Conditions for using the model

The following conditions for using (results obtained from) the model are derived from the assumptions made in the calculation method for a (SF)UCF.

- Euler-Bernoulli approach should be applicable for the case in which the model is used. This means that each cross-section is assumed to remain perpendicular to the neutral axis. Euler-Bernoulli does not take into account shear deformation.
- Normal force has a positive effect on the resistance of a UCF. Losses due to resistance between the soil and tensile elements are not taken into account. Precaution should be taken when piles with large cross-section and bending stiffnesses are used as these can decrease the normal force in the UCF.
- For the bending resistance of a SFUCF, there should be enough rotation capacity for all hinges to form. This means that no hinge may reach the curvature limit of fibre pull-out before all other hinges have formed.
- The hardening factor of a SFUCF should be greater than one to guarantee plastic behaviour and the formation of finely distributed cracks, rather than discrete large cracks.
- This model is only suitable to describe behaviour of UCF's that serve a temporary function.

Moreover, some limitations of the model should be listed:

- The model is only suitable to calculate force distributions for UCF's where a consistent centre to centre distance between the tensile elements is used.

- Only one type of tensile element with identical stiffness can be used along the span.
- FM BF can only be applied for the reference concrete mix design described in 2.2.3. This means that concrete classes C25/30 and C30/37 can not be considered with the addition of fibre reinforcement.
- The bearing resistance of tensile elements is not taken into account.
- This model is not suitable to describe behaviour of UCF's that serve a permanent function.
- A loss of punching shear resistance when punching cones are overlapping is not considered and has to be checked manually.

3.2 Overview of parameters

Table 3.1 gives an overview of all parameters and in which building block they are active.

Table 3.1: Overview of parameters

Parameter	Definition	NS	S	B1	B2	B3	C1	C2	G	FB
N_{ed}	Normal force in UCF	x	x	x	x	x	x	x		x
k_1	Stiffness of retaining wall	x								
k_2	Stiffness of tensile element	x	x							
L	Length of building pit	x	x							
c. t. c.	Centre to centre distance tensile elements	x	x		x	x				x
c − class	Concrete strength class	x	x	x	x	x	x	x	x	
h_{nom}	Thickness of UCF	x	x	x	x	x	x	x	x	x
q_{Ed}	Distributed load on UCF	x	x		x	x				x
a_r	Rib length of pile				x	x			x	
D	Diameter of circular tensile element								x	
B	Width of square tensile element								x	
p	Depth of dish anchor				x	x			x	
tol_{bottom}	Tolerance at bottom of UCF	x	x	x	x	x	x	x	x	x
tol_{top}	Tolerance at top of UCF	x	x	x	x	x	x	x	x	x
$tol_{anchorage}$	Tolerance of connection				x	x			x	
k_3	Membrane spring stiffness					x				
p_{head}	Height of pressure head					x				
d	Diameter of dish anchor								x	
μ	Friction coefficient		x							

3.3 Visualization of the model

The process inside the building blocks is visualized using flowcharts. Corresponding formulas can be found in table 3.3. The definitions of the shapes in the flowchart are given in table 3.2. A visualization of one of the building blocks (FM B2) was shown in this chapter. A complete visualization of the model can be found in annex A.

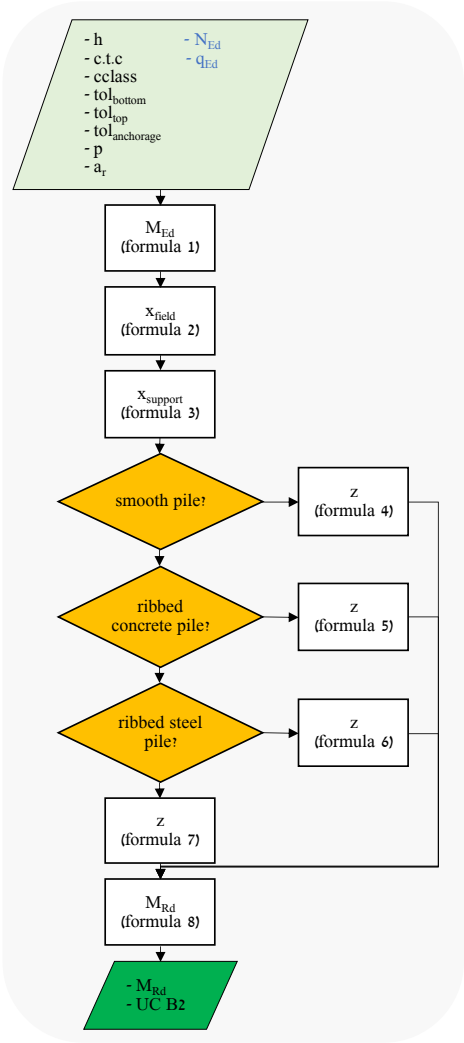

Figure 3.1: Flowchart for building block B2

Table 3.2 Symbols and definition

Symbol	Definition
	Input/output
	Process
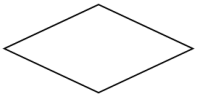	Decision

Table 3.3 Corresponding formulas to flowchart

#	Formula	source
1	$M_{Ed} = q_{Ed} * c.t.c.^2 / 8$	[4]
2	$x_{field} = 2 * N_{ed}/f_{cd,pl}$	[4]
3	$x_{support} = x_{field} / 0.6$	[4]
4	$z = h/2 - tol_{bottom} - 2/3 * N_{Ed}/f_{cd,pl}$	[4]
5	$z = h - tol_{top} - a_r - tol_{bottom} - (x_{field} + x_{support})/3$	[4]
6	$z = h - tol_{top} - a_r - tol_{bottom} - (x_{field} + \max(300mm, x_{support}))/3$	[4]
7	$z = h - tol_{anchorage} - p - tol_{bottom} - (x_{field} + x_{support})/3$	[4]
8	$M_{Rd} = z * N_{Ed}$	[4]

3.4 Verification

The verification process for the model involves a systematic approach where the value of each parameter is initially set to a representative value. Subsequently, each building block is tested by varying the value of one parameter, within a continuous representative domain, at a time and evaluating the unity check for the failure mechanism. Three sample points within this domain are selected for verification using hand calculations and an automated excel sheet provided by BAM Infraconsult bv. The sample points for the force distribution are verified using finite element analysis (FEA). Although this approach does not cover a 100% complete verification of the model, it is deemed sufficient for the intended application due to the verification of results within the representative domain. The complete results of the verification can be found in Annex A, with a summary presented in table 3.4 in the form of average deviation and maximum deviation between the model and the verification results.

Table 3.4: Verification of parametric model

	Method	Average deviation [%]	Maximum deviation [%]
NS (no slip)	FEA	0.42	2.92
S (slip)	FEA	0.08	1.02
FM B1	Hand calculation	0.50	4.39
	Excel	1.09	1.09
FM B2	Hand calculation	0.19	1.96
	Excel	0.22	2.50
FM B3	Hand calculation	0.83	4.69
	Excel	0.53	4.69
FM C1	Hand calculation	0.79	4.17
	Excel	0.00	0.00
FM C2	Hand calculation	0.37	4.17
	Excel	0.29	3.84
FM G	Hand calculation	0.56	1.97
	Excel	0.07	1.49
FM BF	Hand calculation	0.65	2.70

4. Parameter influence on design efficiency

The goal of this chapter is to provide an understanding of how various parameters impact the design of a UCF. By applying the information presented in this chapter, an engineer can identify which parameters to adjust in order to improve the design of a UCF, when following a traditional design approach. Besides, quick estimates can be made to determine whether the chosen parameters provide sufficient resistance. Additionally, the results can help to determine which combinations of parameters should be avoided in specific situations. The chapter aims to answer the sub-question outlined in paragraph 1.1.

1. What parameters influence the resistance of the failure mechanisms to be considered in the design of a UCF and how can these parameters be altered to improve design efficiency in a traditional design approach?

The outline of the chapter mirrors the way the model is broken down into building blocks. A division into several sections was made, where the influence of parameters on force distribution is discussed first, followed by an examination of bending moment resistance in both cracked and uncracked UCF. The influence of parameters on shear force and punching shear force is also described. Building blocks, which are thoroughly detailed in annex A, are utilized to generate data, which is then plotted in graphs to display continuous results. For a comprehensive understanding of which parameters are used in what building block, refer to table 3.1 in chapter 3.

4.1 Force distribution

When determining the force distribution in a UCF, it is assumed to remain uncracked. The force distribution is influenced by its geometry, consisting of the nominal thickness, the full length of the span, and the centre-to-centre distance of the tensile elements. Additionally, the loads applied to the UCF, as well as the stiffness of the spring supports play a role. This paragraph examines the effect of varying with aforementioned parameters and presents the results in four graphs. Output from the force distribution is to be used in failure mechanism for bending resistance and shear force resistance, where the maximum moment in the UCF, as well as the shear force at $x=h_{min/2}$ from the retaining wall are values used as input. For this reason, the influence of parameters on force distribution is expressed in how much they influence the maximum moment and the shear force at beforementioned locations.

Unless specified otherwise, the following values for parameters were used:

- q_{Ed} = 100 kN/m²
- h_{nom} = 1.0 m
- Length = 20 m
- c.t.c. = 2.5 m
- Concrete class = C20/25
- tol_{top} = 0.075 m
- tol_{bottom} = 0.150 m
- k_1 = 60000 kN/m²
- k_2 = 50000 kN/m (20000) when divided by c.t.c.$_y$

Figure 4.1 illustrates how the overlapping boundary disturbance zones behave under different UCF lengths, with the c.t.c. distance fixed to a value of 2.5m. Figure 4.2 examines the impact of varying the c.t.c. distance from a standard value to an extremely large value on the maximum moment and shear force in the UCF. Figure 4.3 shows the effect of the stiffness ratio between the tensile elements and the retaining wall, while figure 4.4 investigates how the bending stiffness of the UCF, which is dependent on h_{nom} and the concrete strength class, affects the force distribution.

It is worth noting that the tolerances were kept constant for the reason for that they only affect the cross-sectional height of the UCF, meaning that their influence is indirectly incorporated in the bending stiffness. Besides, the specified values for execution tolerances are by far most commonly found in practice.

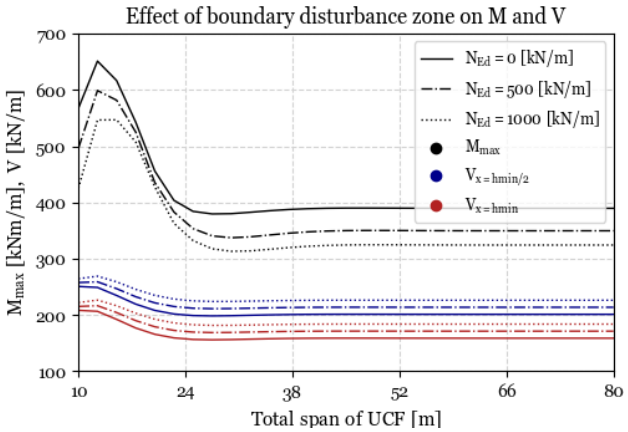

Figure 4.1: Boundary disturbance zone

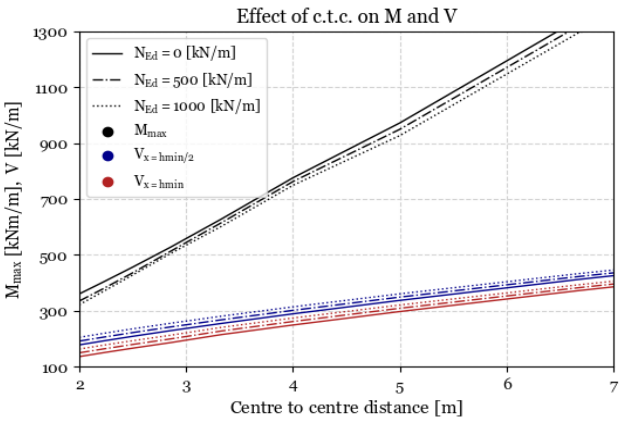

Figure 4.2: Centre to centre distance

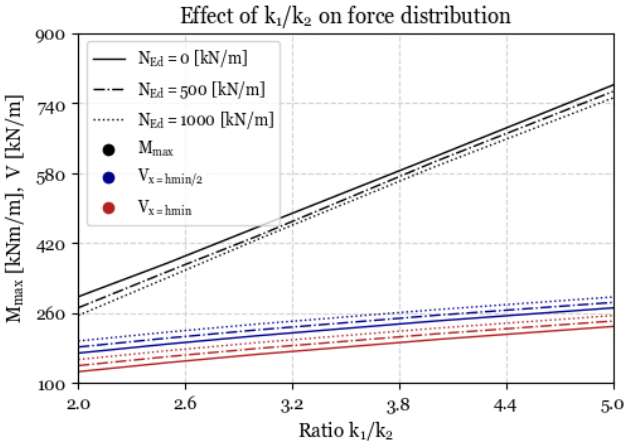

Figure 4.3: k_1/k_2

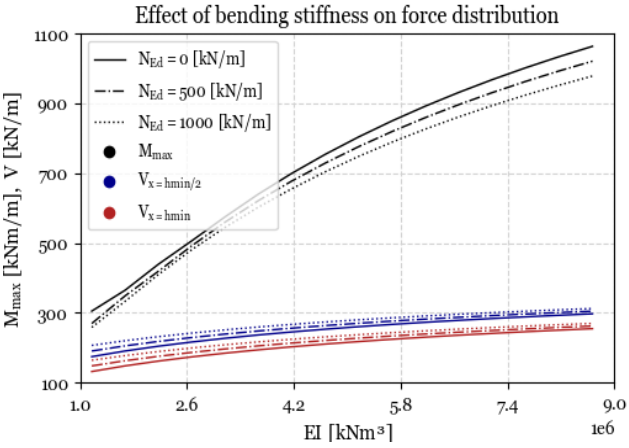

Figure 4.4: Bending stiffness

As illustrated in figure 4.1, the maximum moment in a UCF design with the above-specified parameters is significantly larger when the complete span of the UCF is 10-20m, compared to building pits with greater spans. The large increase of the maximum moment is explained by overlapping boundary disturbance zones which are induced by the k_1/k_2 ratio. The boundary disturbance needs a specific length to dampen, the graph depicts that for a length larger than 20m, the boundary disturbance is dampened sufficiently such that the zones do not overlap. A common conception is that a large normal force positively affects the maximum moment in the UCF, this is confirmed by the graph. However, in the descending branch one can see that an increase of normal force hardly decreases the maximum moment, and the favourable properties of a high normal force are not present. Additionally, with the parameters used to generate this graph, a high normal force negatively affects the shear force at $x = h_{min}/2$. A conclusion to be drawn from this graph is that designing for an uncracked UCF is possible, but may be very difficult when the building pit has a length of 10-20m. This is because the maximum bending moment is increased by a factor of almost 2 due to the overlapping boundary disturbance zones.

As expected, increasing the centre to centre distance between tensile elements greatly increases the bending moment in the UCF. This indicates that for designing for an uncracked UCF, tight c.t.c. distances are advised. The influence of increasing the c.t.c. distance is less pronounced on shear force. Figure 4.2 also shows that a high normal force has a negative effect on the shear force but a positive effect on the bending moment.

Figure 4.3 illustrates that using relatively stiff tensile elements compared to the retaining wall, can make a significant difference in the bending moment in the UCF, which is of importance when keeping the UCF uncracked is desirable. Preventing cracking is difficult when the retaining walls have a high stiffness, as the ratio k1/k2 will become very high. The shear force is influenced by the k_1/k_2 ratio to a lesser degree than the maximum bending moment.

To investigate the influence of cross-sectional bending stiffness on the force distribution, the parameter EI, which represents the bending stiffness of the structure, was varied between a range of values. The minimum value of EI corresponded to a combination of C20/25 with h_{nom} = 0.8m, while the maximum value corresponded to a combination of C30/37 and h_{nom} = 1.5m. The results presented in figure 4.4 indicate that increasing the nominal thickness to prevent cracking of the UCF may not be as effective as one may initially anticipate. This is due to the fact that an increase in the nominal thickness or concrete strength class also leads to an increase in the maximum moment in the UCF, which can be explained by the statically indeterminate nature of the beam model used in the analysis.

4.2 Bending moment resistance

A UCF possesses two methods of resisting bending moments. The first is through its tensile strength capacity, where the UCF can withstand the bending moment by preventing cracking. In this scenario, the force distribution of an uncracked beam model, as illustrated in previous figures, should be used. Should this mechanism prove insufficient, additional resistance can be obtained through the formation of a compression arch, in which the force distribution is dependent on a single field. This paragraph describes the influence of parameters on both methods of resisting bending moments.

FM B1 - Tensile strength

Figure 4.5 illustrates the impact of various parameters on the maximum moment resistance of a UCF. It can be used as a design tool to attain the maximum allowable bending moment for a specific combination of $_{hnom}$, concrete class, and normal force, and determine whether it is sufficient to prevent cracking of the UCF. The graph is based on the assumption that the sum of tol_{top} and $tolb_{ottom}$ equals 225mm, which is a commonly encountered value in practice.

As previously demonstrated, a high normal force has been shown to be beneficial in reducing the maximum moment within the UCF. Figures 4.1-4.4 show that a high normal force is also beneficial for the cracking resistance of the cross-section, meaning that chances to prevent cracking are much larger in a UCF which is loaded by a large normal force. Increasing the nominal floor thickness will greatly increase the bending moment resistance as a result of increased cross-sectional area and tensile zone area. Besides, increasing the concrete strength class can positively affect the bending moment

resistance, explained by the higher tensile strength of the material. Worth noting is that increasing the height as well as the concrete strength class also gives a higher acting moment, as illustrated in figure 4.4.

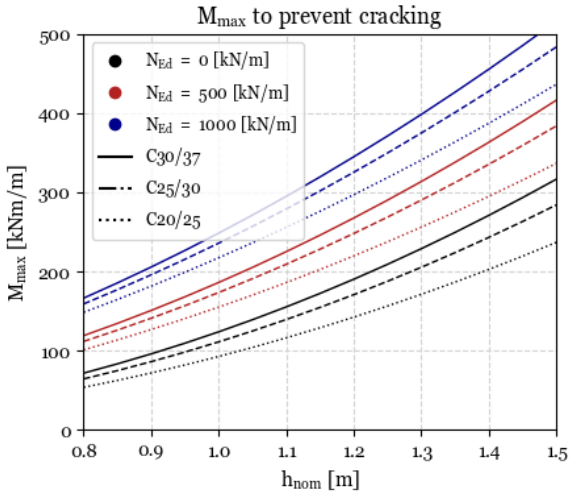

Figure 4.5 Cracking moment under various combinations of parameters

FM B2 – compression arch

In case the tensile strength is not sufficient to provide adequate resistance against the maximum bending moment, a compression arch can be used as an additional means of resistance. The bending moment resistance provided by the compression arch is equal to the product of the normal force acting on the UCF and the effective height of the arch. Figures 4.6 and 4.7 can be utilized as design tools to quickly determine whether a given set of parameters will provide sufficient bending moment resistance. The engineer can use figure 4.6 to determine the acting bending moment in the UCF given a specific distributed load and centre to centre distance between the tensile elements. The bending moment resistance can then be found based on the acting normal force and effective arch height using figure 4.7. Conversely, the graphs can also be used to determine the maximum centre to centre distance for a given distributed load and bending moment resistance of the UCF.

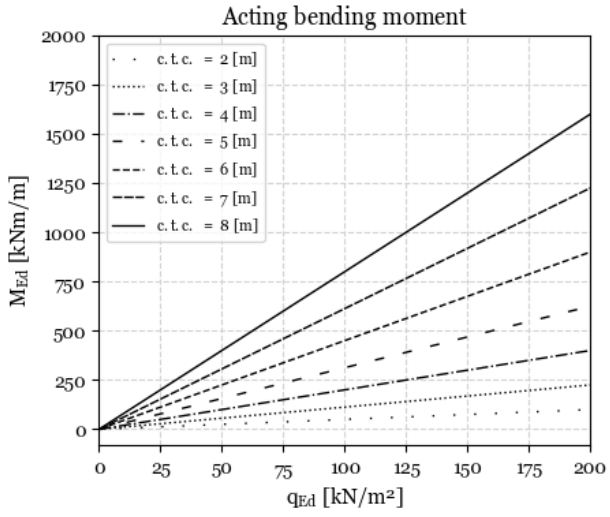

Figure 4.6: Acting bending moment

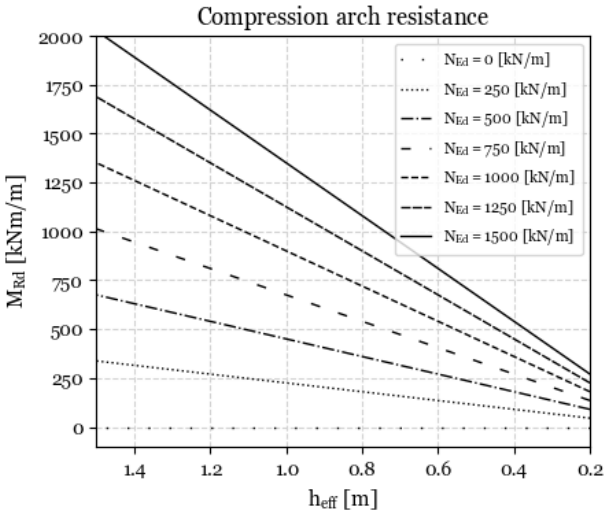

Figure 4.7: Bending moment resistance

Figure 4.7 illustrates the importance of the normal force in providing resistance of the compression arch. When the normal force is close to zero, the compression arch will lack resistance and a cracked UCF will not have sufficient bending moment resistance. The effective height also significantly affects resistance, as a larger effective height leads to a significant increase in bending moment resistance.

The effective height of the compression arch is determined by the type of connection and execution tolerances, as well as specific properties of the connection. The three accompanying graphs allow the engineer to quickly calculate the effective height of the compression arch, which is equal to h_{nom} minus a reduction. The reduction of h_{nom} can be determined from the graph, and the effective height can be computed using the provided formula. The graph is based on the assumption that the sum of tol_{top} and tol_{bottom} equals 225mm.

$$h_{eff} = h_{nom} - reduction$$

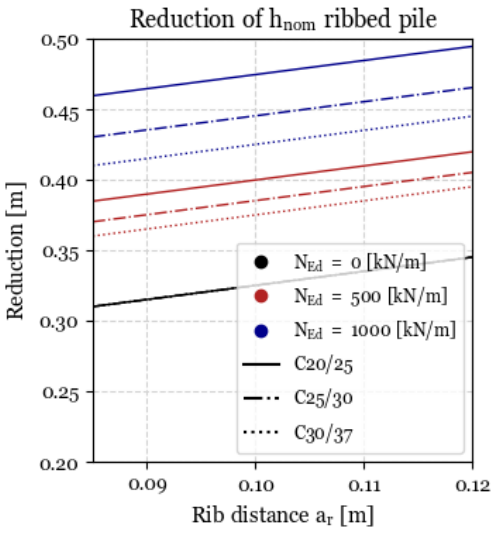

Figure 4.8: reduction h_{nom} ribbed pile

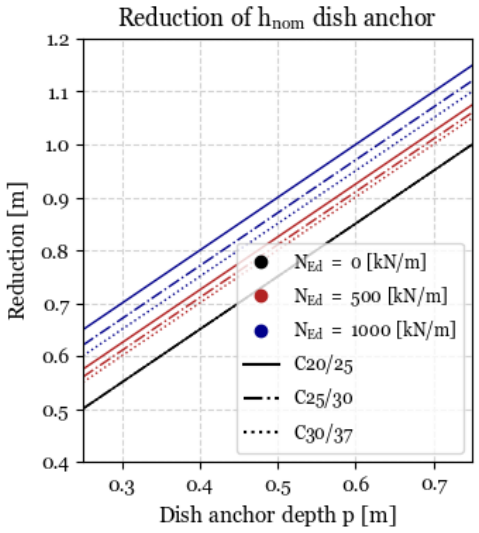

Figure 4.9: reduction h_{nom} dish anchor

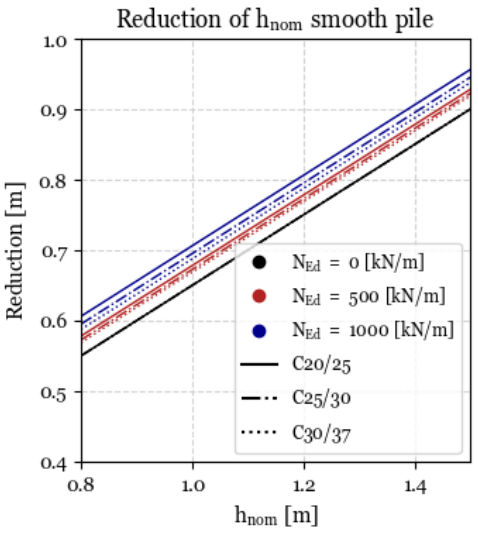

Figure 4.10: reduction h_{nom} smooth pile

The reduction used to calculate h_{eff} for a ribbed pile is dependent on the rib distance as well as a factor depending on the quotient of normal force and compressive strength of the material. For this reason, when the normal force equals zero, the reduction is the same for all concrete classes. According to the graph, the highest compression arch resistance is achieved using a minimum rib distance and a high concrete class.

When a dish anchor is used as connection type, the effective height can be obtained in the same way as for a ribbed pile however the embedment depth of the dish anchor plays a role contrary to the rib distance. Since the minimum value of embedment depth is larger than the minimum value of rib distance, it can be concluded that the effective height of the compression arch is per definition smaller than when using a ribbed pile. This means that a ribbed pile would be the optimal connection type in terms of compression arch resistance.

For a smooth pile, the reduction depends on the nominal thickness, normal force and concrete class, where the greatest reduction is found for a high normal force, high nominal thickness and low concrete class.

FM B3 – Compression arch with membrane action

The rotation of cracked segments of the UCF results in an expansion of the total length, which in turn causes a displacement of the retaining wall. The retaining wall is modelled as a spring, which generates additional normal force when compressed. As depicted in figure 4.7, an increase of normal force results in a corresponding increase of resistance. This means that additional resistance can be obtained by taking this membrane action into account. Figures 4.11 and 4.12 illustrate how the additional normal force in the UCF is dependent on the influencing parameters.

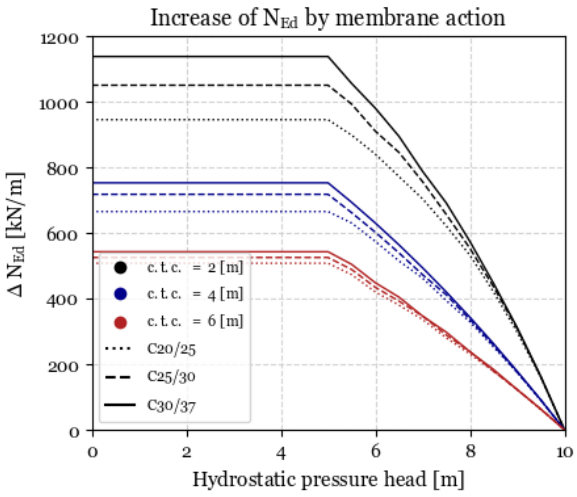

Figure 4.11 effect of c.t.c., c-class and p_{head}

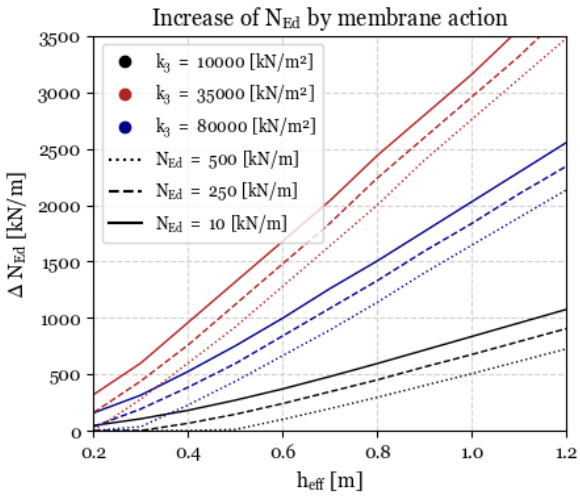

4.12 effect of k_3, h_{eff} and initial N_{Ed}

Figure 4.11 was generated using a fixed h_{nom} of 1.0m, $N_{Ed,initial}$ of 0 kN/m and k_3 of 35000 kN/m². As depicted in the graph, the pressure head has a substantial influence on the additional normal force that can be generated through membrane action. The additional normal force begins to decrease and reaches zero between a pressure head of 5 and 10 meters. This is in accordance with the reduction factor that should be applied according to [4]. Furthermore, the graph illustrates that the centre to centre distance of the elements has a significant impact on the additional normal force. This is a result of the increased rotation and extension that is possible with smaller elements, caused by the ratio between height and length of a segment, which makes snap-through less likely to occur. Changing the concrete class only makes a significant difference in combination with smaller centre to centre distances.

The graph presented in figure 4.12 was generated using a fixed concrete class of C20/25, a pressure head of 0m, and a centre to centre distance of 2.5m. The graph demonstrates that the spring stiffness has a significant influence on the additional normal force generated, which is a direct result of the additional normal force being the product of the spring stiffness and displacement. Furthermore, the graph illustrates that when the initial normal force in the UCF is minimal, a greater amount of additional normal force can be generated through the utilization of membrane action. Specifically, in this graph, a UCF without initial normal force will almost reach the same value of N_{Ed} after membrane action as a case where an initial normal force of 500 kN/m was present. As expected, a UCF with a larger thickness can generate a greater amount of additional normal force, the same reasoning as for the c.t.c. in figure 4.11 applies.

It is important to note that the values for increased normal force can not directly be substituted in figure 4.7, this is because the effective height for a compression arch with membrane action is calculated differently than for a regular compression arch. The difference is that the effective height for a compression arch with membrane action takes into account geometric non-linearities to the rotation of segments and follows an iterative calculation procedure.

4.3 Shear force resistance

There are two methods of determining the sufficiency of shear force resistance in a UCF. The first method, failure mechanism C1, assesses the resistance to bending shear fracture at the location $x=h_{min}$ outside the retaining wall. If this method is inadequate, failure mechanism C2, which includes additional checks C2a, C2b, and C2c, may be used to determine sufficiency. These additional checks are based on the shear force and bending moment at $x=h_{min}/2$ outside the retaining wall.

Bending shear fracture

Bending shear fracture resistance depends on the concrete strength class, nominal thickness of the UCF and the acting normal force. Figure 4.13 contains a design graph that shows the influence of all parameters and can be used as a quick method for determining whether a given UCF has adequate shear force resistance. A boundary condition for applying the figure as a design graph is that the sum of tol_{top} and tol_{bottom} must equal 225mm.

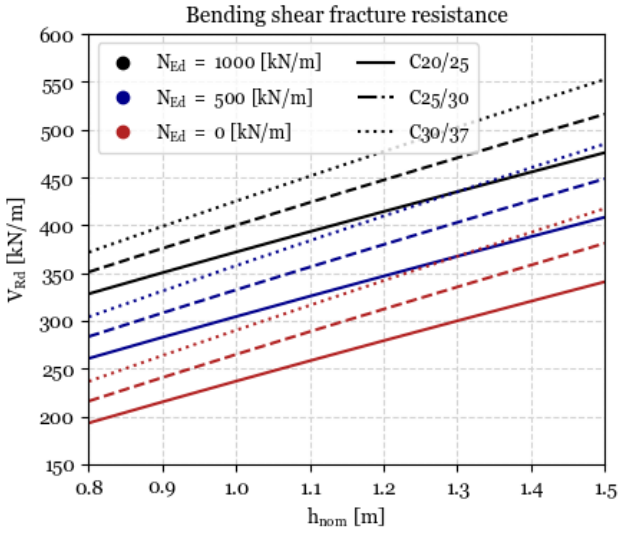

Figure 4.13 Bending shear fracture

Figure 4.13 illustrates that the largest factor of the shear force resistance is the nominal thickness of the UCF, followed by the acting normal force. As a means of increasing resistance if required, increasing the concrete strength class can be a viable option. In absolute terms, increasing the concrete class will have a greater impact on a thick UCF as compared to a slender UCF. However, relatively, a more substantial increase in resistance can be achieved by modifying the concrete strength class in a more slender UCF.

Additional shear force checks

The additional shear force checks of failure mechanism C2 are to be evaluated at the location $x=h_{min}/2$ outside the retaining wall. Check C2a involves a bending moment check for which the graph provided in figure 4.5 can be utilized. A more comprehensive method of determining the sufficiency of shear force resistance is by utilizing the design graphs below. Nine combinations of concrete strength classes and nominal thicknesses are provided. The graphs depict envelopes with boundaries dependent on the normal force. For a specific case, the values for shear force and bending moment can be aligned. If the aligned point falls within the envelope of the corresponding normal force, it indicates there is sufficient shear force resistance.

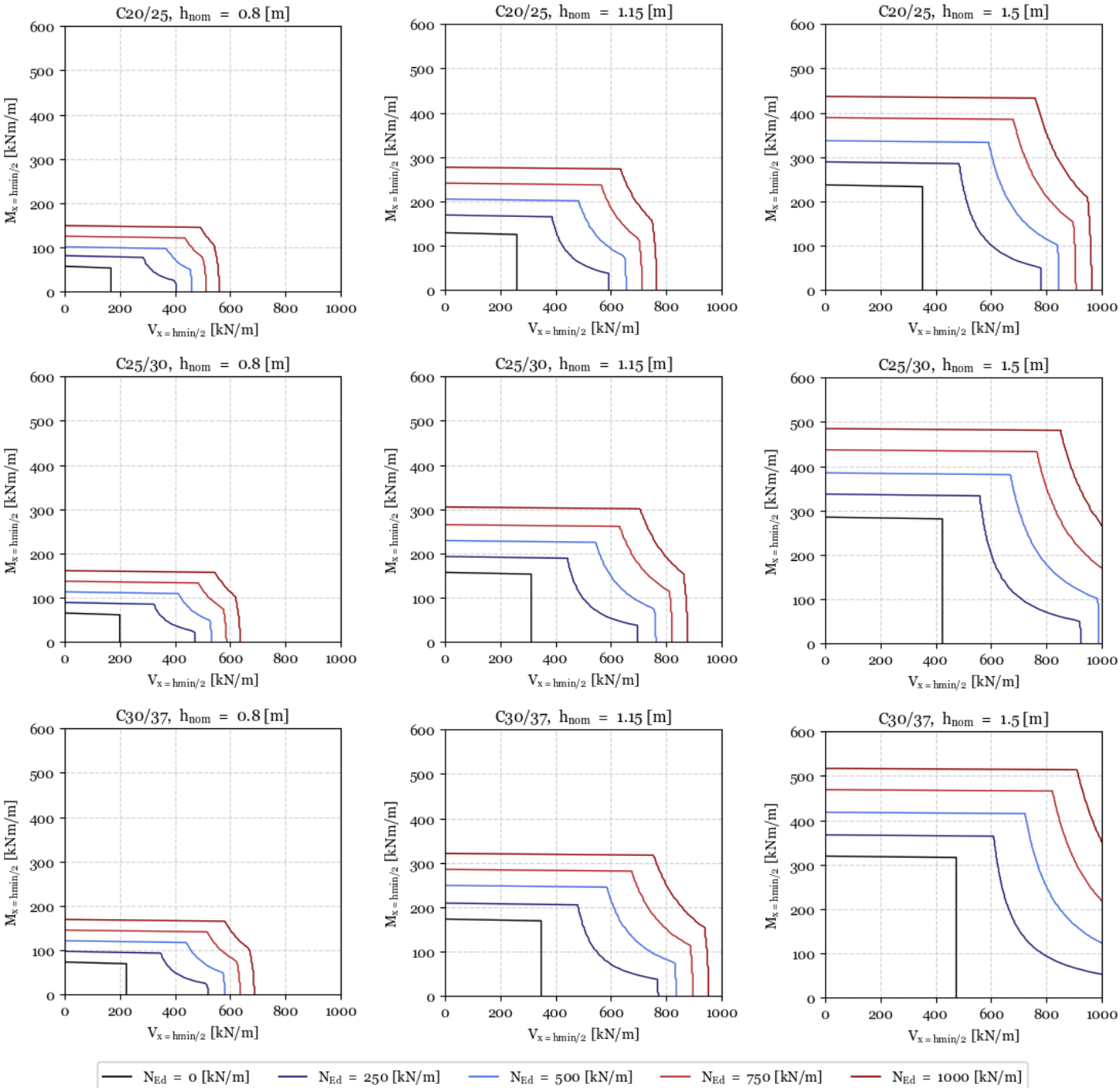

Figure 4.14: Resistance envelope additional shear force checks.

Using the information presented in the graphs, it is possible to determine which parameters are most effective to alter in cases where insufficient resistance is identified. Increasing the nominal thickness and concrete strength class both significantly enhances the allowable combination of shear force and bending moment. However, the increased resistance is more pronounced when increasing the nominal thickness compared to the strength class.

4.4 Punching shear force resistance

The type of tensile element used as connection type for the UCF can significantly affect the punching shear force resistance of the structure. In this paragraph, each type of tensile element will be analysed separately, and the ways in which their parameters influence the punching shear force resistance will be examined and discussed. It is important to note that the values presented in this analysis do not take into account the necessary safety factor for performing the unity check of failure mechanism G.

Smooth piles

The resistance of a smooth steel pile utilized as connection type is dependent upon the friction between the pile shaft and the concrete. The connection resistance is influenced by factors such as the concrete strength class, the diameter of the pile, the effective thickness of the floor, and the roughness coefficient. Two figures are provided, with the left graph displaying the punching shear resistance when a roughness coefficient of 0.1 is applied and the right graph depicting the punching shear force resistance for a roughness coefficient of 0.5. d_{min} indicates the effective height over which friction will be present and can be calculated with:

$$d_{min} = h_{nom} - tol_{top} - tol_{bottom}$$

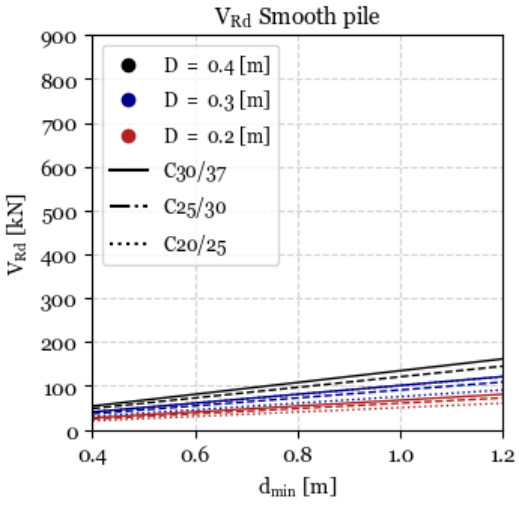

Figure 4.15 : c=0.1

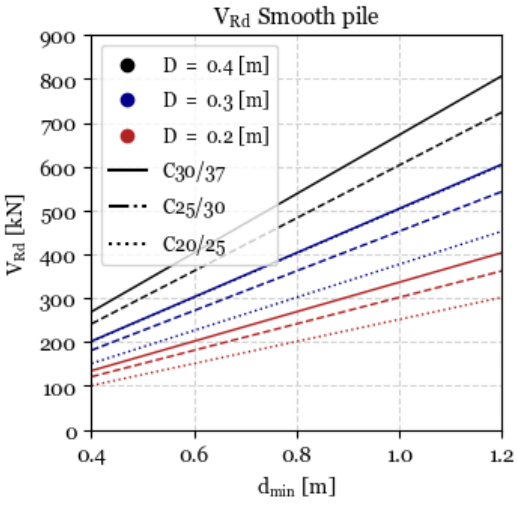

Figure 4.16: c=0.5

The graphs demonstrate that when utilizing a friction coefficient of 0.1, the punching shear resistance obtained is minimal. Although increasing the roughness of the pile surface does provide a slight increase in resistance, it remains very small, particularly when compared to the resistance provided by other types of connections. An increase in pile diameter, results in an increased surface area, providing a greater resistance, as evident in the graph. Furthermore, upgrading the concrete class only yields a minimal improvement in resistance.

Ribbed piles

Two types of ribbed piles were examined in this study. The steel ribbed piles possess a circular cross-section, whereas the concrete ribbed piles have a square cross-section. The graphs in figures 4.17 and 4.18 illustrate that, despite the slight variations in the method of calculating the circumference of the punching cone for the two types of piles, the obtained results are nearly identical.

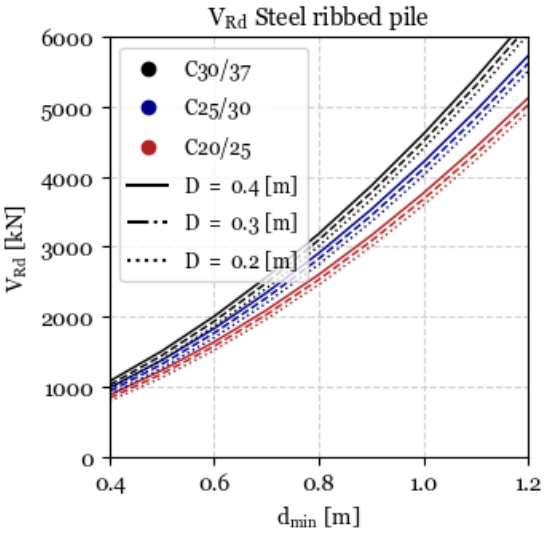

Figure 4.17: steel pile

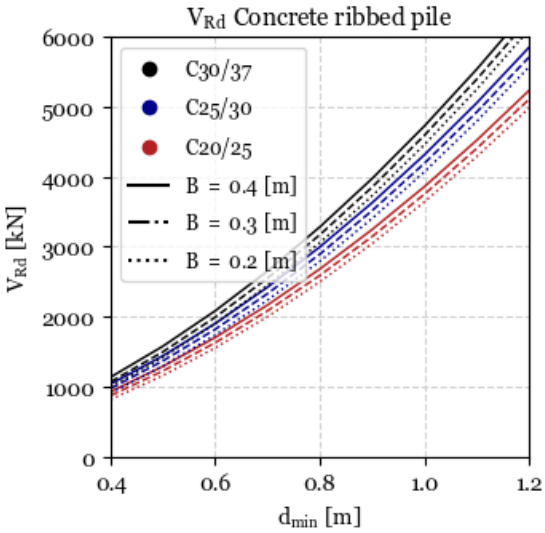

Figure 4.18: concrete pile

In comparison to smooth piles, significantly greater resistance can be obtained by utilizing ribbed piles. Notably, variations in diameter have a minimal impact on the resistance. This can be explained by the diameter of the punching cone on the bottom of the UCF, which does not increase proportionately with the diameter of the pile. Utilizing a higher class of concrete strength results in greater resistance for the punching cone, which is consistent with the data presented in the graph. Increasing the height of the UCF has a substantial effect on the resistance of the punching cone, by a much greater magnitude than other factors. The effective height, which indicates the height of the punching cone, can be calculated with the following formula:

$$d_{min} = h_{nom} - tol_{top} - tol_{bottom} - a_r$$

Modifying the rib distance of the pile has a minimal impact on the resistance, as it is restricted to a narrow range between 0.085 and 0.12 meters.

Dish anchors

The punching shear resistance of dish anchors as a connection type is dependent on various factors, including the diameters of the dish anchor and the steel pile, as well as the effective height of the punching cone and the strength class of the concrete. Dish anchors possess two distinct failure mechanisms: resistance of the punching cone and compressive resistance underneath the dish anchor.

The data presented in the graphs indicate that, for a small effective punching cone height, the punching resistance is the primary governing failure mechanism. However, as the effective punching cone height increases, the compressive stress underneath the dish anchor becomes increasingly significant and governing. This point is reached at an earlier stage for smaller dish anchors, as there is less area available to distribute the force. Using the data presented in the graphs, it can be concluded that increasing the concrete strength class can positively impact the punching resistance, especially when the compressive stress is governing. Additionally, for certain ranges of effective punching cone heights, increasing the size of the dish anchor can also improve resistance. Increasing the diameter of the steel pile does not offer a significant improvement in resistance.

The effective height, which indicates the height of the punching cone, can be calculated with the following formula:

$$d_{min} = h_{nom} - tol_{top} - tol_{bottom} - p$$

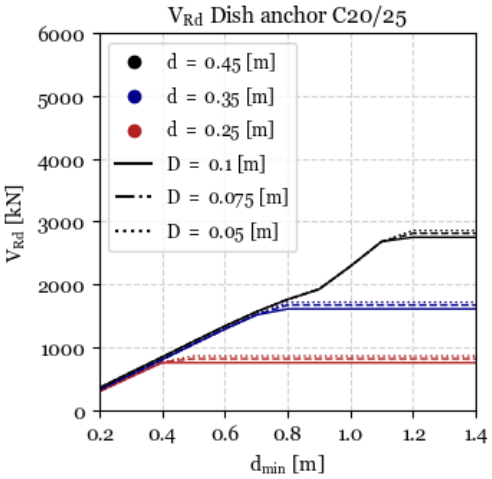

Figure 4.19: C20/25

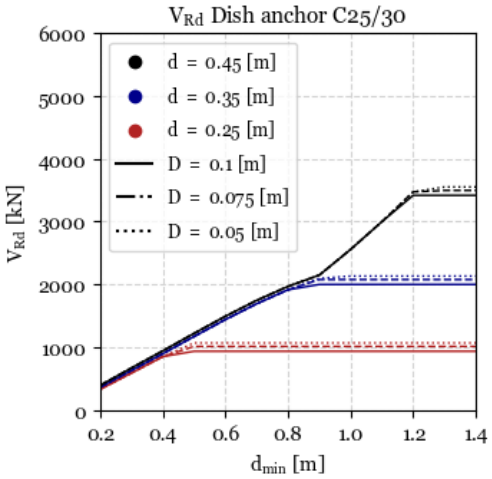

Figure 4.20: C25/30

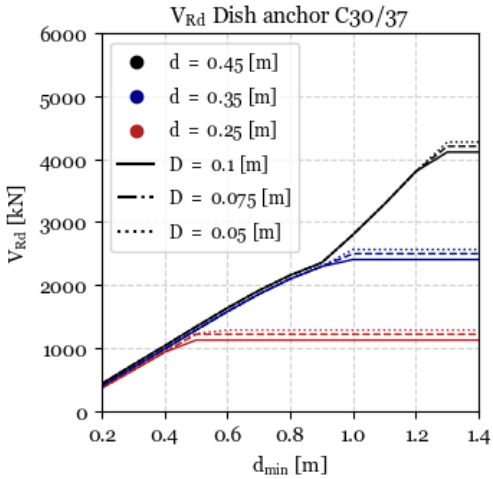

Figure 4.21 : C30/37

4.5 Additional remarks

- The results presented in figures 4.1 through 4.4 are specific to the parameters outlined at the beginning of paragraph 4.1, where only one parameter was varied at a time. As such, it is not possible to directly apply these results to other sets of parameters. However, the conclusions drawn from the graphs can be used as a general indication. The same applies to figures 4.11 and 4.12.
- The figures presented in this chapter can be utilized as direct design graphs, under the condition that the force distribution in the UCF is known. They provide a quick means of determining the feasibility of a particular set of parameters for use in design. However, Figures 4.1 through 4.4 and 4.11 through 4.12 are exceptions to this, as they were not fully parametrized and required fixed parameters in order to be plotted.
- The results presented in this chapter do not consider the bearing resistance of a tensile element, nor the bearing resistance of a dish anchor.

- When applying the results for punching shear resistance, it should be checked whether the punching cone diameter is sufficiently small such that punching cones of neighbouring piles do not overlap. This would decrease the punching shear resistance and require additional analyisis.

5. Enhancing UCF design with steel fibre reinforcement

In this chapter the added value of steel fibre reinforcement as a result of increased cross-sectional resistance is examined. Using the model described in chapter 3, calculations are performed in which results for a conventional UCF are compared to a SFUCF. A complete description of the building blocks relevant for this chapter can be found in Annex A. The aim of this chapter is to answer the following sub-question from paragraph 1.1:

1. How does the addition of fibre reinforcement influence the behaviour of a UCF and in what scenarios can the addition of fibres be beneficial in terms of material savings or resistance gain?

Material savings are used as a way to describe the added value, where minimum required floor thickness $h_{nom,req}$ is used as a basis for comparison between a conventional UCF and a SFUCF. Subtracting $h_{nom,req}$ as in the formula below, for a specific load case (combination of N_{Ed} and q_{Ed}), gives the material savings (h_{saved}). Results presented in this chapter give insight to material savings for a large amount of load cases and sets of variable parameters that are listed in table 3.1. This gives the engineer the opportunity to quickly estimate whether a project may benefit from the application of steel fibre reinforcement.

$$h_{saved} = h_{min,req,UCF} - h_{min,req,SFUCF}$$

Two points regarding the material properties and boundary conditions should be taken into consideration prior to comparing the resistance of a UCF and SFUCF. Firstly, it should be noted that material properties in the stress-strain diagram, as shown in figure 2.19, are based on concrete class B25, which is equivalent but not equal to current concrete class C20/25. The material properties for B25 are described in an outdated guideline that was replaced by [8]. In order to apply results of this thesis, expired material properties should be substituted by currently accepted values. It is important to study whether this approach is safe. Secondly, the boundary conditions for applying the calculation method described in paragraph 2.2.5 should be taken into account.

5.1 Substitution of concrete strength class

The concrete mix design used as reference in this thesis is classified as B25, which is equivalent to C20/25. However, with the release of new guidelines, the characteristic tensile- and compressive strength properties of the material have changed. This affects the cracking moment resistance (M_{cr}) and plastic moment resistance (M_p) of a cross-section. As seen in figure 5.1, substituting material properties of C20/25 into the stress-strain diagram used in the calculation method results in a decrease of M_{cr} and M_p. This substitution can be viewed as an added safety measure by using reduced moment resistance. Since the concrete mix design was determined to be safe for use at Botlekspoortunnel after thorough research, it is assumed that substituting the material properties is a safe approach, because it gives further reduction of resistance.

Material properties for concrete strength class B25 and for C20/25 according to [8] are outlined in table 5.1. The reduction of M_p and M_{cr} was calculated using the following formula:

$$reduction\ [\%] = 100 - \frac{100 * M_{p/cr,C20/25}}{M_{p/cr,B25}}$$

Table 5.1: Material properties

Stress-strain diagram (paragraph 2.2.4)	Equivalent to current value in [8]	Value for B25 [N/mm²]	Value for C20/25 [N/mm²]
f_b	f_{cd}	15	13.33
f_{br}	$f_{ctd,pl}$	1.15	1.0
E	E_{cm}	28500	27500

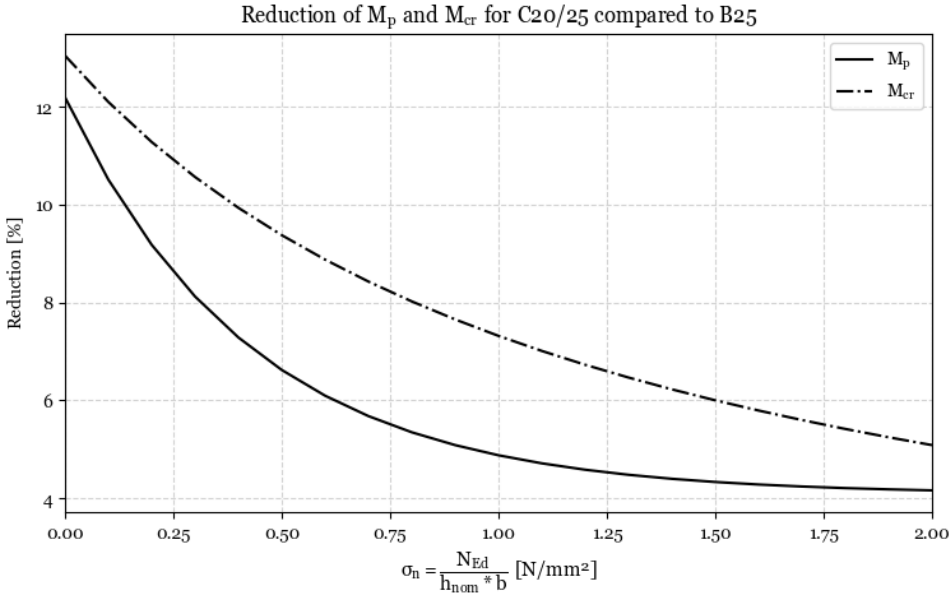

Figure 5.1: Reduction of M_{cr} and M_p

It was found that the reduction only depends on the change of material properties and the compressive stress caused by the normal force in the SFUCF. The reduction is most significant when the compressive stress is low. The substitution of material properties has a greater impact on M_p than on M_{cr}. This also implies that the hardening factor for C20/25 will be slightly lower than for B25. It is worth noting that b in the formula on the x-axis is equal to 1 meter.

5.2 Boundary conditions

Two boundary conditions related to the hardening factor and maximum curvature are outlined in paragraph 2.2.4. These conditions must be met for the calculation method to be appropriate and for the results to be applicable.

The hardening factor, as illustrated in figure 5.2, is dependent on the compressive stress caused by N_{Ed}. The graph demonstrates that M_p benefits more from a high normal force than M_{cr}, resulting in an increase of the hardening factor for higher compressive stress. Most importantly, the hardening factor is always greater than 1, even when there is no normal force present in the UCF. This indicates that plastic behaviour with finely distributed cracks is always guaranteed for the concrete mix design used

as a reference, which is a boundary condition for the calculation method outlined in paragraph 2.2.5 to be applicable.

A second boundary condition for the situation in figure 2.24 to be valid, is that the curvature limit in a hinge may not be exceeded. The curvature limit depends on N_{Ed} and the nominal thickness of the SFUCF and can be obtained from figure 5.3. The limit value corresponds to the curvature where the ultimate tensile strain (ε_{svu}) is exceeded in the outer fibres of the cross-section, and fibre pull-out starts. In the M-N-k diagram in figure 2.21 this point is marked with 2.

Figure 5.3 illustrates that a SFUCF loaded by a high normal force can withstand more curvature than a SFUCF with a low normal force. This can be explained by the compressive zone height in the cross-section, which is greater when the normal force is high, resulting in a smaller tensile zone. For a given curvature, the strain in the ultimate tensile fibres will therefore be smaller when the normal force is high. This reasoning also applies to the floor thickness. A slender SFUCF can withstand more curvature than a thick SFUCF because the tensile zone for a given curvature is smaller, leading to smaller strains in the outer fibre of the cross-section.

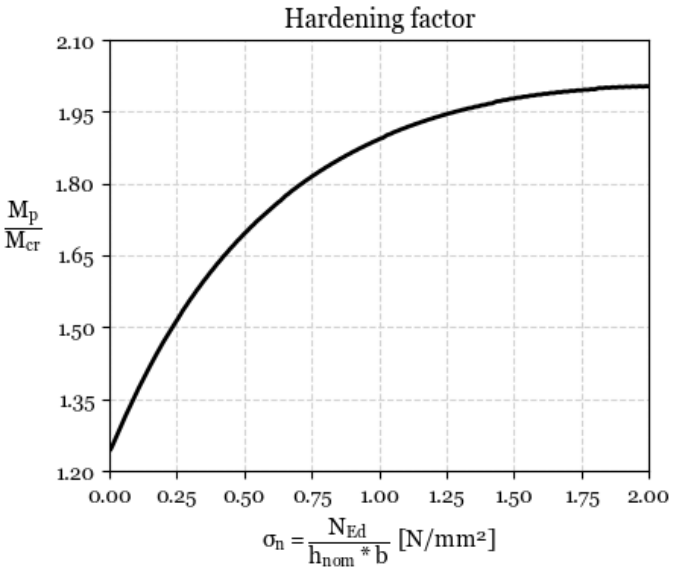

Figure 5.2: Hardening factor

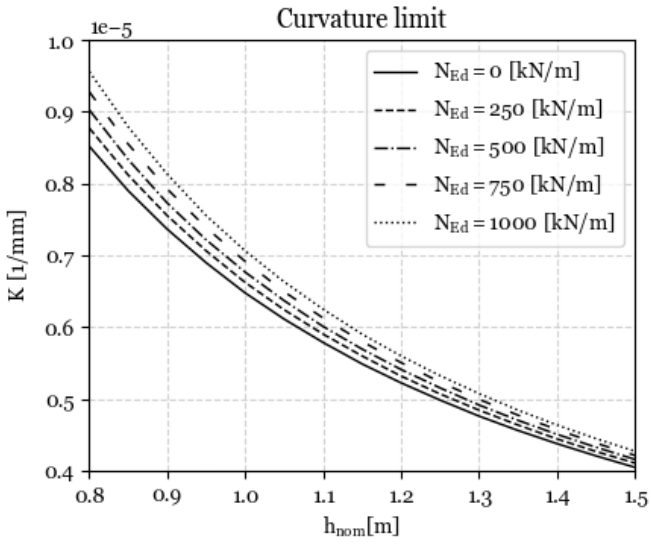

Figure 5.3: Curvature limit

This thesis does not investigate the actual curvature in a hinge. Further research into the rotation of hinges in a SFUCF is suggested. When utilizing the results presented in the following paragraph, it is crucial to verify that the curvature limit for the specific case is not exceeded.

5.3 Material savings by additional bending moment resistance

Assuming that the boundary conditions are satisfied, possible material savings are presented in graphs where the loading condition is set out on the axes. The results in this paragraph can only directly be applied when bending moment resistance is governing over (punching) shear force resistance. The load case of a specific project can be aligned on the axes after which the possible material savings can be read in the graph. The contours in the graphs are coupled to a colorbar where the value of h_{saved} is

specified. For the comparison between $h_{nom,req}$ for a UCF and SFUCF, a cracked situation is assumed. This means that bending moment resistance for a conventional UCF is obtained from failure mechanisms B2 and B3: compression arch (with membrane action). The reason for this assumption is that an uncracked UCF introduces too many variables for the comparison, because its resistance is largely dependent on the force distribution. Moreover, in an uncracked situation, the behaviour of a SFUCF does not differ from a conventional UCF. When applying the results presented in this chapter, the engineer should always examine whether the UCF actually cracks, such that the above assumption is valid. In practice this is often the case.

Standard values of parameters which are representative for a realistic UCF design are used as basis for the comparison. To demonstrate how each variable parameter affects the possible material savings, it will be changed within a representable domain. The standard set of parameters is listed below and uses dish anchors as standard connection type.

- c.t.c. = 2.50 m
- p_{head} = 0.00 m
- k_3 = 35000 kN/m²
- p = 0.25 m
- a_r = 0.085 m
- tol_{top} = 0.150 m
- tol_{bottom} = 0.075 m
- $tol_{anchorage}$ = 0.100 m

Reduced UCF thickness – Changing the c.t.c. distance

The centre to centre distance was changed from a typical 2 meters to a very unusual 8 metres. The colorbar applies to all graphs on it's left side, unless specified otherwise.

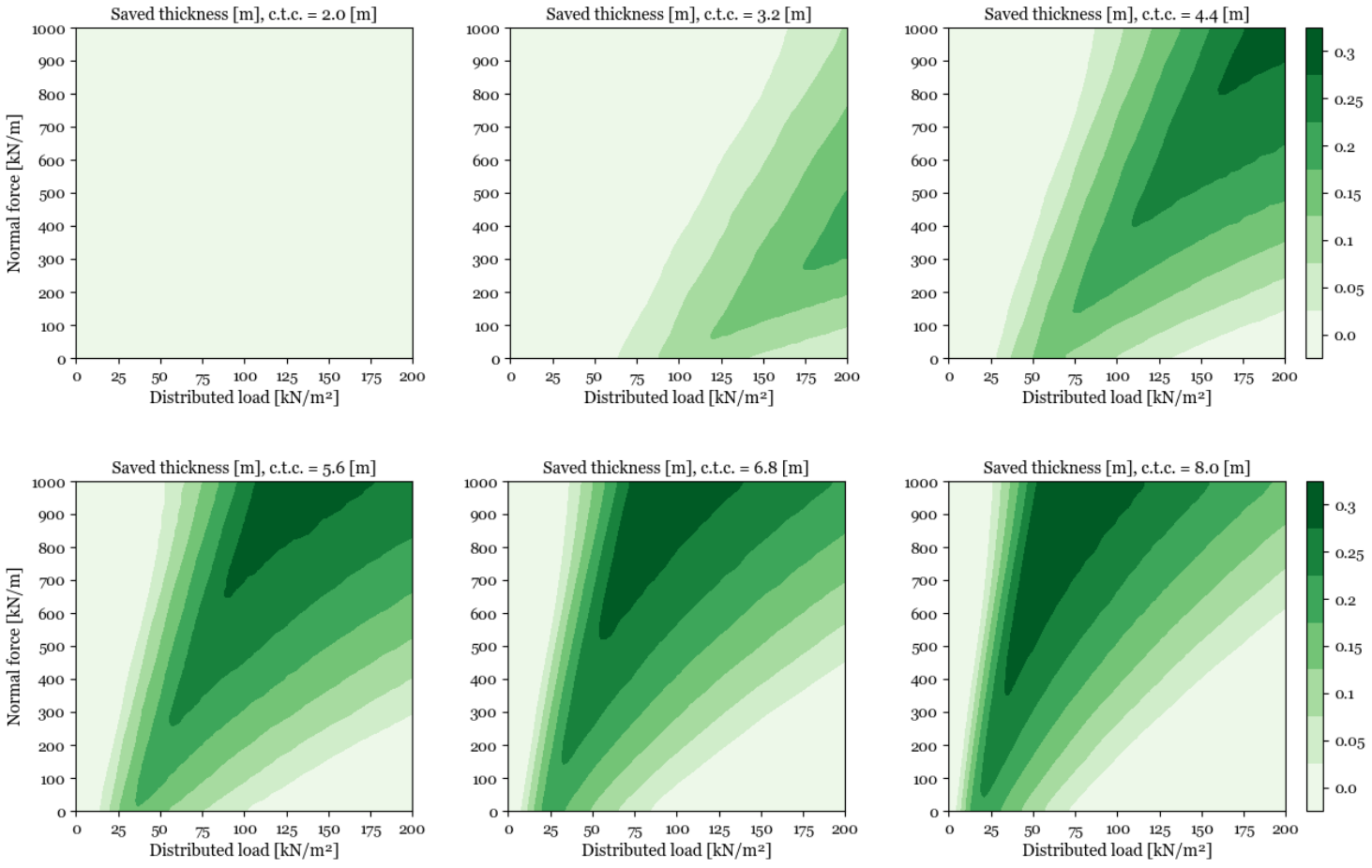

The graphs show that for the typical centre to centre distance range of 2 to 3.2 meters, minimal material savings can be achieved. For c.t.c. distances between 3.2 and 4.4 meters, substantial savings are possible, but only under load conditions with a large distributed load. For larger c.t.c. distances, significant material savings of up to 0.3m are possible when the normal force is substantial. Since the distributed load is primarily dependent on the hydrostatic pressure head, it can be argued that material savings where a small c.t.c. distance is applied, will only be applicable in deep building pits where a large pressure head is present. However, for large c.t.c. distances, material savings are also possible even with a low distributed load. An example is the underpass at Heinesoweg in Zwolle, where despite the low distributed load, material savings were still obtained because large c.t.c. distances had to be applied.

Reduced UCF thickness – Changing p_{head}

The results were analysed by varying the hydrostatic pressure head from 0 to 10 meters, while keeping other parameters at their standard values. It should be noted that the scale of the colorbar for the bottom-right graph was adjusted. Moreover, it's worth mentioning that the hydrostatic pressure head is measured relative to the top of the (SF)UCF.

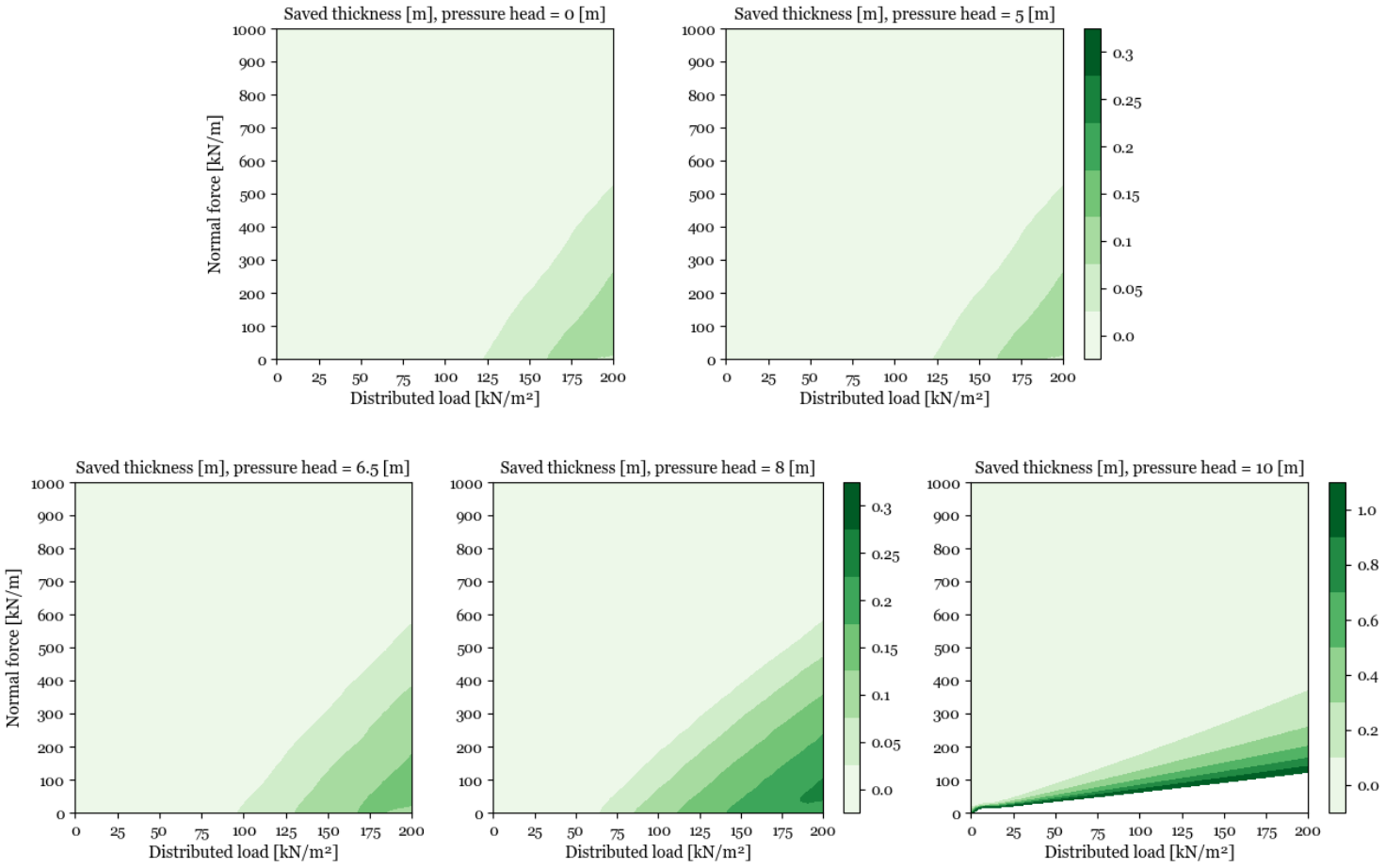

The results show no difference between a hydrostatic pressure head of 0 and 5 meters, which is expected as no reduction coefficient for membrane action is to be applied within this range. However, for higher pressure heads, the additional resistance by membrane action is reduced. The plots demonstrate that material savings are possible at larger pressure heads, especially when the distributed load is high. It is important to note that the distributed load is highly dependent on the pressure head,

hence a pressure head of 8 meters in combination with a distributed load of 150 kN/m² may not be commonly encountered in practice.

For pressure heads of 10 meters or higher, the membrane action is no longer applicable, which significantly reduces the resistance of the compression arch. This allows for serious material savings, even when both the distributed load and normal force are low. The white area in the graph indicates load cases where a conventional UCF with a moderate thickness is not feasible, but a SFUCF can still be applied. The primary challenge in this area is the lack of normal force, which renders the compression arch almost ineffective. Even though the pressure head at projects of Groninger forum and Mauritshuis was not necessarily 10m or higher, the common problem was a lack of normal force even after taking membrane action into account. These projects are examples where a SFUCF was essential to making the project feasible, and this is also shown by the results in the graph.

Reduced UCF thickness – changing k_3

The membrane spring stiffness was altered between 10000 and 60000 kN/m². The graphs indicate that in case of a membrane stiffness of 35000 to 60000 kN/m², no significant amount of material can be saved by applying a SFUCF. This is due to the high normal force generated by the compression of the spring, which is beneficial for the compression arch. As a result, a smaller floor thickness can be used and the application of a SFUCF becomes redundant.

When the membrane spring stiffness is low, similar issues arise as when the pressure head is high. The lack of additional normal force that can be generated by membrane action makes the use of a SFUCF beneficial. In this case, the lack of normal force is not caused by a reduction coefficient, but because of the physical low stiffness of the membrane spring.

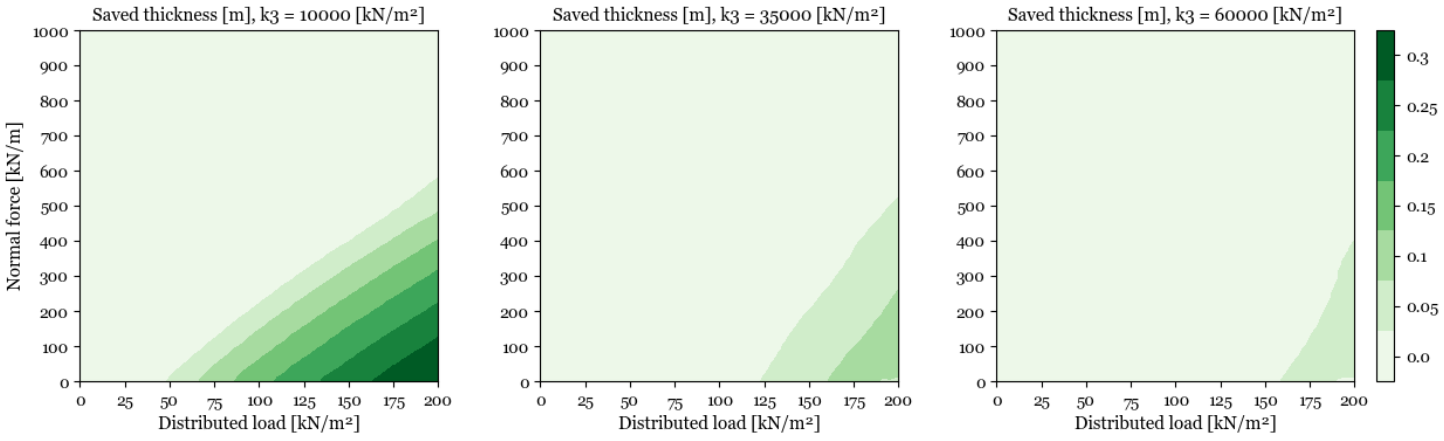

Reduced UCF thickness – changing p

Increasing the embedment depth for a dish anchor significantly reduces the effective height of the compression arch. In practice, the dish anchor is typically placed as close to the top of the UCF as possible. The reason for this can be observed in the graphs. When the dish anchor is deeply embedded in the UCF, like in the right graph, a lot of resistance of the compression arch is lost. This explains the potential for material savings when a deeper embedment depth is applied. It is important to note that the scale on the colorbar has changed compared to previous graphs.

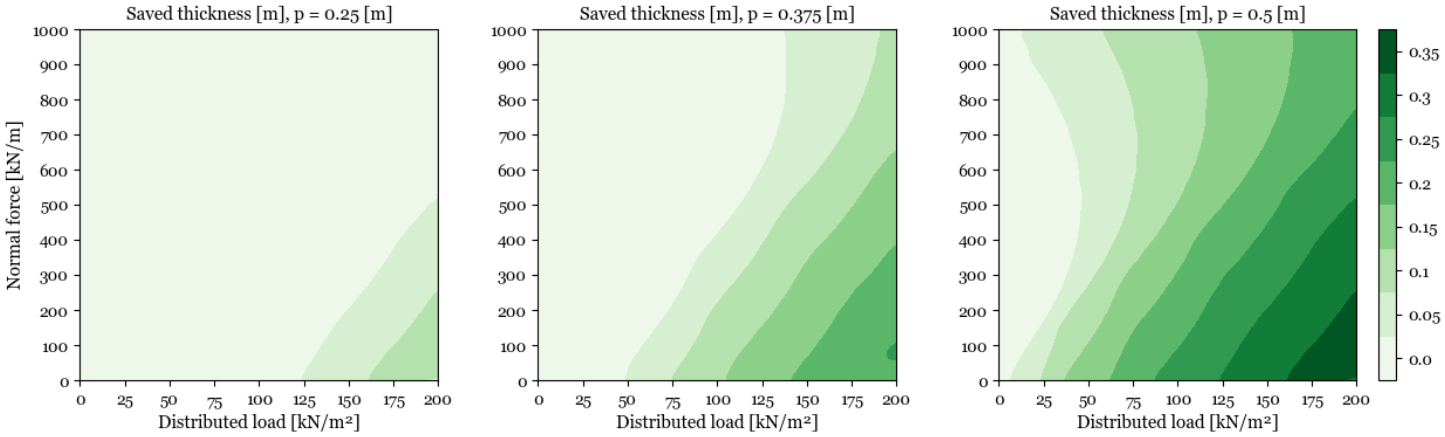

Reduced UCF thickness – changing the connection type

So far, all graphs have utilized dish anchors on steel rods as the standard connection type. It is worth studying whether material savings are possible when using different types of connections. It is important to note that changing the tensile elements also changes the k1/k2 ratio and affects the force distribution along the UCF. This may increase the likelihood that the floor remains uncracked which would eliminate the need for steel fibre reinforcement. However, the graphs below are based on the assumption of cracking, and the engineer should always verify if cracking actually occurs.

The graphs show that when changing the connection type to ribbed steel or ribbed concrete piles, there are no material saving possible in combination with the other standard parameters. However, for a smooth pile, a substantial difference can be made under certain load conditions. These load conditions are most likely to occur in deep building pits. A factor to consider is the execution for each type of tensile element, a reason for the common application of dish anchors for deep building pits is that they are considered to be easier to execute at this depth. The results of the graphs are in line with the formulas for effective height of the compression arch, where a smooth pile gives the least effective height and a ribbed pile gives the most effective height.

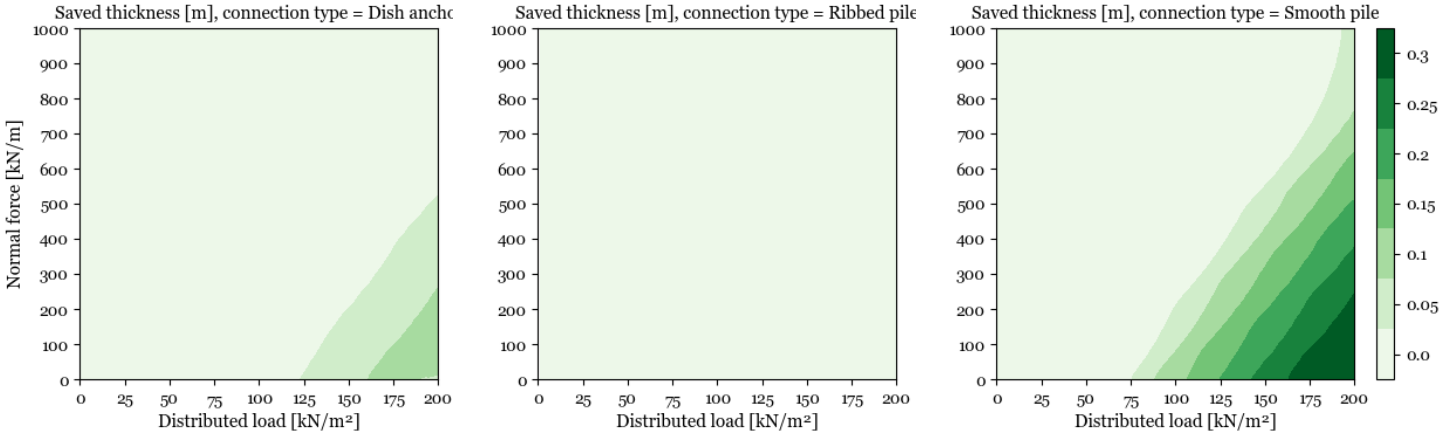

Reduced UCF thickness – changing a_r

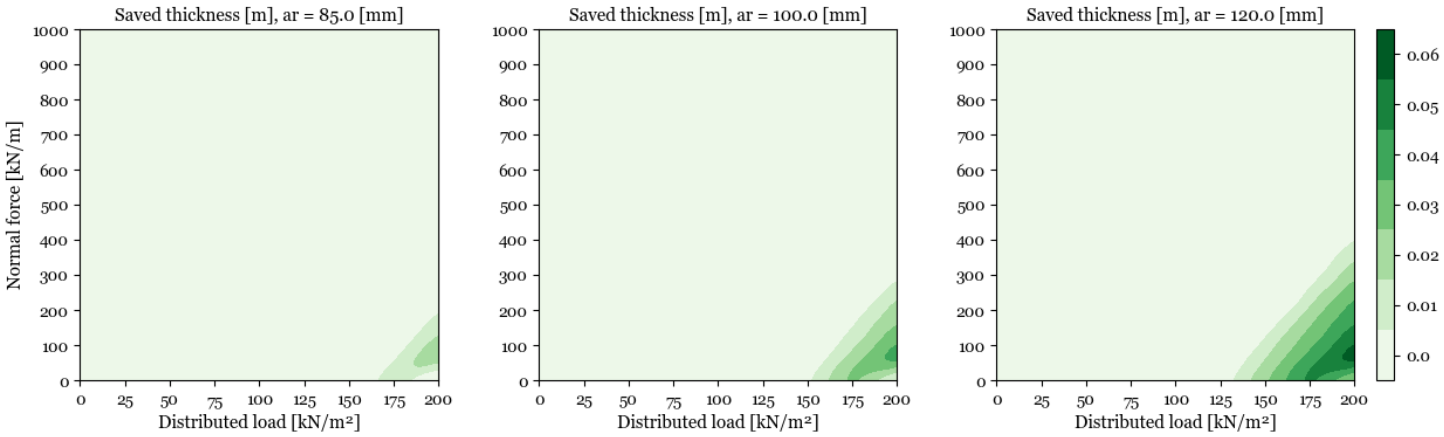

Changing the rib distance only applies when using ribbed piles, therefore the connection type for plotting these graphs was set to steel ribbed piles. Applying concrete ribbed piles does not alter the results. Other parameter are kept at their standard values listed at the beginning of this paragraph. As seen on the colorbar with changed scale, changing the rib depth hardly changes the possibility to save material. The small difference is explained by the slight decrease of effective height of the compression arch.

Material savings by additional bending resistance expressed in percentages

Previous results have presented material savings in terms of the required thickness for a SFUCF subtracted from the required thickness for a conventional UCF. This provides an absolute value, but does not indicate the relative material savings that can be achieved. Expressing the material savings as percentages addresses this issue and gives a different perspective on the results. The formula used to calculate the percentage of material saved is listed below. An example is provided using the standard set of parameters and a c.t.c. distance of 3.2m.

$$saved\ concrete\ [\%] = 100 - \frac{100 * h_{min,req,SFUCF}}{h_{min,req,UCF}}$$

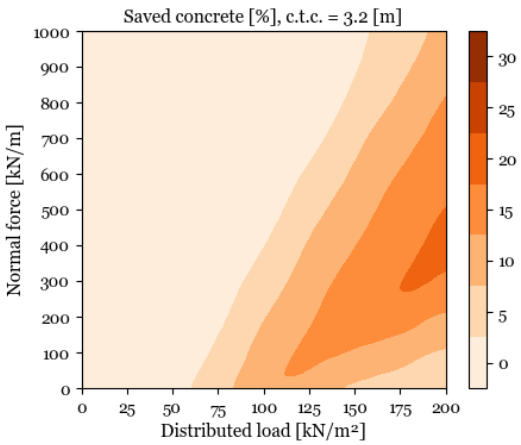

Annex C includes additional graphs that complement the results presented in this paragraph, where material savings are expressed in percentages. Combining the graphs presented in this chapter and the graphs in chapter C, gives the opportunity to calculate the required thickness for a UCF and SFUCF, for all load cases plotted in the graphs

5.4 Additional remarks

- The results in this chapter apply only to the specific combinations of standard parameters listed in paragraph 5.3, where one parameter was varied at a time. While this provides insight into circumstances under which the application of steel fibre reinforcement can result in material savings, it may be more useful for an engineer to obtain an exact answer for a unique set of parameters not covered in this chapter, rather than making an estimate based on the provided results. For this purpose the engineer can use the optimization tool discussed in the next chapter. By inputting specific parameters for a project, the output of the tool will suggest whether or not the use of a SFUCF is advantageous as well as provide a list of optimal design parameters.
- The reference steel fibre reinforced concrete mix design was categorized as strength class B25, equivalent to C20/25. The properties of this concrete mix were determined through four-point bending tests. The input of the stress-strain diagram used in the calculation procedure for a SFUCF is in correspondence with the material properties obtained with the four-point bending tests. Since material properties for higher concrete strength classes following four-points bending tests were not available, only comparisons could be made to UCF's executed in concrete class C20/25. It is recommended to conduct further research to material properties that can be used as input to the calculation method, such that a comparison can be made between a SFUCF and UCF executed in higher concrete strength classes.
- Due to execution tolerances and the behaviour of a conventional UCF, a lower bound of 800 mm is used as minimum nominal floor thickness. For the comparison in this chapter the same lower bound was used for a SFUCF. However, it is possible that allowing a floor thickness smaller than 800mm could result in greater material savings, as in many load cases, a unity check below 1.0 was obtained for a SFUCF thickness of 800mm. Additional research is recommended to investigate whether the ductile behaviour of a SFUCF could allow a floor thickness smaller than 800mm to be safely executed.
- As described in the literature study, steel fibre reinforcement potentially has a positive impact on the shear force- and punching shear force resistance of a UCF. Methods for taking these positive effects into account are outlined in [23]. The calculation requires the use of post-cracking tensile strength values obtained from three-point bending tests as input. These tests were not performed on the reference concrete mix design, so the additional resistance for (punching) shear cannot be determined using this method. A conservative approach is to treat a SFUCF as if it is not reinforced with steel fibres, however this makes a comparison between UCF and SFUCF on (punching) shear force resistance redundant. It is recommended that additional three-point bending tests be conducted to determine the necessary material properties for the described calculation method, as this could provide valuable information on potential material savings when the bending moment resistance is not governing over (punching) shear force resistance.

6. Cost optimization by parametric design

The previous chapters provided a thorough analysis of how design parameters can impact the design of an underwater concrete floor. Additionally, the effects of incorporating steel fibre reinforcement were investigated and scenarios where material savings as a result of the fibre reinforcement are possible, were illustrated through graphical representations. These results were obtained by generating data with the parametric model and can assist an engineer in decision-making in a traditional design approach for a UCF.

This chapter describes a different way in which the parametric model can be used to assist the engineer, namely by creating a new design approach for (SF)UCF's. Given the complexity and large number of parameters involved in the design of UCF, an optimization tool was developed to evaluate and compare different designs (sets of parameters), and identify the optimal set of parameters. The optimization tool uses the total material cost of the UCF, including tensile elements, as the basis of comparison between different designs.

The optimization tool can be utilized for a specific case, as prescribed by the user. Certain parameters, such as the dimensions of the building pit and the load case, are specific to the given case and must be provided by the user. For other parameters, such as the nominal thickness, amount of tensile elements and concrete strength class, the optimization tool will iterate through a large pool of combinations. By calculating the total price for each combination of variable parameters, the most cost-effective design for the prescribed case is found.

The parametric model and various building blocks outlined in chapter 3 and annex A contain all necessary calculation steps to develop the optimization tool. The challenge is to connect these building blocks in an appropriate sequence that accurately reflects the design process of a (SF)UCF. Once this is done, it is possible to iterate through different sets of parameters to generate a range of designs and identify the design with the lowest cost.

This chapter will provide an overview of the input and output of the optimization tool, and will describe the factors taken into account in the comparison between different designs. Additionally, the process within the optimization tool will be visualized by a flowchart.

6.1 Input and output of the optimization tool

The user is required to provide an Excel file where all required information for the optimization process is inputted and stored as a database. The Excel file includes various data sheets where case-specific parameters, as well as material prices are listed. Additionally, there are data sheets for each connection type, where the engineer can input different variations and corresponding parameters of a specific connection type to be considered. The decision to use an Excel file as the method of input was based on the assumption that it is a user-friendly method for most engineers, and allows for easy modification of material prices or other parameters, as well as the ability to save multiple versions.

In addition to the excel file, the user is required to provide a standard template used to present the output. After the optimization tool has iterated through the entire pool of parameters and determined the most cost-efficient configuration, the python script automatically generates a calculation report. The report includes cross-sections of the construction, as well as calculations and diagrams illustrating the moment, shear force and displacement distributions. The process of transforming input to output, through the use of a python script, is visually presented in figure 6.1.

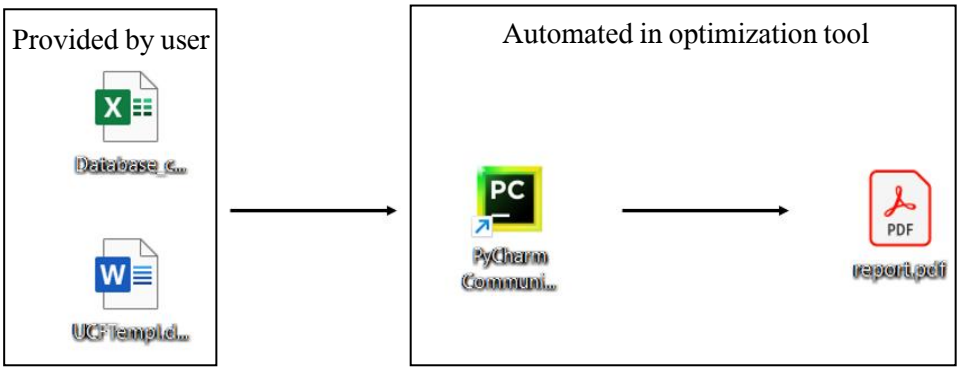

Figure 6.1: Process of going from input to output

Input: case specific parameters

The user is required to provide input for case-specific parameters in a designated table within the Excel file. Table 6.1 lists the necessary parameters and provides a brief explanation.

Table 6.1: Case-specific parameters (dummy values)

Parameter	Value		Description
$Length_x$	20	[m]	Length of short span
$Length_y$	30	[m]	Length of long span
Top_{pit}	+1	[m]	Level of top of retaining wall
Top_{UCF}	-7	[m]	Level of top of UCF
p_{head}	5	[m]	Hydrostatic pressure head relative to top_{UCF}
N_x	300	[kN/m]	Normal force along short span
N_y	300	[kN/m]	Normal force along long span
μ_x	0.3	[-]	Friction coefficient between retaining wall and UCF - short span
μ_y	0.3	[-]	Friction coefficient between retaining wall and UCF - long span
f_y	505	[N/mm²]	Yield stress steel piles
k_{1x}	60000	[kN/m²]	Spring stiffness retaining wall – short span
k_{1y}	60000	[kN/m²]	Spring stiffness retaining wall – long span
k_3	35000	[-]	Membrane spring stiffness
Conseq.class	2	[-]	Consequence class according to Eurocode
tol_{top}	0.075	[m]	Execution tolerance for top level UCF
tol_{bottom}	0.15	[m]	Execution tolerance for bottom level UCF
$tol_{anchorage}$	0.1	[m]	Execution tolerance for connection
$Pile_{depth,est}$	15	[m]	Estimated required tensile element depth

Input: connection types

The Excel file consists of data sheets for each connection type, allowing the user to specify multiple variants for consideration in the optimization process. Required parameters, including spring stiffness, for the chosen variants must be entered to accurately determine force distribution. Additionally, the base price of the tensile elements (expressed in €/m) should be entered. The circular diameter must be provided for smooth and ribbed steel piles, while the square diameter must be entered for ribbed concrete piles. The diameters of both the pile and anchor must be specified when dish anchors are used as connection type. Table 6.2 presents an example, demonstrating how two variants for each connection type are entered.

Table 6.2: Connection types to be considered (dummy values)

	Datasheet: Smooth pile			Datasheet: Ribbed concrete pile			Datasheet: Ribbed steel pile			Datasheet: Dish anchor			Unit
variant	**1**	**2**	**..**	**1**	**2**	**..**	**1**	**2**	**..**	**1**	**2**	**..**	
k_2	60000	70000		70000	80000		60000	70000		50000	50000		[kN/m]
D	0.2	0.3					0.2	0.3		0.0635	0.0635		[m]
B				0.2	0.3								[m]
d										0.25	0.35		[m]
€	120	150		120	150		120	150		60	60		[€/m]

Input: additional costs

In addition to the cost of the tensile element, a separate data sheet within the Excel file allows the user to provide additional costs. The prices for underwater concrete of various strength classes considered, as well as the price of steel fibre reinforcement, must be provided. When considering a dish anchor, additional costs must be taken into account, including the grout for ensuring friction and bearing resistance between the tensile elements and soil, the cost of the dish anchor itself, and a connection bolt for secure placement. Table 6.3 serves as an illustration, presenting dummy values as an example.

Table 6.3: Additional prices (dummy values)

Item	Price	Unit
Underwaterconcrete C20/25	115.00	[€/m³]
Underwaterconcrete C25/30	120.00	[€/m³]
Underwaterconcrete C30/37	125.00	[€/m³]
Steel fibre reinforcement (30kg/m³)	120.00	[€/m³]
Grout	5.00	[€/m]
Dish anchor	3.00	[€/kg]
Connection bolt	32.50	[€/piece]

Process: iterating through pool of parameters

The pool of parameters is comprised of arrays of variable parameters with iterable values. These arrays possess upper and lower boundaries and a step size, which have a fixed value in the python script but could be altered by the user if desired. The variable parameters, to be iterated over by the optimization tool are listed below:

- h_{nom}
- concrete strength class
- s_x
- s_y
- connection type and variant
- c
- a_r
- p

The nominal thickness parameter is iterated over values ranging from 0.8m to 1.5m, with a step size of 0.025m. The array for concrete classes includes C20/25, C25/30, and C30/37. Due to a lack of appropriate data, the implementation of steel fibre reinforcement can only be considered when the set of parameters contains strength class C20/25.

The process for determining the number of fields along the span (s_x and s_y) is based on a minimum and maximum centre to centre distance of 2m and 7.5m, respectively. Using these values, the upper and lower bounds for the number of fields in the UCF are determined and will be iterated over with a step size of 1.

The iteration of connection types and their variants is dependent on the data input by the user. If the set of parameters being calculated includes smooth piles as the connection type, the roughness coefficient will be iterated through values of [0.1, 0.2, 0.4, 0.5]. If the set of parameters includes ribbed piles, the rib distance will be varied through [0.085m, 0.09m, 0.095m, 0.1m, 0.105m, 0.12m]. If dish anchors are used as the connection type, the embedment depth will be varied from tol_{top}+$tol_{anchorage}$ to $h_{nom}/2$ m with a step size of 0.025m.

Process: basis of comparison

The price calculation of a design is performed if a set of parameters is determined to have sufficient resistance and meets the requirements on all necessary failure mechanisms. The price calculation is based solely on the material prices for the UCF and tensile elements. The formulas used to calculate the price of the design vary depending on the connection type. An additional cost should be added to the formulas in case steel fibres are applied in the design.

Smooth/ribbed piles: $length_x * length_y * h_{nom} * €_{concrete} + (s_x - 1) * (s_y - 1) * pile_{est,depth} * €_{pile}$

Dish anchor: $length_x * length_y * h_{nom} * €_{concrete} + (s_x - 1) * (s_y - 1) * pile_{est,depth} * (€_{pile} + €_{grout}) + (s_x - 1) * (s_y - 1) * (€_{dish} + €_{bolt})$

Addition of steel fibres: $length_x * length_y * h_{nom} * €_{fibres}$

Output: calculation report

A comprehensive report is automatically generated for the optimal design. This report comprises the case-specific parameters, as well as the set of optimal parameters and pool of parameters from which they were selected. It also presents calculation results such as distributions of bending moments, shear forces, and displacements, and provides illustrations of cross-sections of the building pit. An example of the automated report generated for the case study presented in the following chapter, can be found in Annex E.

6.2 Calculation process and visualization

This paragraph further explains the calculation process in the optimization tool and visually illustrates it using a flowchart. The building blocks of the parametric model, mentioned in chapter 3, are sequenced in a specific order to create a complete design process for a (SF)UCF. Visualization and verification of the building blocks can be found in Annex A.

The process starts by determining the governing loads through the load combinations specified in paragraph 2.1.1. The resulting force distributions are then calculated for both non-slipping and slipping beam models along the short span, taking into account variations of stiffness coefficients. This results in a total of four force distributions. The resulting governing bending moment is subjected to FM B1. If it fails to meet the requirements, FM B2 is performed. Depending on the pressure head and concrete class, FM B3 and FM BF may be used if FM B2 does not suffice. If no bending moment failure mechanism satisfies the requirements, a new iteration will start by selecting a different set of parameters.

If the set of parameters passes the bending moment resistance check, the FM C1 shear force check can be performed. If it is insufficient, the FM C2 check can be performed. If both the FM C1 and FM C2 checks do not meet the requirements, a new set of parameters will be selected and the iteration process will be repeated.

The requirement for performing the same analysis for the long span as for the short span is determined by evaluating conditions specified in paragraph 2.1.2. If the analysis of the long span is not necessary, check A will be performed. However, if the conditions are not met, the analysis of the long span must be performed through the previously described process that was performed for the short span.

The punching shear force check will be performed if it is found that the both the short and long span have sufficient bending moment and shear force resistance. The governing punching shear force of all previously calculated load distributions is used. Depending on the connection type, a new iteration process starts for c, a_r or p. If FM G indicates that there is sufficient punching shear force resistance, the price of the set of parameters is calculated. The price and parameters are saved in lists.

The final step in the optimization tool involves finding the optimal design. This is achieved by identifying the index corresponding to the lowest value in the list of prices obtained from all the iterations. The parameters with corresponding indexes are then considered as the optimal design.

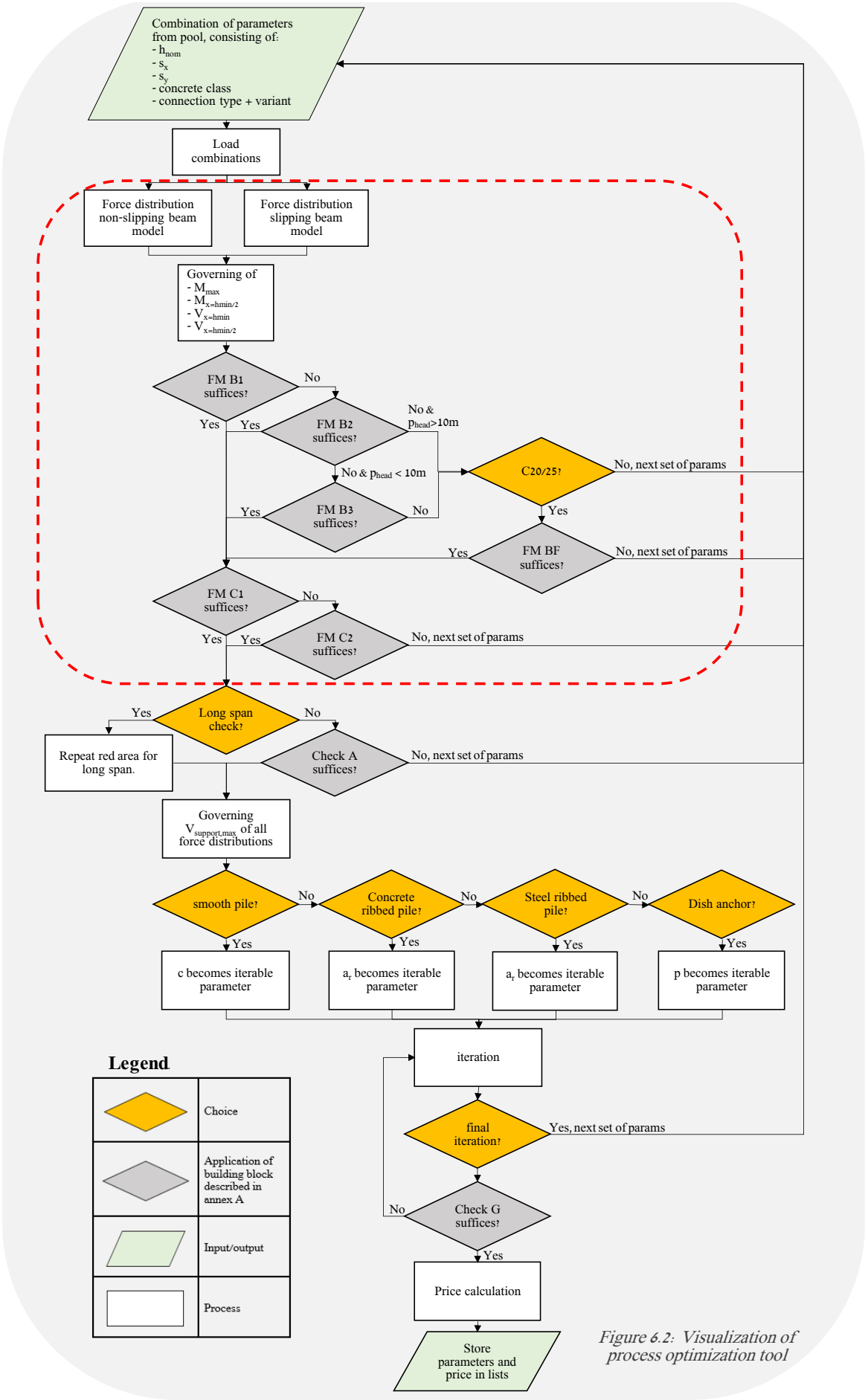

Figure 6.2: Visualization of process optimization tool

6.3 Reproducibility of optimization tool

This chapter and the annexes do not contain the precise Python code required to replicate the parametric model and optimization tool. However, it is still possible to reproduce these elements. Annex A provides a comprehensive visual representation of the building blocks of the parametric model through flowcharts, accompanied by the relevant formulas. Additionally, Annex B describes a parametric method for determining the force distribution in a UCF. By combining these resources, the parametric model can be reproduced.

The optimization tool is derived from the building blocks of the parametric model. By utilizing the flowchart presented in figure 6.2, one can replicate the design process of a (SF)UCF, as well as the iterative process used in the optimization model.

The input, consisting of an Excel database and a Word template, as well as the output in the form of an automated calculation report, cannot be directly reproduced based on the information provided in this thesis. However, it should be noted that these components simply serve as a means of presenting input and results, and are not integral to the optimization process itself. Furthermore, they are not strictly necessary, as the entire optimization process can be performed in PyCharm or another preferred development environment.

7. Case study Rotterdamsebaan

The optimization tool described in chapter 6 will be utilized to assess the design of a UCF in a completed deep excavation project on the Rotterdamsebaan. This project involved constructing the entrance of a drilled tunnel, requiring deep excavations with UCF's. The entrance to the tunnel was divided into a series of building pits. The case study focusses specifically on building pit V1, which is the final building pit before entering the drilled section of the tunnel. The aim of this comparison is to determine if the tool's results align with those of an engineer-optimized design and to study whether the original design could have been improved from an economical viewpoint. Additionally, the possibility of enhancing the design by adding steel fibre reinforcement will be evaluated. An analysis of the project's specific parameters and user-specified parameters will be conducted to effectively apply the tool.

7.1 Analysis of design Rotterdamsebaan

The objective of the analysis is to identify the project-specific parameters as well as the parameters that were optimized by the engineer to arrive at the final design. Furthermore, the analysis will examine the choices made regarding materials and connection types in the design process.

Geometry

The figures below were obtained from the calculation report concerning the UCF [28] and depict a cross-section and top view of the building pit. They include all essential parameters related to the geometry of the UCF.

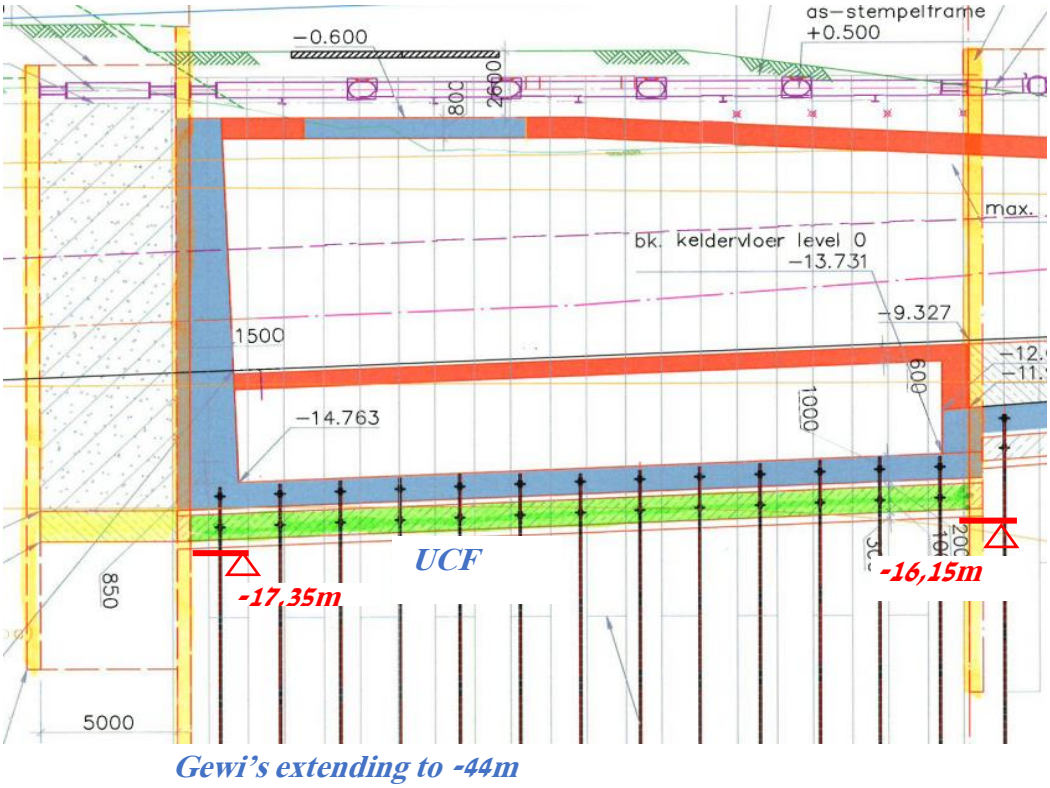

Figure 7.1: cross section of building pit [28]

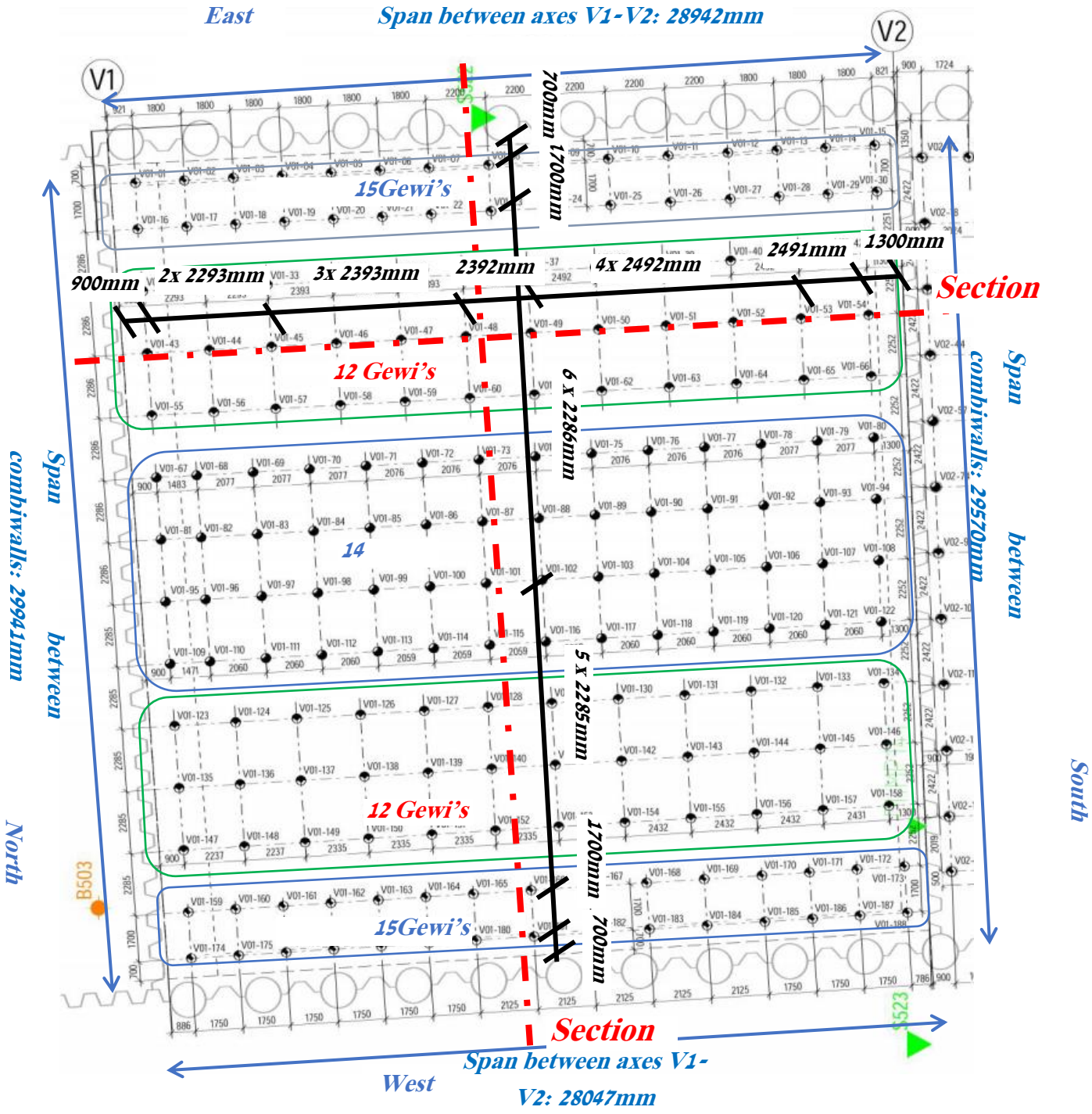

Figure 7.2: Top view of building pit [28]

Figure 7.1 illustrates the excavation levels in relation to Nationaal Amsterdams Peil (NAP). By combining the calculated required thickness h_{nom} of 1.0m and a 0.3m gravel layer, the necessary top levels of the UCF can be determined. At axis V1 the required top_{UCF} is -16.05m, whilst at axis V2 the required top_{UCF} is -14.85m. The average top_{UCF}, in reference to NAP, is -15.45m. In determining the governing load combination, the top level of the retaining wall is also important and was found to be +1.5m in relation to the NAP. The UCF is connected to Gewi piles with dish anchors, which extend to -44m.

The east and west sides of the building pit feature combi-walls, while sheet piled walls are used on the north and south sides to conduct a retaining function. The width of the construction floor cast on top of the UCF ranges from 28.05m to 28.94m between axis V1 and V2. However, taking into account additional space between the UCF and retaining wall, results in a complete span of 29.46m along section 2, as mentioned in the calculation report. Along section 1, following the same approach, a total length of 30.76m is found. From this point on, the span between the combi-walls will be referred to as the "long span" and the span between the sheet piles will be referred to as the "short span", based on their respective lengths.

The foundation design uses irregular centre to centre distance between the tensile elements as a way to positively affect the force distribution. The long- and short span were divided into respectively 15 and 13 fields of which the centre to centre distances are:

Long span (14 piles):	1x 1.11m,	1x 1.70m,	5x 2.85m,	6x 2.86m,	1x 1.70m,	1x 1.11m
Short span (12 piles):	1x 1.30m,	2x 2.29m,	4x 2.39m,	5x 2.49m,	1x 1.55m	

Design consideration: governing sections

Two cross-sections were used for the design of the UCF. The middle of the span typically experiences the highest deformation and dominant forces in the tensile elements. Therefore, section 1 was selected as the design section for the long span. For the short span, the governing cross-section was determined to be section 2, which intersects the green box with only 12 tensile elements along the span. The force distribution in the green box was found to be more critical than the force distribution in the blue box, due to the lower number of tensile elements.

Hydrostatic pressure head

Under normal conditions, the phreatic level at the location of the building site is -1.4m relative to NAP. However, during the construction phase, the level was lowered to -2.5m. Since the UCF serves a temporary function and the forces in the tensile elements will be relieved after the construction floor and tunnel elements are cast, the latter was used for the design. This results in a pressure head of 12.95m with reference to top_{UCF}.

Loads and combinations

The UCF was designed in accordance with the safety approach of [4], using corresponding load factors and load combinations. In compliance with [6], the structure was classified in consequence class CC2.

The distributed load was calculated from the following factors:

- A specific weight of 23 kN/m³ was applied for the self-weight of the UCF. Using this value and the calculated h_{nom}, it was determined that $q_{self} = 23$ kN/m².
- The upward distributed load caused by hydrostatic pressure was calculated as the difference between the $bottom_{UCF}$ and the phreatic level, multiplied by the specific weight of water. The resulting value was found to be $q_{water} = 139.5$ kN/m².
- The UCF is located in a Pleistocene soil layer that is not prone to heave. As a result $q_{heave} = 0$ kN/m²

The normal forces in the UCF were determined through retaining wall analysis and were found to be 1170 kN/m along the long span and 1100 kN/m along the short span.

Design considerations: pressure head and normal force
Since the UCF is slanted along the short span, the hydrostatic load is higher at axis V1 than at axis V2. The middle tensile elements in section 2 will experience the greatest load as the displacement of the UCF is largest in the middle of the span. To account for this, the average pressure head along the slanted UCF was used, as it corresponds to the location of the most heavily loaded tensile elements.

Because the excavation levels for section 2 vary, the normal force at the edge on V1 is greater than the normal force at the edge on V2. For safety reasons, the lowest value was used.

Connections
The spring stiffnesses of the sheet piled walls (k_{1x}), combi-walls (k_{1y}) and Gewi-piles (k_2) were obtained from the calculation report and are listed below. Because of the high pressure head, membrane action may not be taken into account, hence the membrane spring stiffness is not relevant for this case study. A friction coefficient of 0.3 is used to calculate the maximum friction force between the UCF and retaining wall.

k_{1x} = 60000 kN/m²
k_{1x} = 100000 kN/m²
k_2 = 50000 kN/m²
$\mu_{x,y}$ = 0.3

The Gewi-piles have a diameter of 63.5 mm and are connected to the UCF with dish anchors which have a diameter of 350 mm. The embedment depth of the dish anchor is 0.2 m.

Design considerations: Connection UCF-retaining wall and use of Gewi-piles
To be able to retract and reuse the retaining walls, no connection between the UCF and the retaining wall may be utilized. This requires additional evaluations to determine if there is sufficient friction between the UCF and the retaining wall. If there is insufficient friction, the force distribution must be recalculated using a slipping beam model, where all checks regarding bending moment and (punching) shear resistance must still suffice.

The use of Gewi-piles and dish anchors was predetermined as the preferred method for constructing this building pit, as they provide advantages in terms of construction speed and execution phases that could not be obtained with other pile types. The construction phases are listed below:

1. Piling sheet piles and combi-walls
2. Applying Gewi-piles from ground level
3. Applying strutting system between retaining walls
4. Dry excavation of top clay layers

5. Wet excavation to ultimate excavation depth
6. Applying gravel layer (300mm)
7. Casting UCF
8. Emptying building pit

Materials

The applied concrete strength class is C20/25. Material properties of this strength class are listed in table 2.3. The yield strength of the Gewi-piles is equal to 505 MPa.

Tolerances

The tolerances are dependent on the execution methods and soil-type underneath the UCF, this is explained in paragraph 2.1.1. For the UCF in this case study, the following tolerances were taken into account:

tol_{top} = 0.075 m
tol_{bottom} = 0.150 m
$tol_{anchorage}$ = 0.100 m

Results

The unity checks of the different failure mechanisms are summarized in the table below. The governing failure mechanism is punching shear.

Table 7.1: Results UCF building pit V1 [28]

	FM B1	FM B2	FM B3	FM C1	FM C2a	FM C2b	FM C2c	FM G
Section 1 (long span)	5.72	0.24	-	0.66	-	-	-	0.98
Section 2 (short span)	5.33	0.30	-	0.66	-	-	-	0.96

7.2 Input for optimization tool

Case-specific parameters were identified through analysis in the previous paragraph. Arrays of variable parameters with representative boundary values are chosen such that the case study relies on realistic values. Material prices were determined with advice from multiple employed cost-estimators and material suppliers of BAM Infra.

Case specific parameters

A summary of the analysis, resulting in the case-specific parameters needed as input for the optimization tool, is given in the table 7.2.

Table 7.2: Case-specific parameters

Parameter	Value	
$Length_x$	29.46	[m]
$Length_y$	30.76	[m]
Top_{pit}	+1.5	[m]
Top_{UCF}	-15.45	[m]
p_{head}	12.95	[m]
N_x	1100	[kN/m]
N_y	1170	[kN/m]
μ_x	0.3	[-]
μ_y	0.3	[-]
f_y	505	[N/mm²]
k_{1x}	60000	[kN/m²]
k_{1y}	100000	[kN/m²]
k_3	n.a.	[-]
Conseq.class	CC2	[-]
tol_{top}	0.075	[m]
tol_{bottom}	0.15	[m]
$tol_{anchorage}$	0.10	[m]
$Pile_{depth,est}$	27.5	[m]

Variable parameters

Table 7.3 lists arrays of variable parameters that are iterated through. For every combination of these parameters, the force distribution is calculated and failure mechanisms are checked. If all checks are satisfactory, a cost estimate is calculated for that specific combination of parameters.

Table 7.3: Variable parameters – iterable values

Variable parameter	Value	Unit
h_{nom}	[0.8, 0.825, 0.85, 0.875, 0.9, 0.925, 0.95, 0.975, 1.0, 1.025, 1.05, 1.075, 1.1, 1.125, 1.15, 1.175, 1.2, 1.225, 1.25, 1.275, 1.3, 1.325, 1.35, 1.375, 1.4, 1.425, 1.45, 1.475, 1.5]	[m]
s_x	[4, 5, 6, 7, 8, 9, 10, 11, 12, 13, 14]	[-]
s_y	[5, 6, 7, 8, 9, 10, 11, 12, 13, 14, 15]	[-]
Concrete class	[“C20/25”, “C25/30”, “C30/37”]	[-]
Fibres	[“yes”, “no”]	[-]
c	[0.1, 0.2, 0.4, 0.5]	[-]
a_r	[0.085, 0.09, 0.095, 0.1, 0.105, 0.12]	[m]
p	[tol_{top} + $tol_{anchorage}$, h_{min}/2, stepsize=0.05]	[m]
Connection type	[“Dish anchor”]	[-]

The optimization tool allows for multiple variants of a specific connection type to be inputted via an accessory Excel file. As the tool iterates through different connection types, it also iterates through the variations of each type, which may differ in geometric properties or spring stiffness. In this case study, only dish anchors connected to Gewi-piles were used for reasons explained in paragraph 7.1. The spring stiffness of a Gewi-pile with a diameter of 63.5mm was obtained from the calculation report of the applied design. Two variations of this type were applied, differentiated by the diameter of the dish anchor.

Table 7.4: Connection type variants

	Smooth pile			Ribbed concrete pile			Ribbed steel pile			Dish anchor			Unit
variant	**1**	**2**	**..**	**1**	**2**	**..**	**1**	**2**	**..**	**1**	**2**	**..**	
k_2	-	-	-	-	-	-	-	-	-	50000	50000	-	[kN/m]
D	-	-	-				-	-	-	0.0635	0.0635	-	[m]
B				-	-	-							[m]
d										0.25	0.35	-	[m]

Remaining columns in figure 7.4 are added for context but are purposefully left empty as these connection types are not examined in this case study. The arrays for c and a_r in table 7.3 contain standard values, however they may be neglected due to aforementioned reasons.

s_x and s_y indicate the amount of fields the span of the UCF is divided over (with equal lengths). Given the values in the array, this means that for the short span a c.t.c. distance of 2.10m to 7.37m is considered. For the long span, a c.t.c. distance of 2.05m to 6.15m is considered. These boundaries are determined by a minimum and maximum field size set in the optimization tool, equal to respectively 2m and 7.5m.

Material prices

Material price of the complete construction forms the basis of comparison and exist of the following items, the prices were determined with advice from employees and material suppliers.

Table 7.5: Material prices

Item	Price	Unit
Underwaterconcrete C20/25	122.50	[€/m³]
Underwaterconcrete C25/30	126.55	[€/m³]
Underwaterconcrete C30/37	130.00	[€/m³]
Steel fibre reinforcement (30kg/m³)	120.00	[€/m³]
Grout	3.15	[€/m]
Gewi Ø65,5mm	56.80	[€/m]
Dish anchor	3.00	[€/kg]
Connection bolt	32.50	[€/piece]

For the price-determination of grout, a weight of 70kg/m was considered. In combination with a volumetric weight of 24 kN/m³ and a price of 105 €/m³, this results in the price listed in table 7.5.

The price for the dish anchor is based on weight. For a dish anchors with a diameters of 0,25m and 0.35m, this results in a price of respectively €42.00 and €75.00. A bolt is needed to secure the dish anchor in place and has a price of €32.50.

7.3 Results

A calculation report containing results concerning the optimal design was automatically generated after inputting the required parameters. The calculation report can be found in Annex E, however the most important information is provided in this paragraph.

Table 7.6: Results

Parameter	Optimal value according to optimization tool	Optimal value according to engineer-optimized design	Unit
h_{nom}	1.025	1.0	[m]
s_x	13 → c.t.c. = 2.27 m	13 → c.t.c. = variable	[-]
s_y	9 → c.t.c. = 3.41 m	15 → c.t.c. = variable	[-]
Concrete class	C30/37	C20/25	[-]
Fibres	No	No	[-]
p	0.175	0.2	[m]
Connection type	Dish anchor	Dish anchor	[-]
k_2	50000	50000	[kN/m]
D	0.0635	0.0635	[m]
d	0.35	0.35	[m]
Total cost	€294,584.-	€416,128.-	

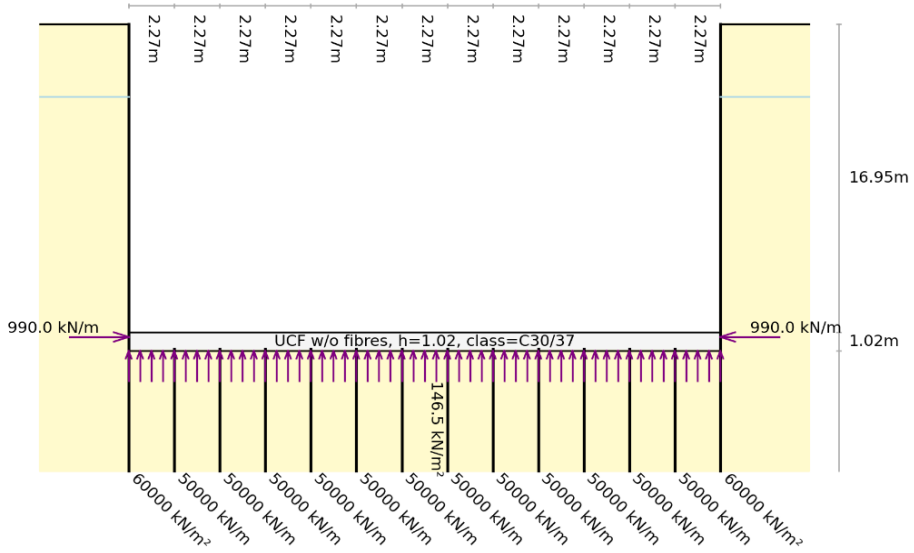

Figure 7.3: Cross-section along short span

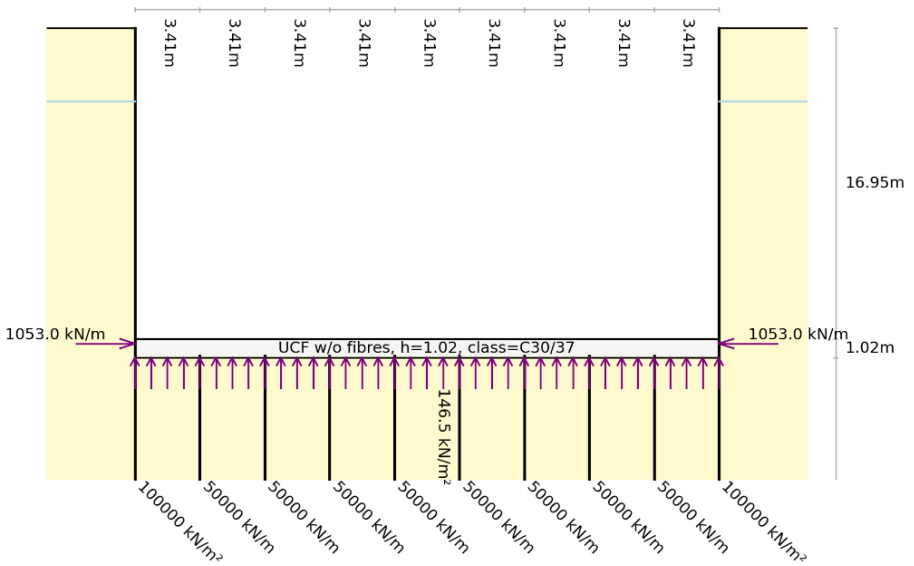

Figure 7.4: Cross-section along long span

Table 7.7: Unity checks

		FM B1	FM B2	FM B3	FM C1	FM C2a	FM C2b	FM C2c	FM G
Applied design	**Short span**	5.33 (no slip)	0.30	-	0.66 (no slip)	-	-	-	0.96 (slip)
	Long span	5.72 (no slip)	0.24	-	0.66 (no slip)	-	-	-	0.98 (slip)
Optimal design	**Short span**	5.40 (no slip)	0.19	-	0.76 (no slip)	-	-	-	0.98 (no slip)
	Long span	6.02 (no slip)	0.42	-	0.85 (no slip)	-	-	-	0.99 (no slip)

Moment distribution optimized design and applied design - short span

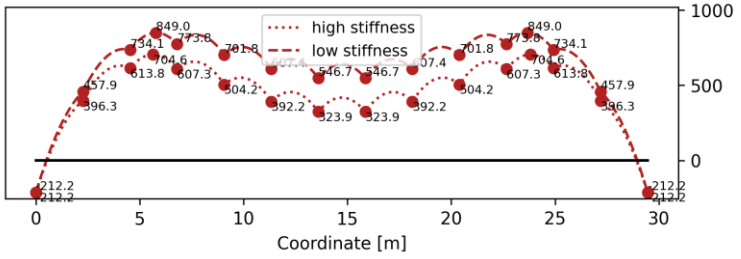

Figure 7.5: M-line, optimal design, non-slipping model

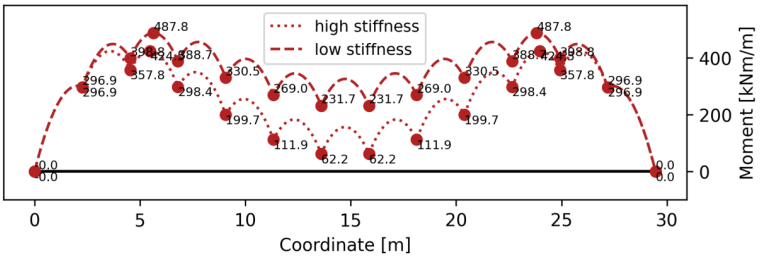

Figure 7.6: M-line, optimal design, slipping model

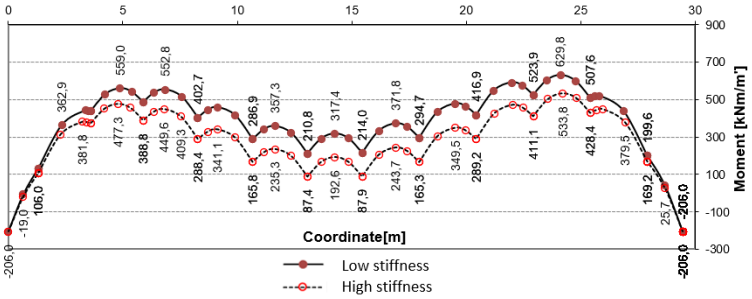

Figure 7.7: M-line, applied design, non-slipping model

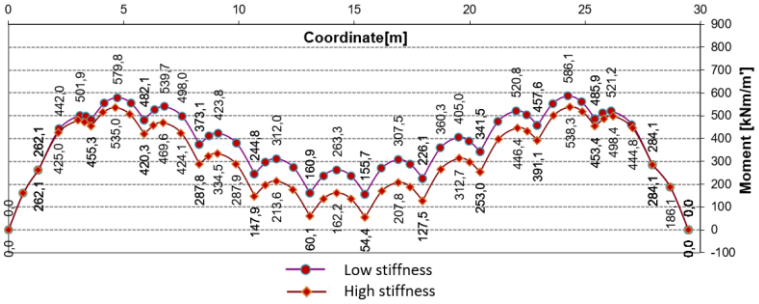

Figure 7.8: M-line, applied design, slipping model

Moment distribution optimized design and applied design - long span

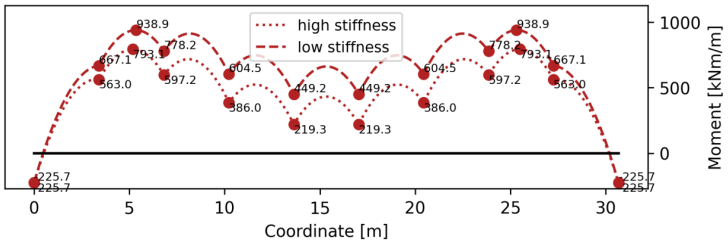

Figure 7.9: M-line, optimal design, non-slipping model

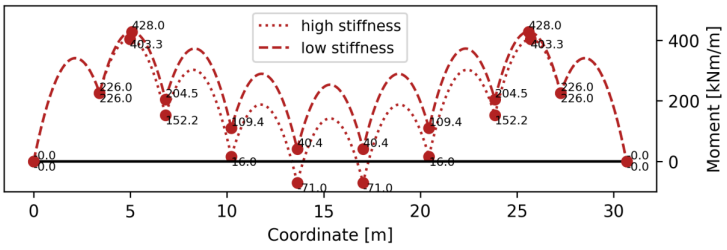

Figure 7.10: M-line, optimal design, slipping model

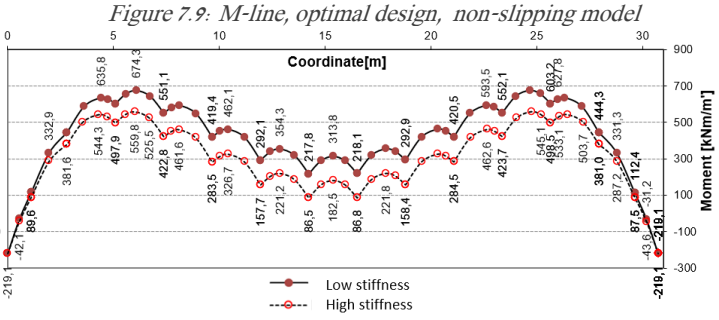

Figure 7.11: M-line, applied design, non-slipping model

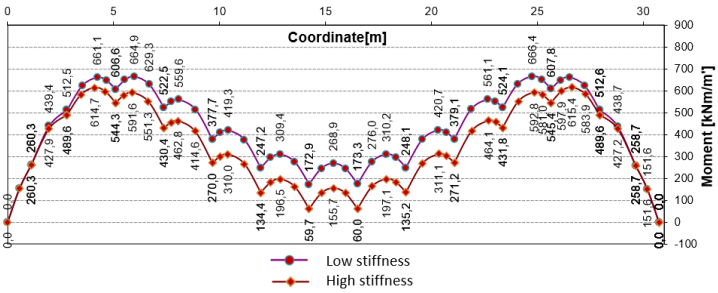

Figure 7.12: M-line, applied design, slipping model

Shear force distribution optimized design – short span

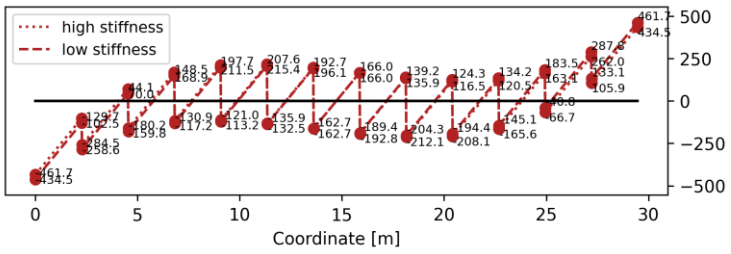

Figure 7.13: V-line, optimal design, non-slipping model

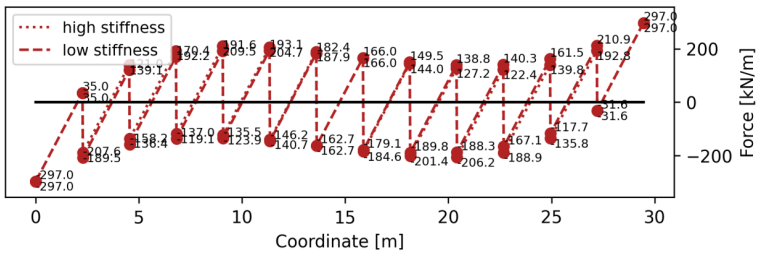

Figure 7.14: V-line, optimal design, slipping model

Shear force distribution – long span

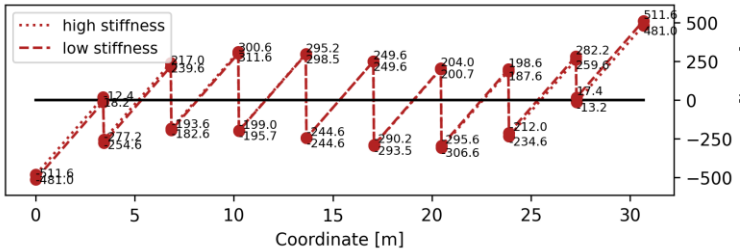

Figure 7.15: M-line, optimal design, non-slipping model

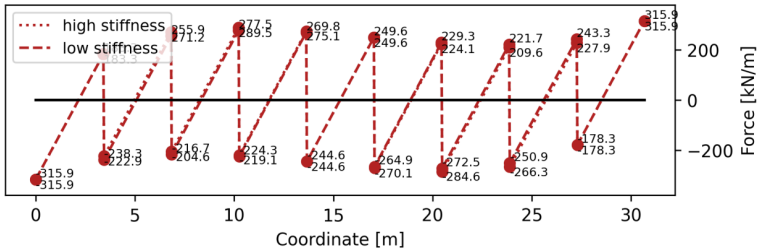

Figure 7.16: M-line, optimal design, slipping model

SLS Displacement optimized design and applied design – short span

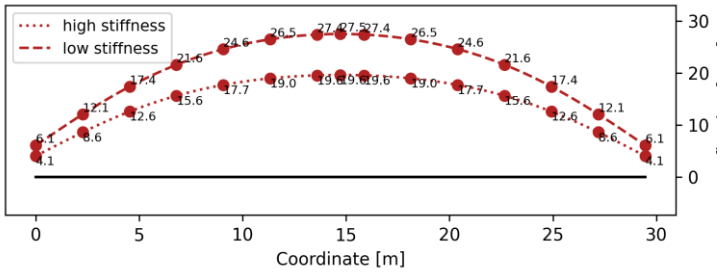

Figure 7.17: Displacements, optimal design, non-slipping model

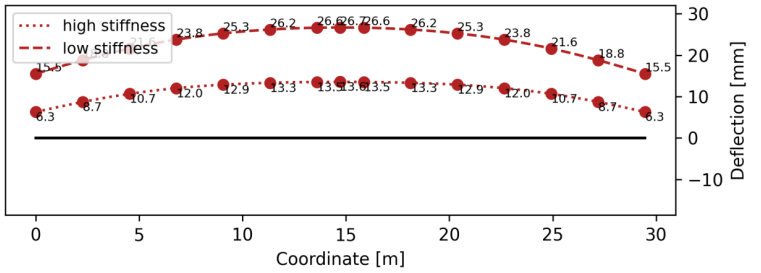

Figure 7.18: Displacements, optimal design, slipping model

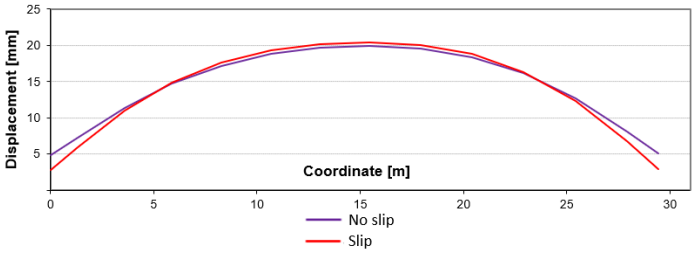

Figure 7.19: governing displacements, applied design

SLS Displacements optimized design and applied design – long span

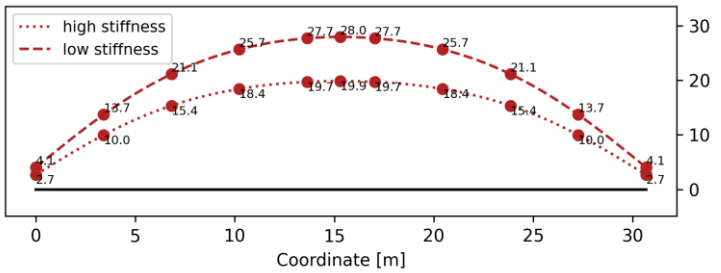

Figure 7.20: Displacements, optimal design, non-slipping model

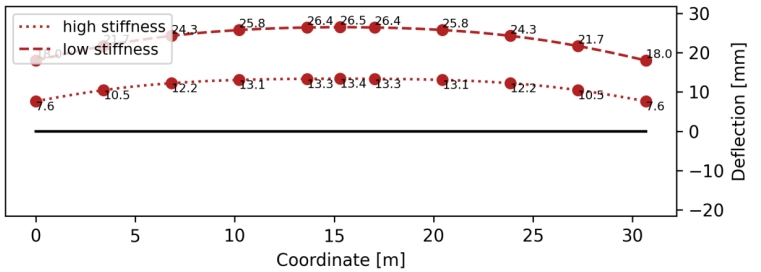

Figure 7.21: Displacements, optimal design, slipping model

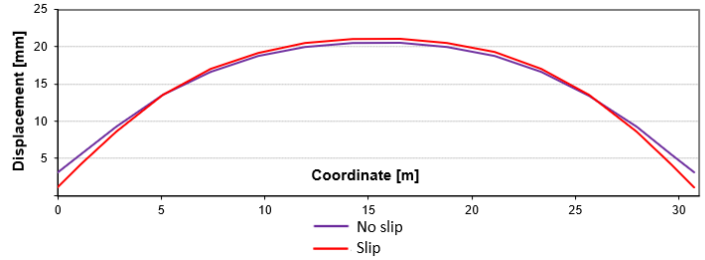

Figure 7.22: governing displacements, applied design

7.4 Suboptimal design alternatives

The optimal design presented in the previous paragraph may be very close to other near optimal designs in terms of price. This paragraph displays five suboptimal alternatives, of which some are very close to the optimal design, and of which some have a specific characteristic which may be of importance for the designer.

1. *Optimization on UCF thickness:*
   For this design the minimum attainable UCF thickness is found whilst keeping the arrays of variable parameters identical to the ones listed in table 7.3.

2. *Least amount of tensile elements:*
   The aim of this design is to find a configuration of parameters that uses as few tensile elements as possible, whilst retaining a UCF thickness smaller than 1.5m.

3. *One extra row of piles:*
   An extra row of tensile elements was added along the long span to study how this influences the required UCF thickness and how this affects the total cost of the construction.

4. *UCF thickness as applied in project:*
   The UCF thickness has a fixed value of 1.0m, identical to the final design applied at Rotterdamsebaan. An optimum set of other parameters is found.

5. *Concrete class as applied in project:*
   In this case, the concrete class is fixed to C20/25 whilst an optimal set of other parameters is found.

Table 7.8 presents the results of suboptimal design, but does not include the connection type, diameter of the Gewi-pile, and spring stiffness of the tensile element, as these values remain constant given the supplied parameters in table 7.4 and do not affect the results.

Table 7.8: Suboptimal configurations of parameters

	h_{nom} [m]	s_x [-] & c.t.c.$_x$ [m]	s_y [-] & c.t.c.$_y$ [m]	Concrete -class	p [m]	d [m]	fibres	Total Cost [€]
1.	0.825	14 → c.t.c.= 2.10	14 → c.t.c. =2.19	C30/37	0.175	0.25	No	€396,002.-
2	1.2	10 →c.t.c. = 2.95	11 → c.t.c. = 2.80	C30/37	0.325	0.35	No	€305,148.-
3	0.975	10 → c.t.c. = 2.95	13 → c.t.c. = 2.37	C30/37	0.175	0.35	No	€310,178.-
4	1.0	14 → c.t.c. = 2.10	9 → c.t.c. = 3.42	C30/37	0.175	0.35	No	€306,016.-
5	1.275	12 → c.t.c. = 2.46	9 → c.t.c. = 3.42	C20/25	0.275	0.35	No	€302,043.-

7.5 Discussion

As can be observed in table 7.6, the total cost for materials in the optimized design is €294,584, representing a reduction of nearly 30% in comparison to the applied UCF design at the Rotterdamsebaan. The primary factor accounting for this substantial cost difference is the significant reduction in the number of tensile elements utilized. Specifically, the applied design uses a grid of Gewi-piles with variable centre to centre distances, resulting in a total of 168 tensile elements. Conversely, the optimized design uses a fixed centre to centre distance along both spans, resulting in a total of 96 required tensile elements. Other differences between the applied and optimized design include variations in floor thickness, with the optimized design having a 25mm increase of thickness compared to the applied design. Furthermore, there is a difference in concrete strength class, with the applied design utilizing C20/25 and the optimized design utilizing C30/37. Additionally, the optimized design uses the minimum required embedment depth for the dish anchor, while the applied design uses a depth that is 25mm larger. The optimization tool also evaluated the addition of steel fibre reinforcement, it was determined that its inclusion would not have a positive impact on the cost of the optimal design. In short, the optimized design trades a thicker floor and higher concrete class for a lower amount of tensile elements.

The primary reason for the greater number of tensile elements required in the applied design is the reduction in size of the edge fields. This design choice is often implemented to positively affect the moment distribution. A comparison of the moment distributions illustrated in figures 7.5-7.12 reveals that the applied design yields a more favourable governing moment distribution, in this case for the non-slipping beam model. However, it is questionable whether this effect is relevant for this particular design. Both the applied and optimized designs utilize a compression arch as the governing failure mechanism for bending moment resistance, which means that cracking will occur in both designs. Therefore, optimizing the moment distribution with the aim of sufficing failure mechanism A for bending moment resistance may not be necessary. Figure 2.7 in chapter 4 shows that for normal forces of the magnitude in this case, the compression arch resistance becomes very substantial, which is also shown in the unity check numbers for check B2.

For both the applied and optimized design, punching shear resistance is the governing failure mechanism with unity checks of respectively 0.98 and 0.99. Given the lower amount of tensile elements to carry roughly the same load, it is expected that the forces in the tensile elements in the optimized design are higher than in the applied design. When looking at the displacement diagrams in figures 7.17 – 7.22, this is confirmed. The force in a tensile element can be calculated as the product of axial stiffness and displacement, meaning that the optimized design has higher forces in the tensile elements due to more significant displacement. Three factors in the optimized design ensure that the required extra punching shear resistance for the tensile elements is obtained. Firstly, the effective height of the punching cone is increased by the slightly larger h_{nom} and smaller embedment depth of the dish anchor. Secondly, the increase of concrete strength class gives extra punching shear resistance. These effects were also stated in paragraph 4.4 and are illustrated in figures 4.19-4.21. Thirdly, the distributed load in the optimized design is slightly decreased compared to the applied design. This can be explained by the higher specific weight of concrete compared to water. Worth mentioning is that the tensile elements and concrete were also checked on yielding, however these failure mechanisms were not governing.

The use of Gewi-piles with larger diameters could result in greater spring stiffnesses for the tensile elements, reducing displacement and punching force along the span, potentially allowing for further optimization of the design in this case study. However, there is currently no available data on the spring stiffnesses of larger Gewi-piles in the specific soil layers to investigate these effects.

The optimal design does not include steel fibre reinforcement. Although the figures in paragraph 5.3 do not perfectly match the parameters of the optimal design, they suggest that using steel fibre reinforced concrete would not result in material savings for the load case present in this case study, due to the high resistance of the compression arch caused by the large normal force. While there are methods available to account for the positive effects of steel fibre reinforcement on punching shear resistance, as stated in paragraph 2.2.5, there is no appropriate data for the reference concrete mix design used in this optimization tool to apply these methods. Further research on the properties of the concrete mix in relation to punching shear resistance can potentially lead to an optimal design with a thinner UCF or greater centre to centre distances.

Suboptimal design alternatives reveal that there are several options that have a total cost similar to the optimal design. These results suggest that optimizing for UCF thickness would not be the best approach in this case, as the large number of tensile elements required would increase the cost significantly. Optimizing for the minimum number of tensile elements is close to the optimal design, but would require deeper excavation levels due to the thicker UCF. For certain projects, it is possible that a standard concrete mix design should be used for all underwater concrete in the project. Applying this principle to this case study and optimizing with a fixed concrete class of C20/25 would result in a thicker UCF with fewer tensile elements than the applied design, and a significant cost reduction. Similarly, fixing the nominal floor thickness would lead to a design with a higher concrete class and fewer tensile elements, resulting in significant cost savings.

Additional remarks

- An aspect not considered in this optimization is the impact of changing the thickness of the UCF on the acting normal forces. Increasing the thickness requires a deeper excavation, resulting in increased normal forces in the UCF. Besides, incorporating excavation depth into cost calculations for a set of parameters would be beneficial in finding the optimal design.
- In this optimization, only material price of the UCF was considered. Including labour costs in the cost-estimation of a set of design parameters may affect the outcome. Moreover, incorporating other methods of comparison, such as MKI, construction speed or complexity, could provide a more comprehensive analysis of the optimal design.
- The calculation of force distribution along the UCF is limited to using fields of equal lengths. Further optimization may be achieved by incorporating the option of variable centre to centre distances. In this specific case, it might have been beneficial to position the tensile piles closer to each other around the centre of the building pit, in order to limit the displacement and punching shear force (which governs the design).

- The optimization tool does not consider the impact of varying centre to centre distances on the spring stiffness and required depth of tensile elements. It is suggested to expand the tool to incorporate this factor for further optimization.

8. Conclusion

The research question of this thesis was divided into a series of sub-questions as outlined in paragraph 1.1. These sub-questions were addressed in four distinct parts of the thesis:

- Part 1: Literature study & parametric model
- Part 2: Parameter influence on design efficiency
- Part 3: Fibre-reinforced UCF
- Part 4: Optimization tool

Part 1 formed the basis for addressing the research question by gathering information from literature and creating a parametric model of a (SF)UCF. This parametric model facilitated data generation regarding the effects of parameters on (SF)UCF design and the benefits of steel fibre reinforcement. The results described in parts 2 & 3 provide engineers with knowledge that can assist in design efficiency when using a traditional design approach for a (SF)UCF.

The parametric model also served as a foundation for the development of the optimization tool. This tool enables a new design approach for a (SF)UCF, where an optimal set of variable parameters is determined based on price, given case-specific parameters provided by the engineer for a particular project. The optimization tool allows for a faster workflow and enhanced design efficiency. However, it is always up to the engineer whether a traditional design approach or the optimization tool is used.

In this chapter, the conclusions drawn from the results in the different parts of the thesis will be elaborated. Additionally, research contributions to this specific field of civil engineering will be discussed.

Improving design efficiency by altering design parameters

Chapter 4 described relations between parameters and resistance of a conventional UCF in continuous graphs. This allows conclusions to be drawn on what parameters to alter such that additional resistance can be obtained.

To avoid cracking in a UCF, increasing the concrete class or nominal thickness can enhance bending moment resistance. When the normal force is 0, increasing the nominal thickness by a factor of 1.14 has a similar effect as upgrading the concrete class from C20/25 to C30/37. However, when the normal force is 1000 kN/m, this factor decreases to 1.08, indicating that as the normal force increases, the relative advantage of increasing floor thickness over the concrete class becomes more pronounced.

To increase bending moment resistance of the compression arch, the effective height of the arch must be increased. The most efficient way to do so, besides increasing h_{nom}, is by using ribbed piles, followed by dish anchors and smooth piles. For high normal forces, increasing the concrete class becomes relatively more beneficial. If membrane action can be taken into account, a small height-to-length ratio of a single span increases the amount of normal force that can be generated. It was found that for a close c.t.c. distance of 2m and a h_{nom} of 1m, taking full membrane action into account, upgrading the concrete class from C20/25 to C30/37 can generate an extra 20% of normal force.

However, with a larger c.t.c. distance of 6m, upgrading the concrete class only leads to an 8% increase in resistance.

To enhance resistance to bending shear fracture in failure mechanism C1, the concrete strength class or h_{nom} can be increased. Multiplying h_{nom} by a factor of 1.27 offers a resistance gain equivalent to upgrading the concrete class from C20/25 to C30/37. This factor remains constant regardless of the normal force in the UCF, implying that for slender UCF's, increasing h_{nom} over the concrete class offers relatively more gained resistance.

Among the connection types studied in this thesis, ribbed piles offer the most resistance to punching shear force. The resistance is mainly influenced by the effective height of the punching cone and the concrete class. Upgrading the strength class from C20/25 to C30/37 offers the same improvement in resistance as increasing the effective punching cone height by a factor of 1.14. The pile diameter has a moderate effect on resistance and changing it results in limited gains. For an effective punching cone height of 0.4m, changing the diameter from 0.2m to 0.4m results in the same resistance gain as increasing the punching cone height by a factor of 1.05. However, this factor decreases to 1.03 when the effective punching cone height is 1.1m, implying that increasing the pile diameter becomes relatively less effective for larger nominal thicknesses.

For dish anchors, only minor changes in punching shear resistance can be obtained by modifying the diameter of the dish anchor or the concrete class in cases where the punching cone failure mechanism governs. The most effective alteration in this situation is to increase the height of the punching cone. If the compressive stress under the dish anchor governs, the most effective way to improve resistance is to increase the diameter of the dish anchor, followed by the concrete strength class.

Addition of steel fibre reinforcement

The study aimed to compare the required nominal thickness for a conventional UCF and a SFUCF using the reference concrete mix design employed at Botlekspoortunnel, under the assumption that the curvature limit was not exceeded. A standard set of representative parameters was utilized, with one parameter being altered at a time to determine the conditions under which the addition of steel fibre reinforcement could result in material savings.

The results indicated that for a typical c.t.c. distance range of 2 to 3.2 meters, only minimal material savings were achievable. However, for c.t.c. distances between 3.2 and 4.4 meters, significant savings could be realized, but only under load conditions with a substantial distributed load and normal force. When larger c.t.c. distances were considered, significant material savings of up to 0.3m were possible when the normal force was substantial, which equates to a reduction of material usage by 30%.

Other circumstances where it was found that the application of fibre reinforcement can result in reduction of required floor thickness, are situations where the effective height of the compression arch is small. This scenario occurs when the embedment depth of a dish anchor is large or when smooth piles are used as tensile elements. Under certain load conditions, reductions of 0.25m were achievable, representing a 30% reduction in material usage.

Perhaps the most significant use case for a SFUCF is when the normal force is close to zero, and additional normal force cannot be obtained through membrane action. Examples of such scenarios include rounded retaining walls or strutting windows applied closely above the UCF in combination with a large pressure head, or building pits in series. In such cases, if the UCF cracks, there is little resistance to be obtained from the compression arch, and the use of a UCF becomes infeasible unless a very significant nominal thickness is employed. In these situations, the application of a SFUCF can make an otherwise near impossible project feasible.

Optimization tool

This study involved the development of an optimization tool for the design of a (SF)UCF as a derivative of the parametric model. The tool was applied to a UCF project on the Rotterdamsebaan and through the exploration of a wide range of combination of parameters, it was determined that a more cost-effective design could have been achieved, with potential savings of up to 30% in costs. The original design faced limitations due to punching shear force resistance, but the optimized design addressed this by increasing the effective height of the punching cone and upgrading the concrete strength class. By slightly increasing the floor thickness, a more favourable distributed load was obtained. These changes resulted in sufficient punching shear resistance for the tensile elements while reducing the quantity of such elements and the overall costs.

Research contributions

This thesis has made significant contributions to the field of civil engineering by providing detailed insights into the impact of various parameters on the design of (SF)UCF's, thereby enabling more informed decision-making when utilizing a traditional design approach hence improving design efficiency. Moreover, the thesis has advanced decision-making with respect to the incorporation of steel fibre reinforcement in UCF's. While the added value of steel fibres was already known in several scenarios, as discussed in paragraph 2.2.3, the parametric approach used in this thesis facilitates exploration of the application of fibre reinforcement across a wide range of load cases and sets of parameters. This allows more exact insight in scenarios where steel fibres provide additional value as well as the quantification of their added value. Furthermore, the plotted results provide a fast and reliable means of determining the viability of using steel fibre reinforcement in a given scenario.

This thesis is also innovative in that it introduces a new design approach for (SF)UCF's. The optimization tool, which was derived from the parametric model, effectively bridges the two disciplines of computer science and civil engineering, enabling the identification of optimal designs for structural elements using computer-based methods. By adopting this parametric approach to structural design through an optimization tool, engineers can work efficiently, saving time and effort, and avoid repetitive tasks. This enables them to focus on higher-level design and analysis.

The limitations of this thesis provide an opportunity for further exploration of the topic, which will be discussed in greater detail in the recommendations presented in the next chapter.

9. Recommendations

The recommendations listed in this chapter follow from limitations of this thesis and provide a chance to conduct further research on the topic.

- The parametric model developed to address the research question has several limitations. Refining the model could lead to more comprehensive results. To improve the model, it is suggested to:
  - Enhance the model to compute force distributions with tensile elements that are irregularly spaced and/or of different types.
  - Consider the bearing resistance of the tensile elements, such that in the optimization tool the chance of generating an optimal result for which the bearing capacity is not sufficient will be prevented. In combination with the previous point, this will also make the optimization tool more applicable for the use phase, where piles may experience compression forces.
  - Take into consideration the effect of changing the centre to centre distance of tensile element on their vertical stiffness and bearing capacity, which in turn influences the force distribution.
  - Take into account the loss of punching shear resistance when punching cones of neighbouring piles overlap, such that it no longer has to be checked manually in cases where the cones overlap.

- In this thesis, the optimization tool only considered the material cost of the UCF. It is suggested to add the option to find the optimal design based on various comparison criteria, such as MKI, construction speed, or execution complexity. This would result in a more thorough analysis of the optimal design.

- It is recommended to conduct further research on the post-cracking material properties for higher concrete strength classes that were obtained using laboratory tests that align with the calculation method used in this thesis. Including the option to generate data on the impact of fibre reinforcement in higher concrete strength classes would provide additional insights.

- In this thesis, Dramix 3D fibres with properties listed in paragraph 2.2.3 were considered. However, recent innovations have provided new types of steel fibres with better properties due to improved shapes and materials. It is recommended to research how the application of these types of fibres would influence the results of this thesis.

- Due to execution tolerances and the brittle behaviour of a conventional UCF, a lower bound of 800 mm is used as minimum nominal floor thickness. Results presented in chapter 5 found that in many cases, a SFUCF with a thickness of 800mm would have plenty of bending moment resistance. Given the ductile behaviour of a SFUCF, additional research is recommended to investigate whether this could allow a safe implementation of a floor thickness smaller than 800mm.

- Further research is recommended to examine the post-cracking material properties for the reference concrete mix by conducting three-point bending tests such that the calculation method described in [23] can be applied to calculate the shear force and punching shear force resistance of a SFUCF. Considering this resistance may provide additional insight into the benefits of steel fibre reinforcements and may offer extra opportunities for the use of a SFUCF.

10. Bibliography

[1] Gia, T. L., Duy, L. T., Kieu, T. D. T., & Thu, H. N. (2019). The impact of groundwater lowering on pile bearing capacity in Hanoi – Vietnam. In Lecture Notes in Civil Engineering (pp. 137–144). Springer Singapore. https://doi.org/10.1007/978-981-15-2184-3_17

[2] Al-Tamimi, A. K. (2019). Design and evaluation of underwater concrete. In Developments in the Formulation and Reinforcement of Concrete (pp. 325–343). Elsevier. https://doi.org/10.1016/b978-0-08-102616-8.00014-9

[3] Hermawan, Marzuki, P. F., Abduh, M., & Driejana, R. (2015). Identification of Source Factors of Carbon Dioxide (CO2) Emissions in Concreting of Reinforced Concrete. In Procedia Engineering (Vol. 125, pp. 692–698). Elsevier BV. https://doi.org/10.1016/j.proeng.2015.11.107

[4] CUR-Aanbeveling 77: 2014 Rekenregels voor ongewapende onderwaterbetonvloeren. SBRCURnet, Gouda.

[5] Polhaar, A. G. (1998, September). Eindstudie staalvezelgewapend onderwaterbeton [MSc thesis]. TU Delft.

[6] NEN-EN 1990, Eurocode - Basis of structural and geotechnical design.

[7] Arkesteijn, R., Hagenaars, P., De Winter, E., & Van Der Veen, C. (2015). Herziening CUR Aanbeveling 77 (3): Enkele aspecten aanbeveling over onderwaterbetonvloeren nader beschouwd. Cement: vakblad voor de betonwereld, 67(8), 50–57.

[8] NEN-EN 1992-1-1, Eurocode 2: Design of concrete structures – Part 1-1: General rules and rules for buildings.

[9] Welleman, H. C. J. W., & Welleman, H. (z.d.). Toegepaste Mechanica 3. Academic Service.

[10] Welleman, H. (2016, november). Het gebruik van Maple bij ConstructieMechanica. https://icozct.tudelft.nl/TUD_CT/extrainfo/files/werkenmetmaple.pdf

[11] Ir. A.G.Kooiman. (1996, December). Staalvezelbeton in de linings van boortunnels, een state-of-the-art. TU Delft.

[12] BTC boortunnelcombinatie. (n.d.). Botlekspoortunnel Ontvangstschacht Evaluatie staalvezel onderwaterbeton.

[13] Arkesteijn, R., & Menting, M. (2013). Staalvezelversterkt onderwaterbeton. Cement, 3, 44–51.

[14] Fiber Reinforced Concrete – Types, Properties and Advantages of Fiber Reinforced Concrete. (2021, May 23). The Constructor. Retrieved October 1, 2022, from https://theconstructor.org/concrete/fiberreinforced-concrete/150/.

[15] Asbestos in Cement Concrete – Properties, Uses and Benefits. (2019, March 18). The Constructor. Retrieved October 1, 2022, from https://theconstructor.org/concrete/asbestos-concreteproperties/31215/

[16] Ahamad, S., Patel, V. K., & Khan, N. K. (2017, July). Experimental Analysis of Asbestos Fibre Reinforced Concrete Composite. IOSR Journal of Mechanical and Civil Engineering, 14(04), 18–22. https://doi.org/10.9790/1684-1404021822

[17] Saidani, M, Saraireh, D & Gerges, M 2016, 'Behaviour of different types of fibre reinforced concrete without admixture' Engineering Structures, vol 113, pp. 328-334. DOI: 10.1016/j.engstruct.2016.01.041

[18] Selin Ravikumar, C. S. R., & Thandavamoorthy, T. S. (2013, September). Glass Fibre Concrete: Investigation on Strength and Fire Resistant Properties. IOSR Journal of Mechanical and Civil Engineering, 9(3).

[19] Gupta, L., & Singh, H. (2018, February). Steel and Glass Fibre Reinforced Concrete: A Review. IRJET, 05(02).

[20] Bekaert. (z.d.). Dramix 3D fibres. https://www.bekaert.com/en/product-catalog/content/dop/dramix3d

[21] Henke, V. (1998, October). Application of steel fibre concrete for underwater concrete slabs. Cement and Concrete Composites, 20(5), 377–385. https://doi.org/10.1016/s0958-9465(98)00005-5

[22] Boersma, AE., Heijmans, R. W. M. G., & Jansen, J. A. G. (2001). Ruim baan met staalvezelversterkt onderwaterbeton. Cement, 2001/4, 55–59.

[23] Arkesteijn, R. (2014). Rekenen aan onderwaterbeton met vezels. Cement, 2014/2, 52–58.

[24] Arkesteijn, R., Dimensionering van onderwaterbetonvloeren. MSc thesis, March 2012.

[25] Bouwmeester-van den Bos, W. J., & Huisman, C. (2003). Ontvangstschacht Botlekspoortunnel, bouwkuip met staalvezelgewapend onderwaterbeton. Cement, 4.

[26] CEB-FIB Model Code 2010 – Final draft, Volume 1&2, March 2012.

[27] Bemessungsgrundlagen fur Stahlfaserbeton im Tunnelbau; Deutscher Beton-Verein Merkblatt, fassung September 1992.

[28] Combinatie Rotterdamsebaan. (z.d.). Ontwerpberekening onderwaterbeton Vlietzone kuip B - Moot V1.

[29] de Winter, E., Arkesteijn, R., & Barten, P. (2017). Herziening CUR-Aanbeveling 77 (4): Rekenvoorbeelden over onderwaterbetonvloeren. Cement, 4, 42–52.

Figure coversheet: CF Rijnlandroute. (z.d.). Congeo. https://www.congeo.nl/projecten/rijnlandroute

Annex A: Complete visualization and verification of model

As described in the main report, the model consist of building blocks that are listed below:

- Force distribution
- Force distribution with slip
- FM B1: tensile resistance
- FM B2: compression arch
- FM B3: compression arch with membrane action
- FM C1: Bending shear fracture
- FM C2: Additional shear resistance
- FM G: Punching shear
- FM BF: Bending resistance SFUCF

A.1 Visualization

The process within each building blocks exists of a series of calculation steps/choices/processes. This paragraph visualizes the process using flowcharts. Each formula is listed with a number and can be found in table A.1.

Force distribution

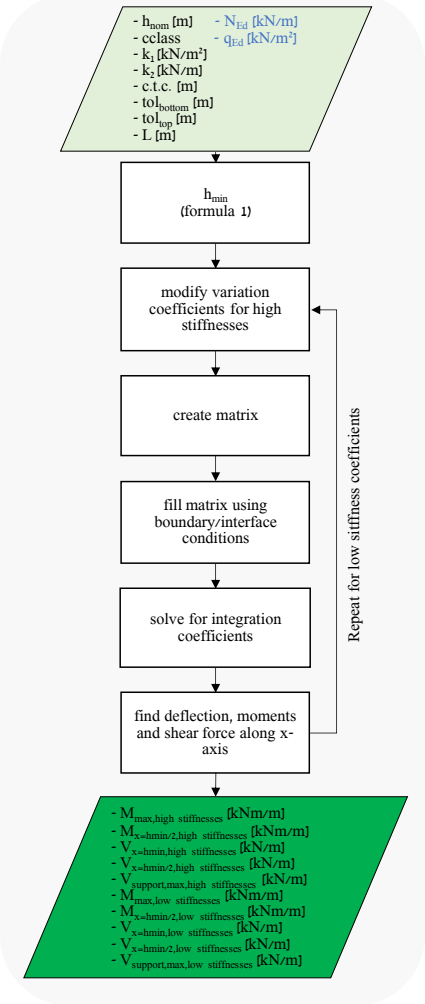

Figure A.1: Force distribution without slip

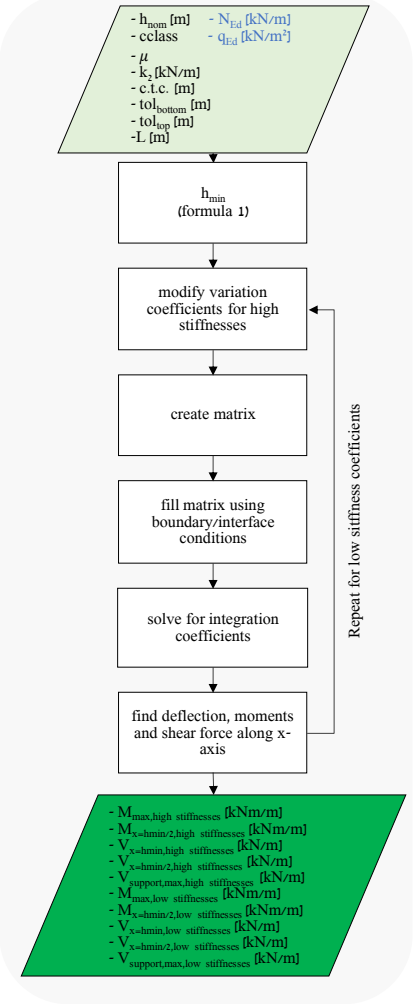

figure A.2: Force distribution with slip

Bending moment resistance

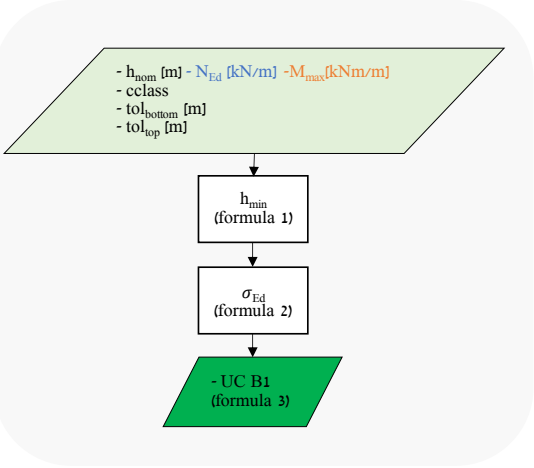

Figure A.3: FM B1

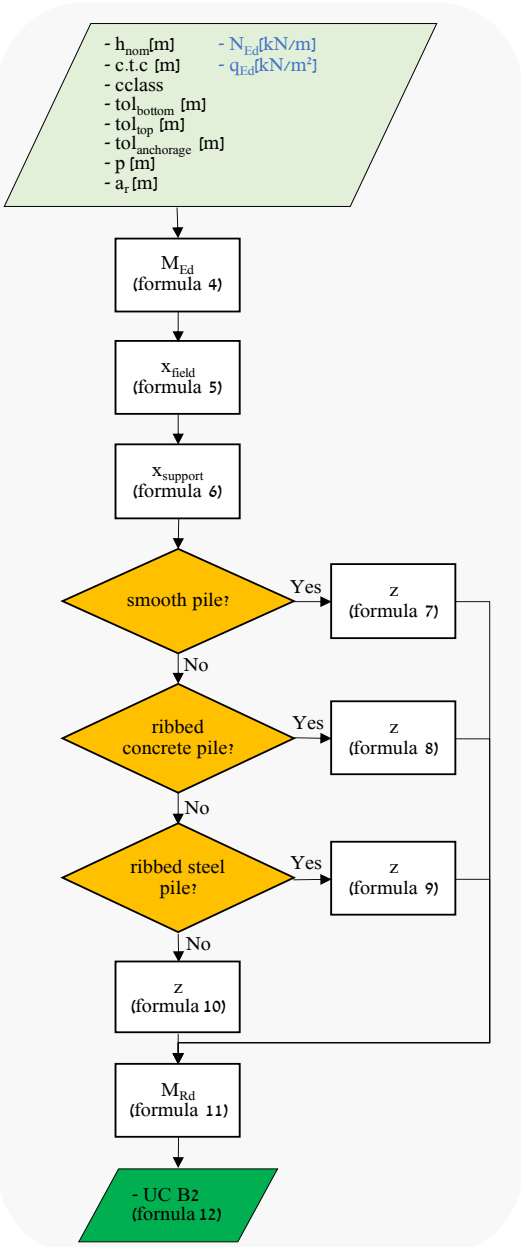

Figure A.4: FM B2

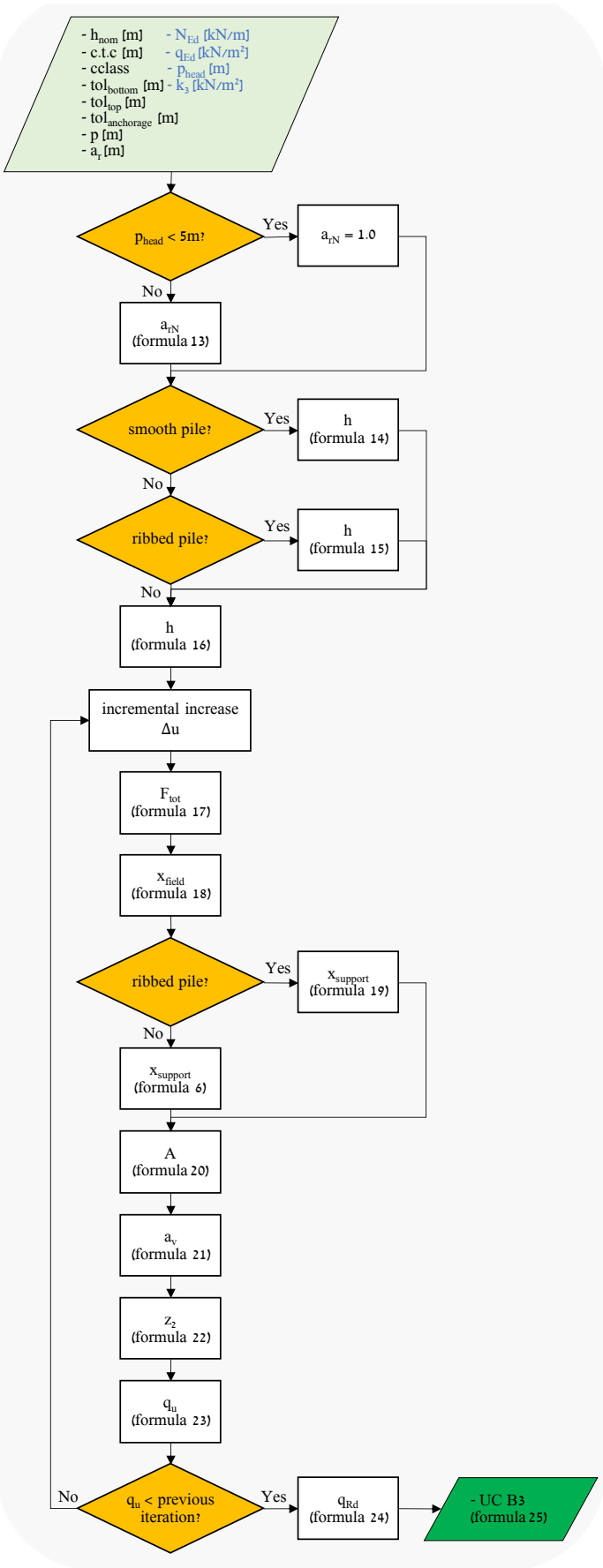

Figure A.5: FM B3

Shear force resistance

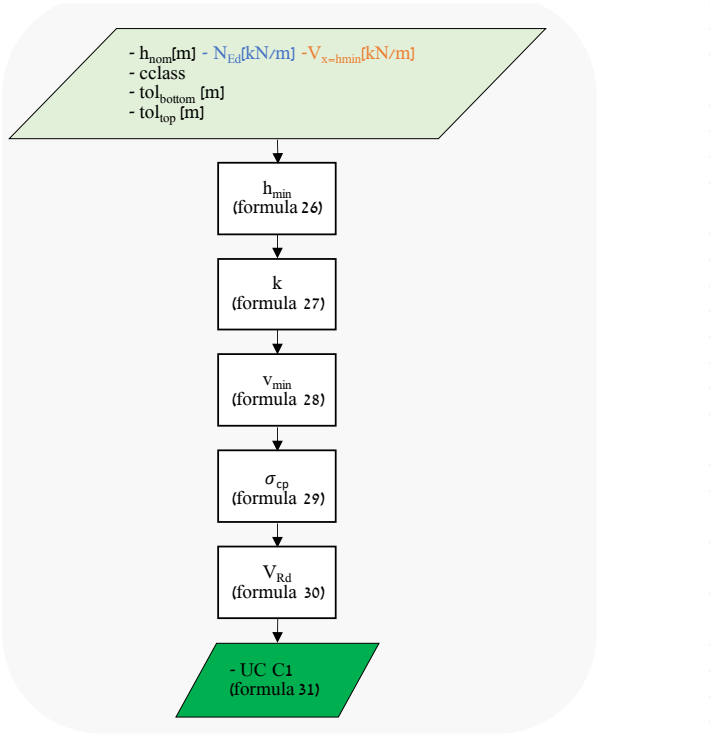

Figure A.6: Bending shear fracture

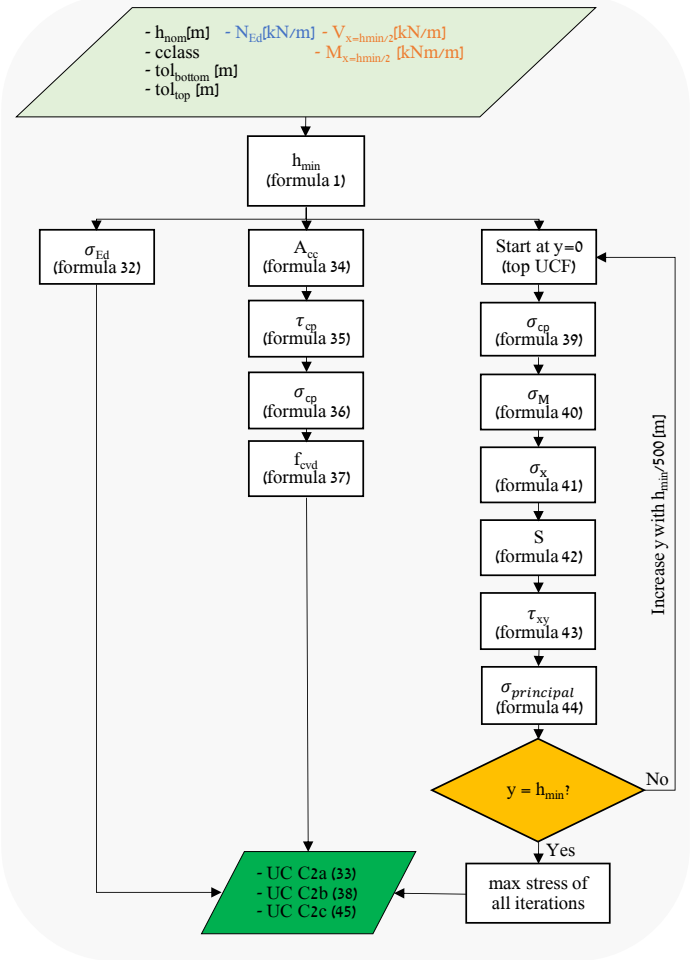

Figure A.7: Additional shear resistance

Punching shear force resistance

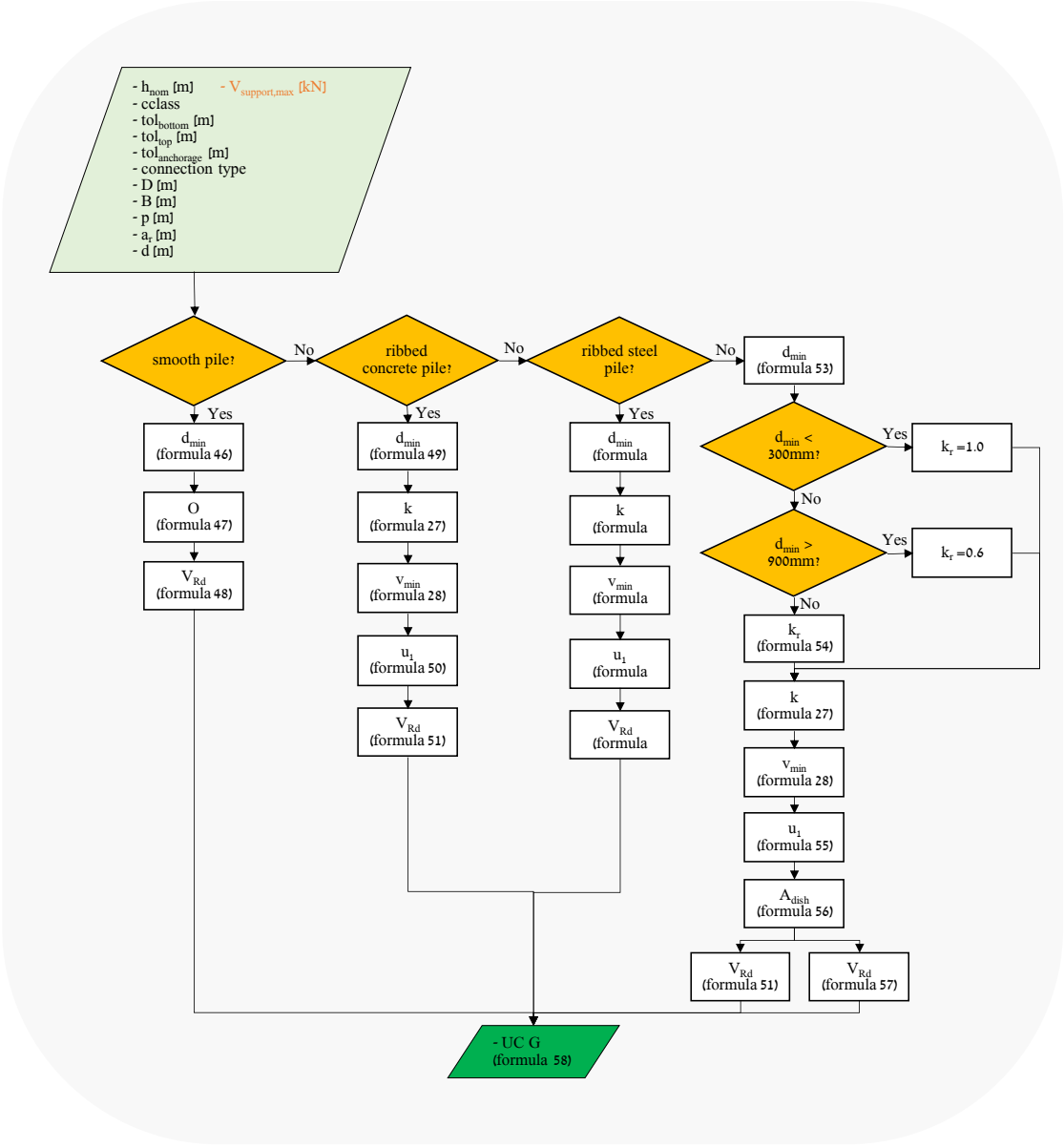

Figure A.8: Punching shear force resistance

Fibre reinforced UCF – bending moment resistance

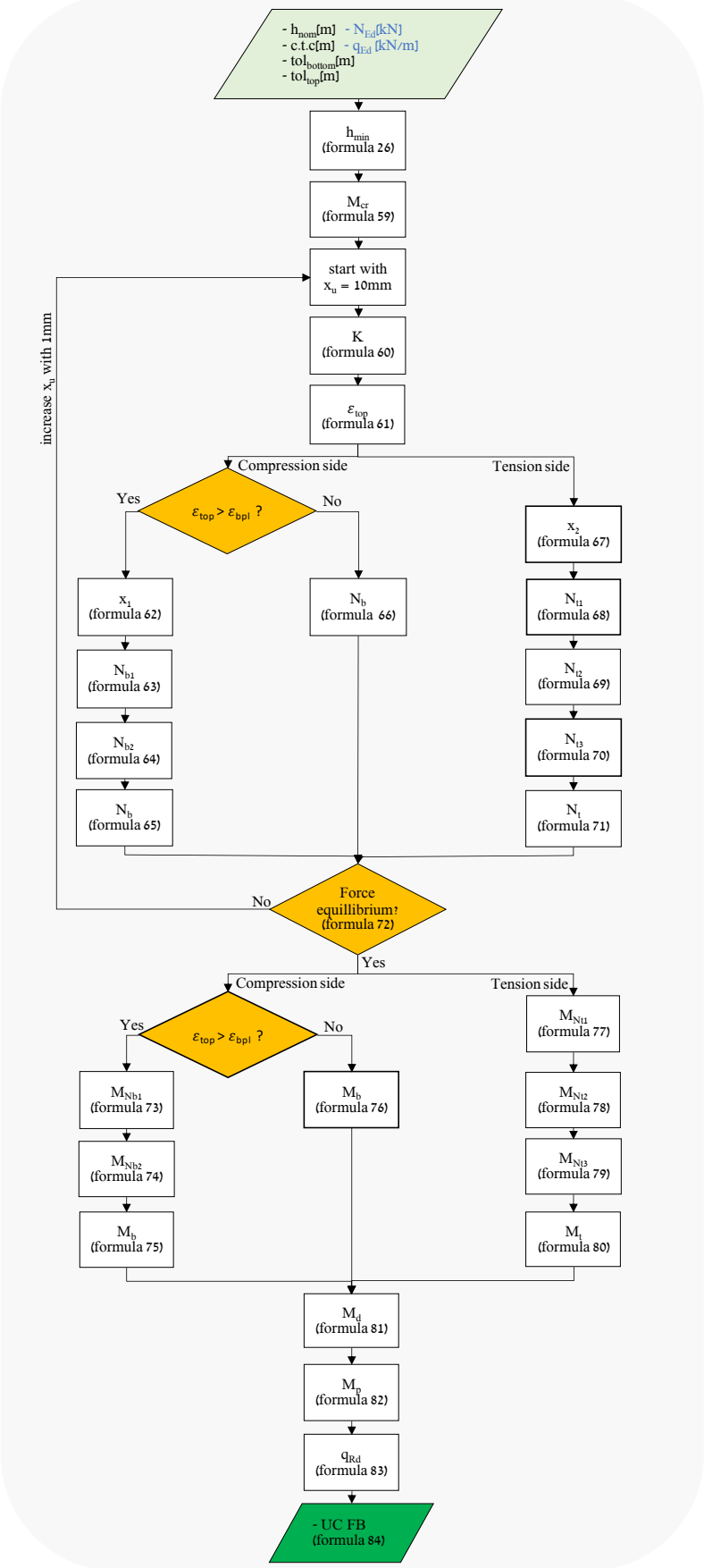

Figure A.8: Bending moment resistance SFUCF

Table A.1: Formulae corresponding with flowcharts

#	**Formulae force distribution and FM B1**
1	$h_{min} = h_{nom} - \sqrt{tol_{top}^2 + tol_{bottom}^2}$
2	$\sigma_{Ed} = (6 * M_{max}/h_{min}^2 - 0.9 * N_{Ed}/h_{min})/10^3$
3	$UC_{B1} = \sigma_{Ed}/f_{ctd,pl}$
#	**Additional formulae FM B2**
4	$M_{Ed} = q_{Ed} * \ c.t.c.^2 \ / \ 8$
5	$x_{field} = 2 * 0.9 * N_{ed}/(f_{cd,pl} * 1000)$
6	$x_{support} = x_{field} \ / \ 0.6$
7	$z = h_{nom}/2 \ - tol_{bottom} - 2/3 \ * 0.9 * N_{Ed}/(f_{cd,pl} * 1000)$
8	$z = h_{nom} - tol_{top} - a_r - tol_{bottom} - (x_{field} + \max(300mm, x_{support}))/3$
9	$z = h_{nom} - tol_{top} - a_r - tol_{bottom} - (x_{field} + x_{support})/3$
10	$z = h_{nom} - tol_{anchorage} - p - tol_{bottom} - (x_{field} + x_{support})/3$
11	$M_{Rd} = z * 0.9 * N_{Ed}$
12	$UC_{B2} = M_{Ed}/M_{Rd}$
#	**Additional formulae FM B3**
13	$a_{rN} = 2 - p_{head}/5$
14	$h = (h_{nom}/2 \ - tol_{bottom}) * 1000$
15	$h = (h_{nom} - tol_{bottom} - tol_{top} - a_r) * 1000$
16	$h = (h_{nom} - tol_{bottom} - tol_{anchorage} - p) * 1000$
17	$F_{tot} = a_{rN} * \Delta u * k_3/2000 + N_{ed}$
18	$x_{field} = 2 * F_{tot}/f_{cd,pl}$
19	$x_{support} = \max(300mm, x_{field}/0.6)$
20	$A = \sqrt{h^2 + (500 * c.t.c.)^2}$
21	$a_v = h - \sqrt{A^2 - (500 * c.t.c. + \Delta u)^2}$
22	$z_2 = h - x_{field}/3 - x_{support}/3 - a_v$
23	$q_u = (8 * F_{tot} * z_2/(1000 * c.t.c. + 2 * \Delta u)^2) * 1000$
24	$q_{Rd} = q_u/1.2$
25	$UC_{B3} = q_{Ed}/q_{Rd}$
#	**Additional formulae FM C1**
26	$h_{min} = (h_{nom} - \sqrt{tol_{top}^2 + tol_{bottom}^2}) * 10^3$
27	$k = \min(1 + \sqrt{200/h_{min}}, 2.0)$
28	$v_{min} = 0.035 * k^{1.5} * f_{ck}^{0.5}$
29	$\sigma_{cp} = \min(0.9 * N_{Ed}/h_{min}, 0.2 * f_{cd,pl})$
30	$V_{Rd} = h_{min} * (v_{min} + 0.15 * \sigma_{cp})$
31	$UC_{C1} = V_{x=hmin}/V_{Rd,c}$

#	Additional formulae FM C2
32	$\sigma_{Ed} = (6 * M_{x=hmin/2}/h_{min}^2 - 0.9 * N_{Ed}/h_{min})/10^3$
33	$UC_{C2a} = \sigma_{Ed}/f_{ctd,pl}$
34	$\mathrm{A_{cc}} = \min(h_{min} * 500 + 0.45 * N_{Ed} * (h_{min} * 10^3)^2/(6 * M_{x=hmin/2} * 10^3), h_{min} * 10^3) * 10^3$
35	$\tau_{cp} = 1.5 * V_{x=hmin/2}/A_{cc} * 10^3$
36	$\sigma_{cp} = 0.9 * N_{Ed}/A_{cc} * 10^3$
37	$f_{cvd} = \sqrt{f_{ctd,pl}^2 + \sigma_{cp} * f_{ctd,pl}}$
38	$UC_{C2b} = \tau_{cp}/f_{cvd}$
39	$\sigma_{cp} = 0.9 * N_{Ed}/(h_{min} * 1000)$
40	$\sigma_M = 6 * M_{x=hmin/2} * 10^3/(h_{min} * 10^3)^2 - y * (6 * M_{x=hmin/2} * 10^3/(h_{min} * 10^3)^2/(500 * h_{min}))$
41	$\sigma_x = \sigma_M - \sigma_{cp}$
42	$S = y * (500 * h_{min} - 0.5 * y) * 10^3$
43	$\tau_{xy} = V_{x=hmin/2} * S/(10^3/12 * (h_{min} * 10^3)^3)$
44	$\sigma_{principal} = s_x/2 + \sqrt{s_x^2/4 + \tau_{xy}{}^2}$
45	$UC_{C2c} = \sigma_{principal}/f_{ctd,pl}$
#	**Additional formulae FM G**
46	$d_{min} = (h_{nom} - tol_{top} - tol_{bottom}) * 10^3$
47	$O = \pi * D * 10^3$
48	$V_{Rd} = c * f_{ctd,pl} * d_{min} * O$
49	$d_{min} = (h_{nom} - tol_{top} - tol_{bottom} - a_r) * 10^3$
50	$u_1 = 4 * (B * 10^3 + \pi * d_{min})$
51	$V_{Rd} = v_{min} * d_{min} * u_1$
52	$u_1 = \pi * (D * 10^3 + 4 * d_{min})$
53	$d_{min} = (h_{nom} - tol_{anchorage} - tol_{bottom} - p) * 10^3$
54	$k_r = 1 - 0.4 * (d_{min} - 300)/600$
55	$u_1 = \pi * (d * 10^3 + 4 * d_{min})$
56	$A_{dish} = \pi * (d * 10^3)^2/4 - \pi * (D * 10^3)^2/4$
57	$V_{Rd} = 1.7 * f_{cd,pl} * A$
58	$UC_G = 1.25 * V_{support,max}/V_{Rd}$
#	**Additional formulae FM BF:**
59	$M_{cr} = \frac{1}{6} * 1000 * h_{min}^2 * (0.9 * \frac{N_{Ed}}{h_{min}} + f_{ctd,pl})/10^6$
60	$K = \varepsilon_{svu}/(h_{min} - x_u)$
61	$\varepsilon_{top} = K * x_u$
62	$x_1 = \frac{\varepsilon_{bpl}}{\varepsilon_{top}} * x_u$
63	$N_{b1} = (x_u - x_1) * f_{cd}$
64	$N_{b2} = 0.5 * x_1 * f_{cd}$
65	$N_b = N_{b1} + N_{b2}$

66	$N_b = 0.5 * x_u * f_{cd} * \frac{\varepsilon_{top}}{\varepsilon_{bpl}}$
67	$x_2 = \frac{\varepsilon_{fbr}}{\varepsilon_{svu}} * (h_{min} - x_u)$
68	$N_{t1} = 0.5 * f_{ctd,pl} * x_2$
69	$N_{t2} = 0.5 * (\beta * f_{ctd,pl} - \mu_{sv} * f_{ctd,pl}) * (h_{min} - x_u - x_2)$
70	$N_{t3} = \mu_{sv} * f_{ctd,pl} * (h_{min} - x_u - x2)$
71	$N_t = N_{t1} + N_{t2} + N_{t3}$
72	$\lvert N_b - N_t - 0.9 * N_{Ed} \rvert < 20\ kN?$
73	$M_{Nb1} = 0.5 * (x_u - x_1) * N_{b1}$
74	$M_{Nb2} = \left(x_u - \frac{2}{3}x_1\right) * N_{b2}$
75	$M_b = M_{Nb1} + M_{Nb2}$
76	$M_b = \frac{x_u}{3} * N_b$
77	$M_{Nt1} = \left(x_u + \frac{2}{3} * x_2\right) * N_{t1}$
78	$M_{Nt2} = \left(\frac{h}{3} + \frac{2}{3}x_u + \frac{2}{3}x_2\right) * N_{t2}$
79	$M_{Nt3} = \left(\frac{h}{2} + \frac{x_u}{2} + \frac{x_2}{2}\right) * N_{t3}$
80	$M_t = M_{Nt1} + M_{Nt2} + M_{Nt3}$
81	$M_d = 0.9 * N_{Ed} * 0.5 * h_{min}$
82	$M_p = (-M_b + M_t + M_d)/\ 10^3$
83	$q_{Rd} = \frac{8}{c.t.c.^2} * (M_p + \frac{M_{cr}}{1.25})$
84	$UC_{FB} = q_{Ed}/q_{Rd}$

A.2 Verification

A standard set of parameters is listed below. For each building block one parameter is set as variable at a time. The unity check of the failure mechanism is calculated for values of the variable parameter inside a representative domain (values that are realistic in practical applications). 3 points within the domain are used as sample and are checked by using hand calculation and Excel sheet from BAM Infraconsult. In the case of force distribution, the samples are checked using FEM. It is clear that this approach does not cover 100% of the required verification, however for the application of this model it is deemed as sufficient. The standard set of parameters and the corresponding values are:

L	=	20	[m]
h_{nom}	=	1.0	[m]
c.t.c.	=	2.5	[m]
p_{head}	=	5	[m]
N_{Ed}	=	300	[kN/m]
q_{Ed}	=	100	[kN/m²]
c-class	=	C25/30	[properties and units according to table 2.3]
k1	=	60000	[kN/m/m]
k2	=	30000	[kN/m/m]
k3	=	35000	[kN/m²]
c	=	0.2	[-]
D	=	0.065	[m]
B	=	0.3	[m]
p	=	0.25	[m]
a_r	=	0.085	[m]
tol_{top}	=	0.15	[m]
tol_{bottom}	=	0.15	[m]
$tol_{anchorage}$	=	0.10	[m]

For some building blocks, output from force distribution should be used as input. These parameters are given a standard value of:

FM C1:

$V_{x=hmin}$	=	100	[kN/m]

FM C2:

$V_{x=hmin/2}$	=	100	[kN/m]
$M_{x=hmin/2}$	=	100	[kNm/m]

Fm G:

$V_{support,max}$	=	100	[kN]

Force distribution without slip

Variation of stiffnesses was not applied. The force distribution was verified using MatrixFrame FEA software.

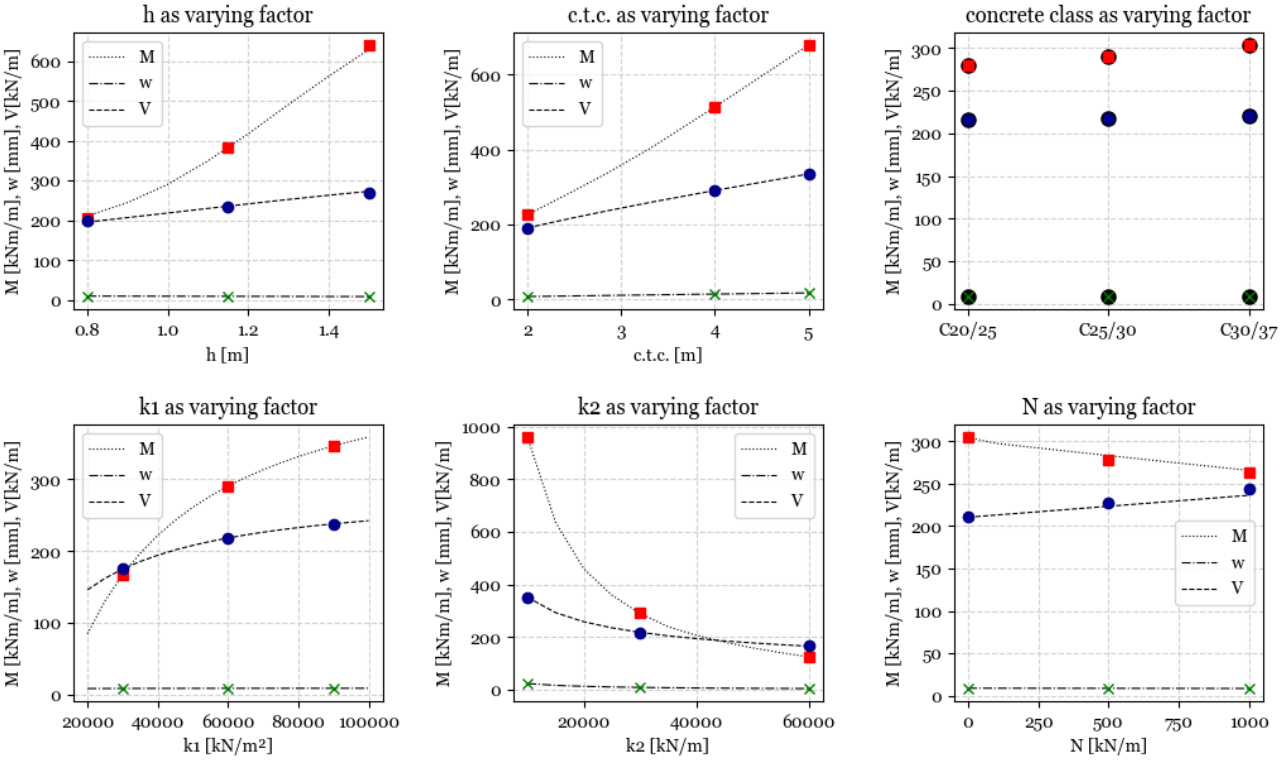

		h_{nom} as variable [m]			c.t.c. as variable [m]			Concrete class as variable		
		0.8	1.15	1.5	2	4	5	C20/25	C25/30	C30/37
Model	M_{Max} [kNm/m]	210.9	380.1	629.1	225.9	514.0	679.4	279.9	290.2	303.6
	w_{Max} [mm]	9.0	8.5	7.82	7.0	13.7	16.8	8.8	8.7	8.7
	V_{max} [kN/m]	195.4	235.4	272.8	190.5	290.8	334.7	216.3	218.1	220.5
FEA	M_{Max} [kNm/m]	205.8	382.6	641.0	225.9	514.0	679.9	279.9	290.2	303.7
	w_{Max} [mm]	9.0	8.5	7.9	7.0	13.7	16.8	8.8	8.7	8.6
	V_{max} [kN/m]	197.7	234.1	269.8	190.4	290.8	334.7	216.3	218.1	220.5

		k_1 as variable [kN/m²]			k_2 as variable [kN/m]			N_{Ed} as variable [kN/m]		
		30000	60000	90000	10000	30000	60000	0	500	1000
Model	M_{Max} [kNm/m]	166.9	290.2	346.2	960.1	290.2	125.1	304.9	283.1	265.7
	w_{Max} [mm]	8.6	8.8	8.8	23.2	8.7	4.3	8.9	8.7	8.5
	V_{max} [kN/m]	174.8	218.1	237.8	351.3	218.1	165.4	210.4	223.3	236.2
FEA	M_{Max} [kNm/m]	166.9	290.3	346.2	960.1	290.3	125.2	304.9	278.4	262.4
	w_{Max} [mm]	8.6	8.7	8.8	23.2	8.7	4.3	8.8	8.6	8.4
	V_{max} [kN/m]	174.8	218.1	237.8	351.2	218.1	165.8	210.4	226.8	243.1

Force distribution with slip

Variation of stiffnesses was not applied. The force distribution was verified using MatrixFrame FEA software.

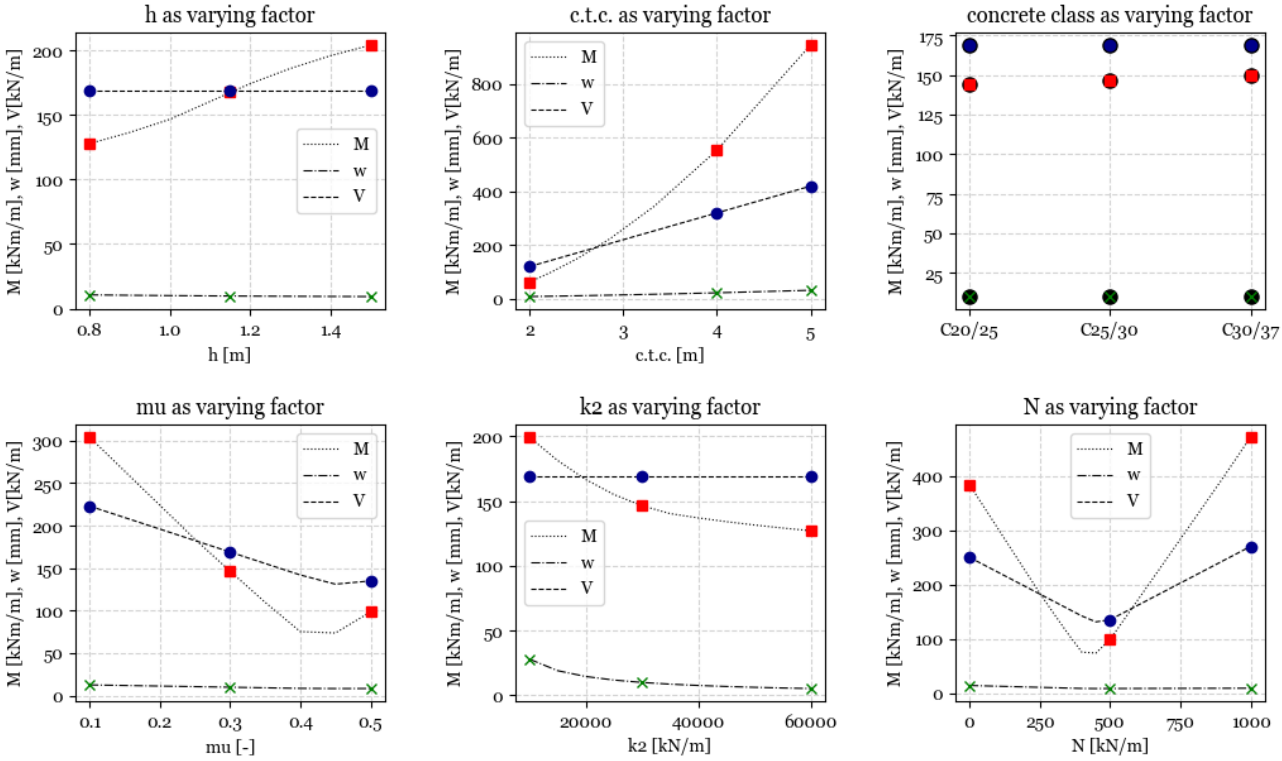

		h_{nom} as variable [m]			c.t.c. as variable [m]			Concrete class as variable		
		0.8	1.15	1.5	2	4	5	C20/25	C25/30	C30/37
Model	M_{Max} [kNm/m]	127.8	167.6	204.1	61.5	552.5	944.8	144.0	146.6	149.7
	w_{Max} [mm]	10.6	9.8	9.3	7.2	21.2	30.6	10.1	10.1	10.0
	V_{max} [kN/m]	169.0	169.0	169.0	119.0	319.0	419.0	169.0	169.0	169.0
FEA	M_{Max} [kNm/m]	127.7	167.5	204.1	61.5	552.5	944.8	144.0	146.6	149.7
	w_{Max} [mm]	10.6	9.7	9.3	7.2	21.2	30.6	10.1	10	10.0
	V_{max} [kN/m]	169.0	169.0	169.0	119.0	319.0	419.0	169.0	169.0	169.0

		μ as variable [-]			k_2 as variable [kN/m]			N_{Ed} as variable [kN/m]		
		0.1	0.3	0.5	10000	30000	60000	0	500	1000
Model	M_{Max} [kNm/m]	304.1	146.6	98.6	199.5	146.6	127.2	384.0	98.6	471.3
	w_{Max} [mm]	12.8	10.1	8.5	28.1	10.1	5.3	14.1	8.5	9.1
	V_{max} [kN/m]	223.0	169.0	135.0	169.0	169.0	169.0	250.0	135.0	270.0
FEA	M_{Max} [kNm/m]	304.1	146.6	98.6	199.5	146.6	127.2	384.0	98.6	471.3
	w_{Max} [mm]	12.8	10.0	8.5	28.1	10.0	5.3	14.1	8.5	9.1
	V_{max} [kN/m]	223.0	169.0	135.0	169.0	169.0	169.0	250.0	135.0	270.0

FM B1: Tensile capacity

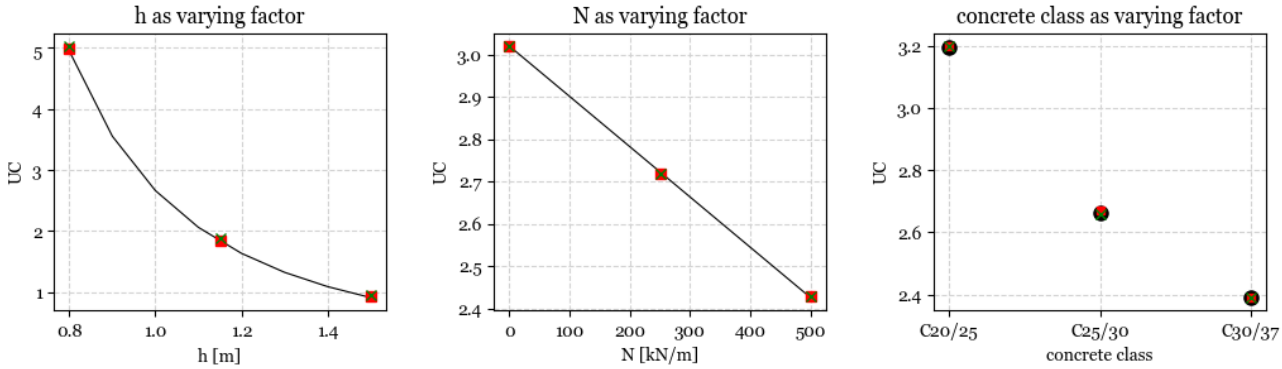

	h_{nom} as variable [m]			N_{Ed} as variable [kN/m]			Concrete class as variable		
	h=0.8	h=1.15	h=1.5	N=0	N=250	N=500	C20/25	C25/30	C30/37
Model	4.95	1.83	0.91	3.02	2.73	2.42	3.20	2.67	2.39
Hand-calculation	4.98	1.85	0.93	3.02	2.72	2.43	3.20	2.67	2.39
Excel	5.03	1.88	0.95	3.02	2.72	2.43	3.20	2.66	2.39

Hand calculation example

With h_{nom}=0.8m and other parameters as stated in introduction:

$$h_{min} = h - \sqrt{tol_{top}^2 + tol_{bottom}^2} = 0.587\ m$$

$$\sigma_{Ed} = (6 * M_{max}/h_{min}^2 - 0.9 * N_{Ed}/h_{min})/10^3 = 4.70\ N/mm^2$$

$$UC_{B1} = \sigma_{Ed}/f_{ctd,pl} = 4.98$$

FM B2: Compression arch

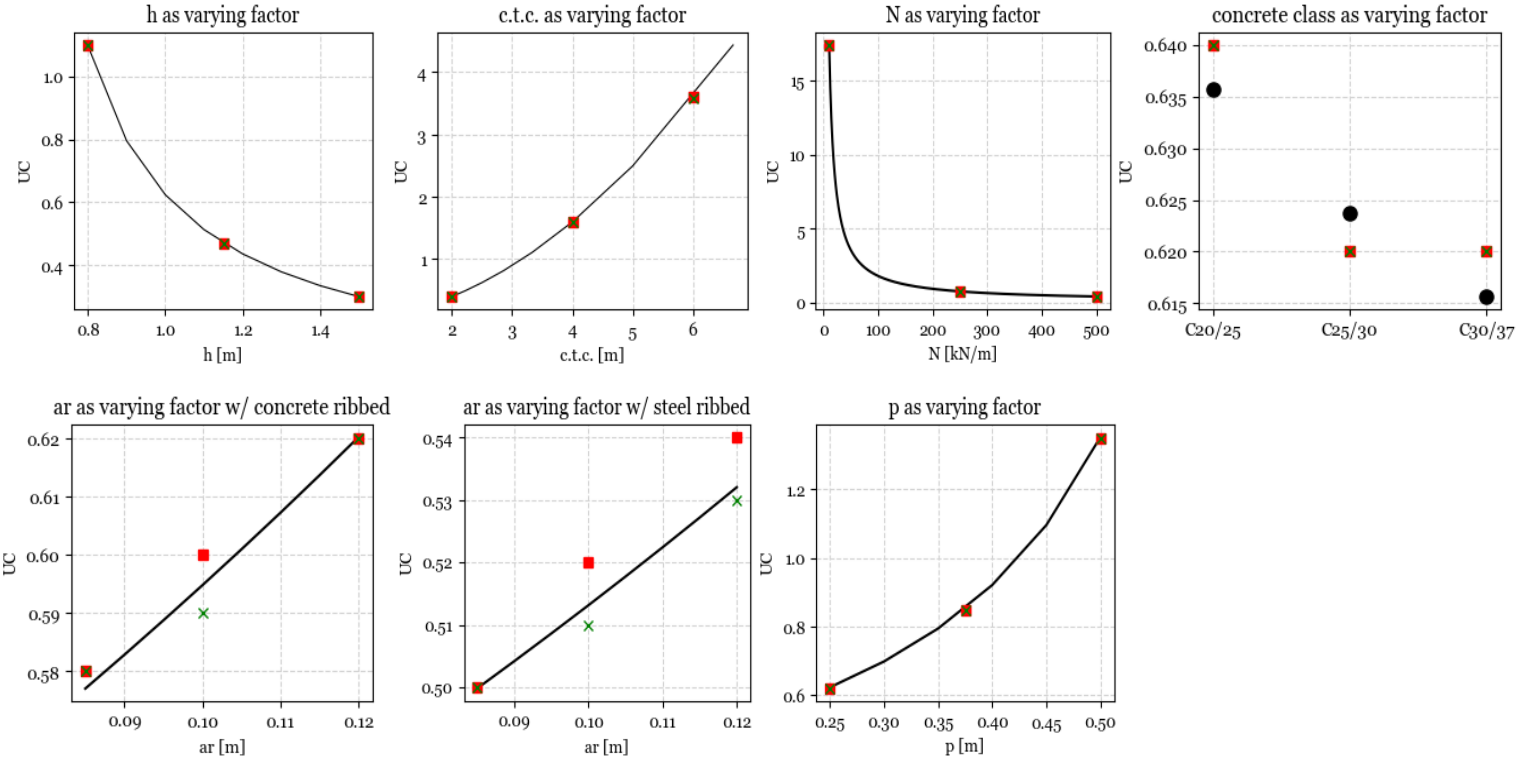

	h_{nom} as variable [m]			c.t.c. as variable [m]			N_{Ed} as variable [kN/m]			Concrete class variable		
	h=0.8	h=1.15	h=1.5	ctc=2	ctc=4	ctc=6	N=10	N=250	N=500	C20/25	C25/30	C30/37
Model	1.10	0.47	0.30	0.40	1.60	3.61	17.40	0.74	0.40	0.64	0.62	0.62
Hand calculation	1.10	0.47	0.30	0.40	1.60	3.60	17.40	0.74	0.40	0.64	0.62	0.62
Excel	1.10	0.47	0.30	0.40	1.60	3.59	17.40	0.74	0.39	0.64	0.62	0.62

	a_r (steel) variable [m]			a_r (concrete) variable [m]			p as variable [m]		
	0.085	0.1	0.12	0.085	0.1	0.12	0.25	0.375	0.5
Model	0.50	0.51	0.53	0.58	0.60	0.62	0.62	0.85	1.35
Hand calculation	0.50	0.52	0.54	0.58	0.60	0.62	0.62	0.85	1.35
Excel	0.50	0.51	0.53	0.58	0.59	0.62	0.62	0.85	1.35

Hand calculation example

With h=0.8m and other parameters as stated in introduction:

$M_{Ed} = q_{Ed} * \ c.t.c.^2 \ / \ 8 = 78.125 \ kNm/m$

$x_{field} = 2 * 0.9 * N_{ed}/(f_{cd,pl} * 1000) = 0.41m$

$x_{support} = x_{field}/0.6 = 0.068m$

$z = h_{nom} - tol_{anchorage} - p - tol_{bottom} - (x_{field} + x_{support})/3 = 0.75m$

$M_{Rd} = z * 0.9 * N_{Ed} = 202.5 \ kNm/m$

$UC_{B2} = M_{Ed}/M_{Rd} = 0.39$

FM B3: Compression arch with membrane action

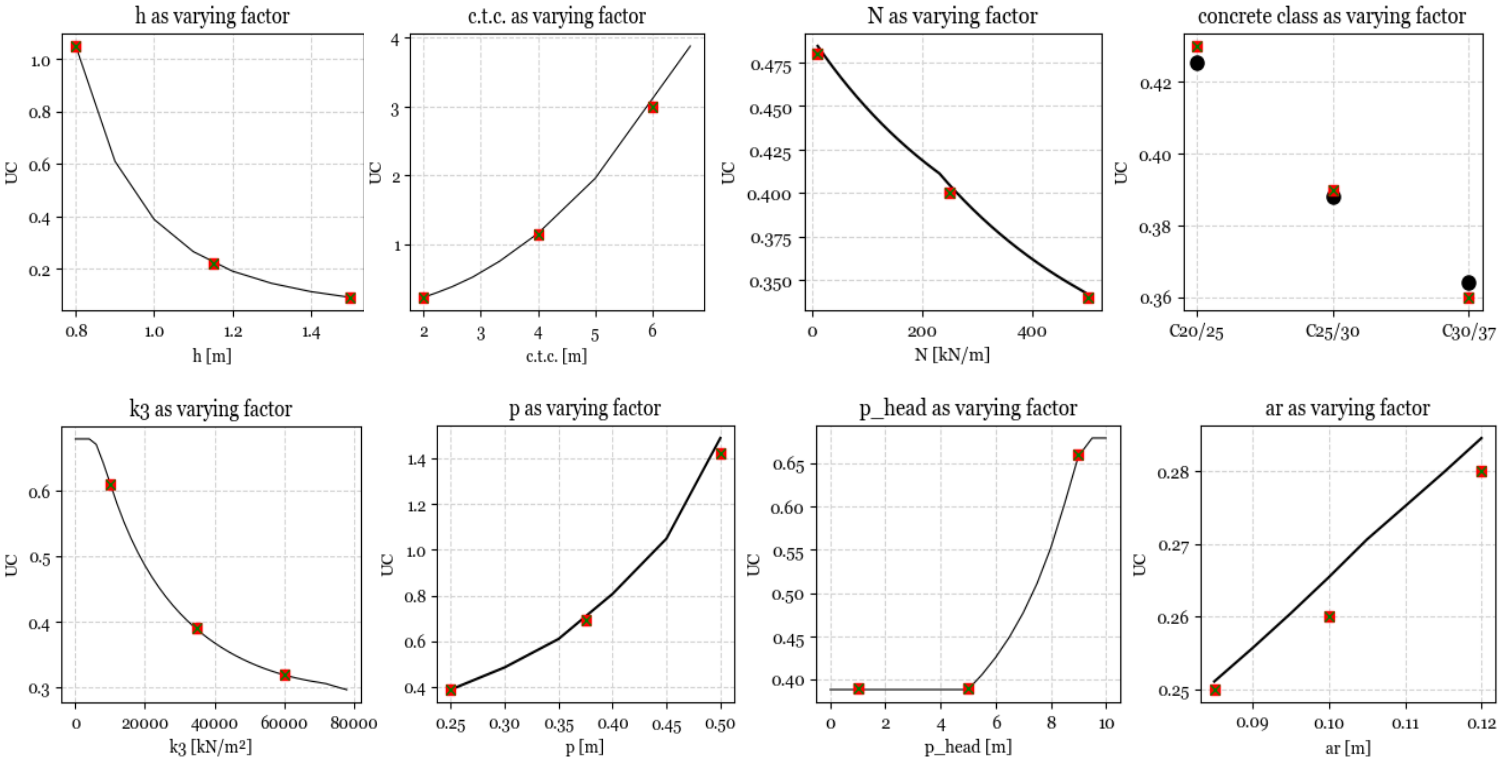

	h_{nom} as variable [m]			c.t.c. as variable [m]			N_{Ed} as variable [kN/m]			Concrete class variable		
	h=0.8	h=1.15	h=1.5	ctc=2	ctc=4	ctc=6	N=10	N=250	N=500	C20/25	C25/30	C30/37
Model	1.05	0.22	0.09	0.24	1.16	3.04	0.48	0.40	0.34	0.43	0.39	0.36
Hand calculation	1.05	0.22	0.09	0.23	1.15	2.99	0.48	0.40	0.34	0.43	0.39	0.36
Excel	1.05	0.22	0.09	0.23	1.15	2.99	0.48	0.40	0.34	0.43	0.39	0.36

	k_3 as variable [kN/m²]			p as variable [m]			p_{head} as variable [m]			a_r as variable [m]		
	10000	35000	60000	0.25	0.375	0.5	1	5	9	0.085	0.10	0.12
Model	0.61	0.39	0.32	0.39	0.70	1.49	0.39	0.39	0.66	0.25	0.27	0.29
Hand calculation	0.61	0.39	0.32	0.39	0.69	1.42	0.39	0.39	0.66	0.25	0.26	0.28
Excel	0.61	0.39	0.32	0.39	0.69	1.42	0.39	0.39	0.66	0.25	0.27	0.29

Hand calculation example

The resistance of the compression arch with membrane action depends on the horizontal displacement of the retaining wall. It should be calculated iteratively at what displacement the peak resistance is found. This is a lot of work hence the displacement for peak resistance is copied from the model. 3 iterations shall be done to verify that the model's displacement indeed gives the peak resistance and that the result is correct. The example will be performed for the standard parameters and h_{nom}=1.5m

According to the model the peak resistance is found at Δu = 100mm, therefor calculations shall be performed for Δu - 10mm, u and Δu + 10mm.

$a_{rN} = 1.0$

$h = (h_{nom} - tol_{bottom} - tol_{anchorage} - p) * 1000 = 1000\ mm$

u=90mm

$F_{tot} = a_{rN} * \Delta u * k_3/2000 + N_{ed} = 1875\ N/mm$

$x_{field} = 2 * F_{tot}/f_{cd,pl} = 281.95\ mm$

$x_{support} = x_{field}/0.6 = 469.9\ mm$

$A = \sqrt{h^2 + (500 * c.t.c.)^2} = 1600.8\ mm$

$a_v = h - \sqrt{A^2 - (500 * c.t.c. + \Delta u)^2} = 125.7\ mm$

$z_2 = h - x_{field}/3 - x_{support}/3 - a_v = 624.3\ mm$

$q_u = (8 * F_{tot} * z_2/(1000 * c.t.c. + 2 * \Delta u)^2) * 1000 = 1303\ kN/m^2$

u=100mm

$F_{tot} = a_{rN} * \Delta u * k_3/2000 + N_{ed} = 2050\ N/mm$

$x_{field} = 2 * F_{tot}/f_{cd,pl} = 308.3\ mm$

$x_{support} = x_{field}/0.6 = 513.8\ mm$

$A = \sqrt{h^2 + (500 * c.t.c.)^2} = 1600.8\ mm$

$a_v = h - \sqrt{A^2 - \left(\frac{ctc}{2} + \Delta u\right)^2} = 141.2\ mm$

$z_2 = h - x_{field}/3 - x_{support}/3 - a_v = 584.7\ mm$

$q_u = (8 * F_{tot} * z_2/(1000 * c.t.c. + 2 * \Delta u)^2) * 1000 = 1315\ kN/m^2$

u=110mm

$F_{tot} = a_{rN} * \Delta u * k_3/2000 + N_{ed} = 2225\ N/mm$

$x_{field} = 2 * F_{tot}/f_{cd,pl} = 334.6\ mm$

$x_{support} = x_{field}/0.6 = 557.6\ mm$

$A = \sqrt{h^2 + (500 * c.t.c.)^2} = 1600.8\ mm$

$a_v = h - \sqrt{A^2 - \left(\frac{ctc}{2} + \Delta u\right)^2} = 157.2\ mm$

$z_2 = h - x_{field}/3 - x_{support}/3 - a_v = 545.4\ mm$

$q_u = (8 * F_{tot} * z_2/(1000 * c.t.c. + 2 * \Delta u)^2) * 1000 = 1312\ kN/m^2$

Hence it is confirmed that the peak resistance occurs at u=100mm. This gives a unity check of:

$UC_{B3} = q_{Ed}/q_{Rd} = 0.091$

FM C1: Bending shear fracture

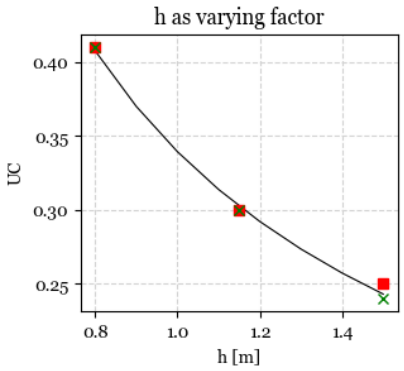

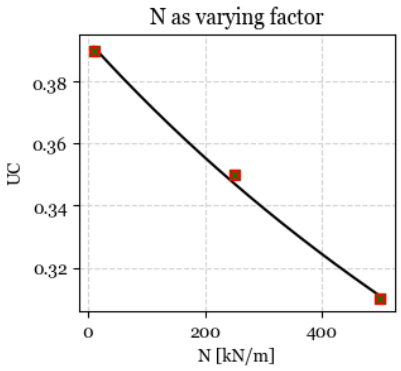

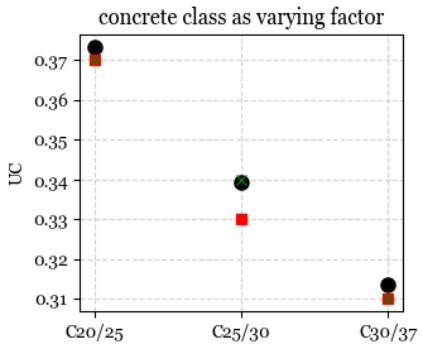

	h_{nom} as variable [m]			N_{Ed} as variable [kN/m]			Concrete class as variable		
	0.8	1.15	1.5	10	250	500	C20/25	C25/30	C30/37
Model	0.41	0.30	0.24	0.39	0.35	0.31	0.37	0.34	0.31
Hand calculation	0.41	0.30	0.25	0.39	0.35	0.31	0.37	0.33	0.31
Excel	0.41	0.30	0.24	0.39	0.35	0.31	0.37	0.34	0.31

Hand calculation example

With h_{nom}=0.8m and other parameters as stated in introduction:

$$h_{min} = (h_{nom} - \sqrt{tol_{top}^2 + tol_{bottom}^2}) * 10^3 = 587\ mm$$

$$k = \min\left(1 + \sqrt{\frac{200}{h_{min}}}, 2.0\right) = 1.58\ N/mm^2$$

$$v_{min} = 0.035 * k^{\frac{3}{2}} * f_{ck}^{\frac{1}{2}} = 0.35$$

$$\sigma_{cp} = \min\left(0.9 * N_{Ed}/h_{min}, 0.2 * f_{cd,pl}\right) = 0.52\ N/mm$$

$$V_{Rd,c} = (v_{min} + 0.15 * \sigma_{cp}) * h_{min} = 244\ kN/m$$

$$UC_{C1} = \frac{V_{x=hmin}}{V_{Rd,c}} = 0.41$$

FM C2: Additional shear resistance

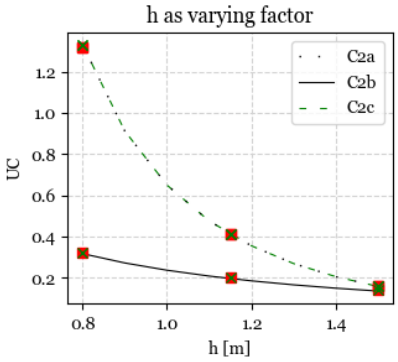

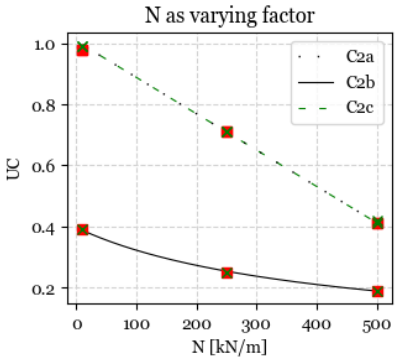

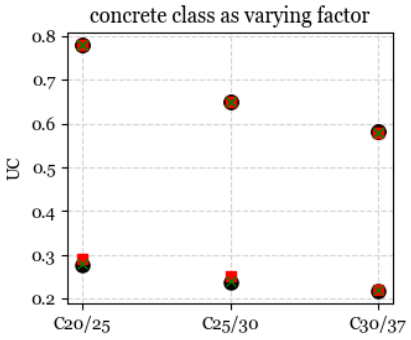

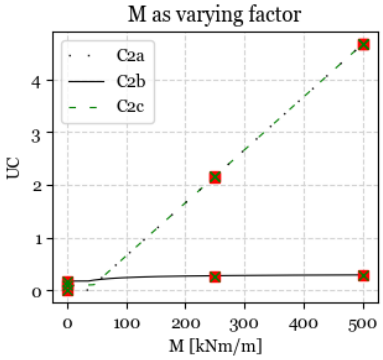

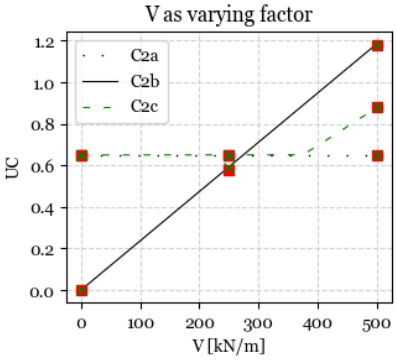

		h_{nom} as variable [m]			N_{Ed} as variable [kN/m]			Concrete class as variable		
		0.8	1.15	1.5	10	250	500	C20/25	C25/30	C30/37
Model	C2a	1.33	0.41	0.16	1.00	0.71	0.41	0.78	0.65	0.58
	C2b	0.32	0.20	0.14	0.39	0.26	0.19	0.28	0.24	0.22
	C2c	1.33	0.41	0.16	1.00	0.71	0.41	0.78	0.65	0.58
Hand calculation	C2a	1.33	0.41	0.16	0.99	0.71	0.41	0.78	0.65	0.58
	C2b	0.32	0.20	0.14	0.39	0.25	0.19	0.29	0.25	0.22
	C2c	1.33	0.41	0.16	0.99	0.71	0.41	0.78	0.65	0.58
Excel	C2a	1.32	0.41	0.16	0.98	0.71	0.41	0.78	0.65	0.58
	C2b	0.32	0.20	0.14	0.39	0.25	0.19	0.28	0.24	0.22
	C2c	1.32	0.41	0.16	0.98	0.71	0.42	0.78	0.65	0.58

		M as variable [kNm/m]			V as variable [kN/m]		
		1	250	500	1	250	500
Model	C2a	0.00	2.16	4.68	0.65	0.65	0.65
	C2b	0.17	0.27	0.29	0.00	0.59	1.19
	C2c	0.09	2.16	4.68	0.65	0.65	0.88
Hand calculation	C2a	0.00	2.14	4.68	0.65	0.65	0.65
	C2b	0.17	0.27	0.29	0.00	0.58	1.18
	C2c	0.09	2.16	4.68	0.65	0.65	0.88
Excel	C2a	0.00	2.16	4.69	0.65	0.65	0.65
	C2b	0.17	0.27	0.29	0.00	0.59	1.18
	C2c	0.09	2.16	4.68	0.65	0.65	0.88

Hand calculation example

With h=0.8m and other parameters as stated in introduction:

C2a

$h_{min} = h - \sqrt{tol_{top}^2 + tol_{bottom}^2} = 0.587\ m$

$\sigma_{Ed} = (6 * M_{x=hmin/2}/h_{min}^2 - 0.9 * N_{Ed}/h_{min})/10^3 = 1.27\ N/mm^2$

$UC_{C2a} = \sigma_{Ed}/f_{ctd,pl} = 1.33$

C2b

$A_{cc} = \min(h_{min} * 500 + 0.45 * N_{Ed} * (h_{min} * 10^3)^2/(6 * M_{x=hmin/2} * 10^3), h_{min} * 10^3) * 10^3 = 371000mm^2$

$\tau_{cp} = 1.5 * \frac{V_{x=\frac{hmin}{2}}}{A_{cc}} * 10^3 = 0.403\ N/mm2$

$\sigma_{cp} = \frac{0.9 * N_{Ed}}{A_{cc}} * 10^3 = 0.72\ N/mm^2$

$f_{cvd} = \sqrt{f_{ctd,pl}^2 + \sigma_{cp} * f_{ctd,pl}} = 1.27\ N/mm^2$

$UC_{C2b} = \tau_{cp}/f_{cvd} = 0.32$

C2c

Principal stress distribution along the height of the UCF is calculated in a large amount of steps. The distribution may have a peak where the maximum principal stress can be found, or the maximum principal stress can be found at an outer fibre of the UCF. The model is used to find at what height the maximum principal stress occurs, hand calculation will check if this is indeed the location with maximum principal stress and whether the value is correct.

According to the model the peak principal stress is found at y = 0 mm (outer fibre at top UCF), therefor calculations shall be performed for y = 0mm to verify the model and y = 2mm to find out whether the peak actually lies at 0mm.

y=0mm

$\sigma_{cp} = 0.9 * N_{Ed}/(h_{min} * 1000) = 0.46\ N/mm^2$

$\sigma_M = 6 * M_{x=hmin/2} * 10^3/(h_{min} * 10^3)^2 - y * (6 * M_{x=hmin/2} * 10^3/(h_{min} * 10^3)^2/(500 * h_{min})) = 1.74N/mm^2$

$\sigma_x = \sigma_M - \sigma_{cp} = 1.28\ N/mm^2$

$S = y * (500 * h_{min} - 0.5 * z) * 10^3 = 0$

$\tau_{xy} = V_{x=hmin/2} * S/(10^3/12 * (h_{min} * 10^3)^3) = 0$

$\sigma_{principal} = s_x/2 + \sqrt{s_x^2/4 + {\tau_{xy}}^2} = 1.28\ N/mm^2$

$UC_{C2c} = \sigma_{principal}/f_{ctd,pl} = 1.33$ → correct result

y=2 mm

$\sigma_{cp} = 0.9 * N_{Ed}/(h_{min} * 1000) = 0.46\ N/mm^2$

$\sigma_M = 6 * M_{x=hmin/2} * 10^3/(h_{min} * 10^3)^2 - y * (6 * M_{x=hmin/2} * 10^3/(h_{min} * 10^3)^2/(500 * h_{min})) = 1.72 N/mm^2$

$\sigma_x = \sigma_M - \sigma_{cp} = 1.26\ N/mm^2$

$S = y * (500 * h_{min} - 0.5 * y) * 10^3 = 586000$

$\tau_{xy} = V_{x=hmin/2} * S/(10^3/12 * (h_{min} * 10^3)^3) = 3.45 * 10^{-3} N/mm^2$

$\sigma_{principal} = s_x/2 + \sqrt{s_x^2/4 + {\tau_{xy}}^2} = 1.26\ N/mm^2$

The principal stress is lower at y=2mm, meaning that the peak indeed lies at y=0mm.

FM G: Punching shear

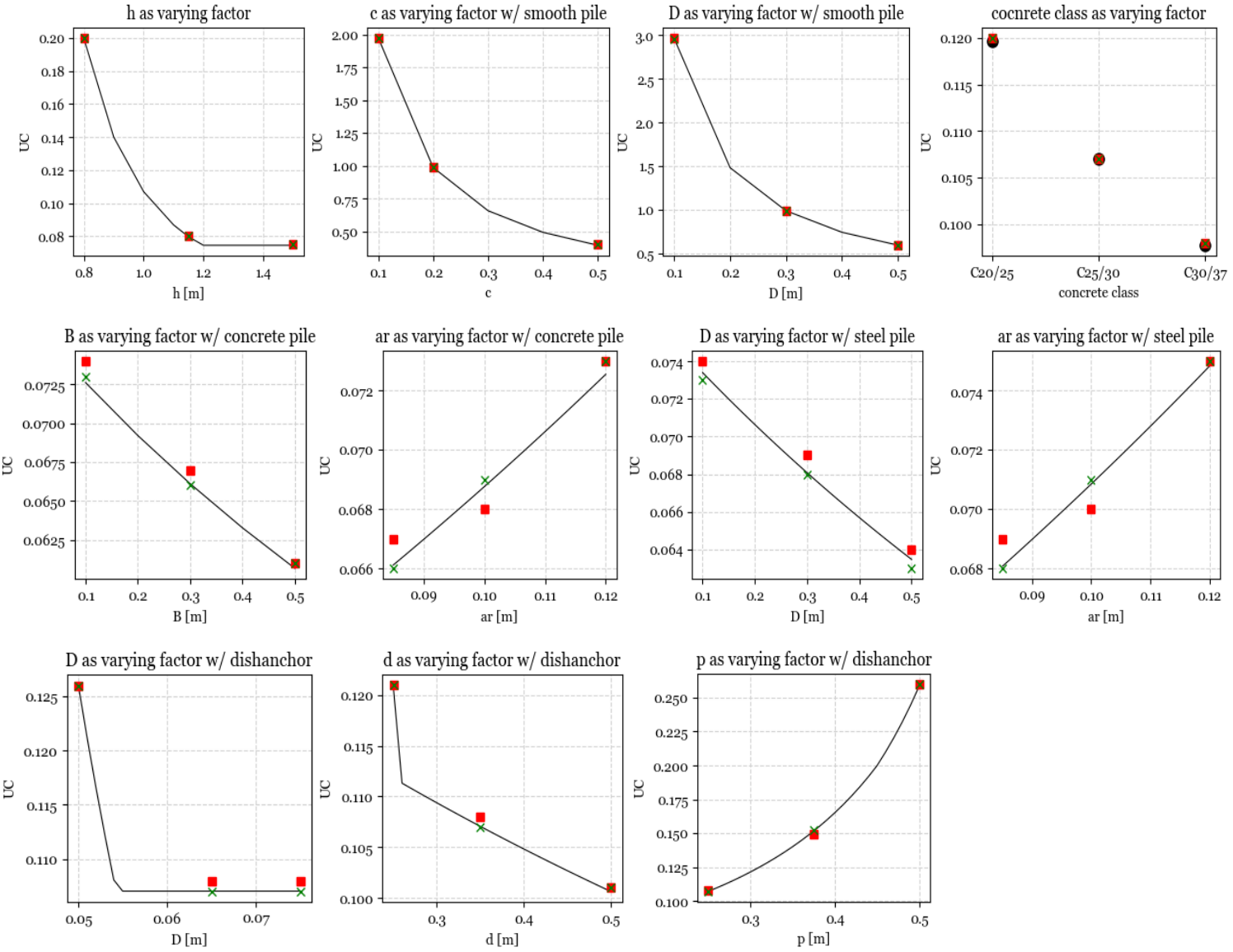

	h_{nom} as variable [m]			c as variable [-]			D variable (smooth)[m]			Concrete class variable		
	h=0.8	h=1.15	h=1.5	c=0.1	c=0.2	c=0.5	D=0.1	D=0.3	D=0.5	C20/25	C25/30	C30/37
Model	0.20	0.08	0.075	1.97	0.99	0.40	2.96	0.99	0.59	0.12	0.11	0.10
Hand calculation	0.20	0.08	0.075	1.97	0.99	0.40	2.97	0.99	0.59	0.12	0.11	0.10
Excel	0.20	0.08	0.075	1.97	0.99	0.40	2.96	0.99	0.59	0.12	0.11	0.10

	B variable (concrete)[m]			a_r variable (concrete)[m]			D variable (steel) [m]			a_r variable (steel) [m]		
	0.1	0.3	0.5	0.085	0.10	0.12	0.1	0.3	0.5	0.085	0.10	0.12
Model	0.073	0.066	0.061	0.067	0.069	0.073	0.073	0.068	0.063	0.068	0.071	0.075
Hand calculation	0.074	0.067	0.061	0.067	0.068	0.073	0.074	0.069	0.064	0.069	0.070	0.075
Excel	0.073	0.066	0.061	0.066	0.069	0.073	0.073	0.068	0.063	0.068	0.071	0.075

	D variable (dishanchor) [m]			d variable (dishanchor) [m]			p variable [m]		
	0.05	0.065	0.075	0.25	0.35	0.5	0.25	0.375	0.5
Model	0.126	0.107	0.107	0.121	0.107	0.101	0.107	0.152	0.258
Hand calculation	0.126	0.108	0.108	0.121	0.108	0.101	0.108	0.149	0.260
Excel	0.126	0.107	0.107	0.121	0.107	0.101	0.107	0.152	0.260

Hand calculation example

With connection type steel ribbed, a_r =0.085m and other parameters as stated in introduction:

$$d_{min} = \left(h_{nom} - tol_{top} - tol_{bottom} - a_r\right) * 10^3 = 665mm$$

$$k = \min\left(1 + \sqrt{\frac{200}{d_{min}}}, 2.0\right) = 1.55$$

$$v_{min} = 0.035 * k^{1.5} * f_{ck}^{0.5} = 0.338$$

$$u_1 = \pi * (D * 10^3 + 4 * d_{min}) = 9299mm$$

$$V_{Rd} = v_{min} * d_{min} * u_1 = 2090\ kN$$

$$UC_G = 1.25 * V_{support,max}/V_{Rd} = 0.06$$

FM BF: Bending moment resistance SFUCF

Contrary to the verification of previous building blocks, the concrete class used is C20/25. This is because C25/30 is not applicable for the results of bending tests from BST. The verification was not performed using excel since there is no excel-sheet for this calculation.

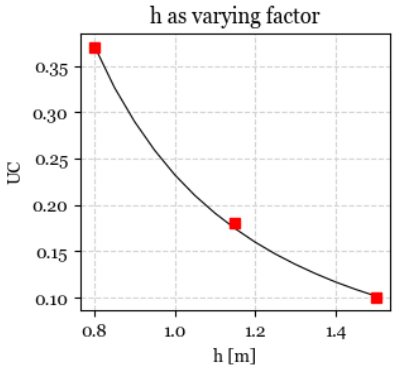

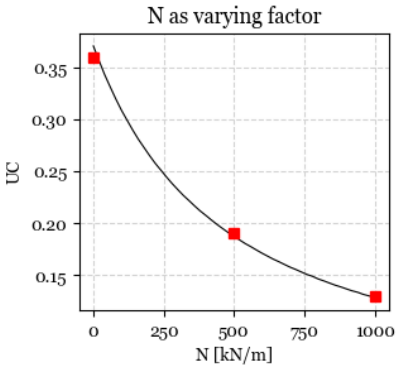

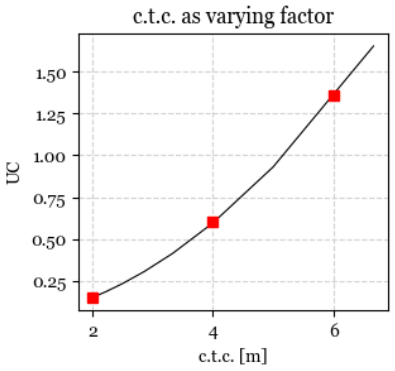

	h_{nom} variable [m]			N variable [kN/m]			c.t.c. variable [m]		
	0.8	1.15	1.5	0	500	1000	2	4	6
Model	0.37	0.18	0.10	0.37	0.19	0.13	0.15	0.59	1.34
Hand calculation	0.37	0.18	0.10	0.36	0.19	0.13	0.15	0.60	1.36

Hand calculation example

With h_{min} = 0.8m and other parameters as stated in introduction. x_u was found to be 62mm, the hand calculation will confirm whether or not this compressive zone height gives equilibrium and calculate the plastic moment and unity check.

$$h_{min} = (h_{nom} - \sqrt{tol_{top}^2 + tol_{bottom}^2}) * 10^3 = 588\ mm$$

$$M_{cr} = \frac{1}{6} * 1000 * h_{min}^2 * (0.9 * \frac{N}{h_{min}} + f_{ctd,pl})/10^6 = 84\ kNm$$

$$K = \varepsilon_{svu}/(h_{min} - x_u) = 9.5 * 10^{-6}\ /mm$$

$$\varepsilon_{top} = K * x_u = 5.89 * 10^{-4}$$

$$x_1 = \frac{\varepsilon_{bpl}}{\varepsilon_{top}} * x_u = 51\ mm$$

$$N_{b1} = (x_u - x_1) * f_{cd} = 146\ kN$$

$$N_{b2} = 0.5 * x_1 * f_{cd} = 340\ kN$$

$$N_b = N_{b1} + N_{b2} = 486\ kN$$

$$x_2 = \frac{\varepsilon_{fbr}}{\varepsilon_{svu}} * (h_{min} - x_u) = 4\ mm$$

$$N_{t1} = 0.5 * f_{ctd,pl} * x_2 = 2\ kN$$

$$N_{t2} = 0.5 * (\beta * f_{ctd,pl} - \mu_{sv} * f_{ctd,pl}) * (h_{min} - x_u - x_2) = 8\ kN$$

$N_{t3} = \mu_{sv} * f_{ctd,pl} * (h_{min} - x_u - x2) = 219\ kN$

$N_t = N_{t1} + N_{t2} + N_{t3} = 229\ kN$

$|N_b - N_t - 0.9 * N_{Ed}| < 20\ kN? \quad \rightarrow \quad 13 < 20 \rightarrow equillibrium\ confirmed$

$M_{Nb1} = 0.5 * (x_u - x_1) * N_{b1} = 803\ kNmm$

$M_{Nb2} = \left(x_u - \frac{2}{3}x_1\right) * N_{b2} = 9520\ kNmm$

$M_b = M_{Nb1} + M_{Nb2} = 10323\ kNmm$

$M_{Nt1} = \left(x_u + \frac{2}{3} * x_2\right) * N_{t1} = 129\ kNmm$

$M_{Nt2} = \left(\frac{h_{min}}{3} + \frac{2}{3}x_u + \frac{2}{3}x_2\right) * N_{t2} = 1920\ kNmm$

$M_{Nt3} = \left(\frac{h_{min}}{2} + \frac{x_u}{2} + \frac{x_2}{2}\right) * N_{t3} = 71613\ kNmm$

$M_t = M_{Nt1} + M_{Nt2} + M_{Nt3} = 73662\ kNmm$

$M_d = 0.9 * N_{Ed} * 0.5 * h_{min} = 79380\ kNmm$

$M_p = (-M_b + M_t + M_d)/10^3 = 142.7\ kNm$

$q_{Rd} = \frac{8}{c.t.c.^2} * \left(M_p + \frac{M_{cr}}{1.25}\right) = 269\ kN/m$

$UC_{FB} = q_{Ed}/q_{Rd} = 0.37$

Annex B: Force distribution in UCF

The literature study in the main report concisely described how to find the force distribution for an uncracked UCF. The process will be described more thoroughly in this annex. A distinction is made between situations where slipping between the UCF and retaining wall does or does not occur. For both situations the same differential equation holds:

$$q_{Ed}(x) = EI * \frac{d^4 w(x)}{dx^4}$$

For the sake of simplicity, the f(x) symbols have been omitted. The following relationships between displacement, rotation, bending moment, and shear force are to be noted:

$$V = -EI * \frac{d^3 w}{dx^3}$$

$$M = -EI * \frac{d^2 w}{dx^2}$$

$$\varphi = -\frac{dw}{dx}$$

For a continuous beam model with n fields, integration of the ODE gives the following formulas for shear force, bending moment, rotation and displacement. Worthwhile noting is that terms including q_{Ed} were changed from negative to positive or vice versa, this is because q_{Ed} acts opposite to the positive z-axis direction.

$$for\ i = 1 \dots n: \quad w_i = C_{4i-3} + C_{4i-2}x + C_{4i-1}x^2 + C_{4i}x^3 - \frac{qx^4}{24EI}$$

$$for\ i = 1 \dots n: \quad \varphi_i = -C_{4i-2} - 2C_{4i-1}x - 3C_{4i}x^2 + \frac{qx^3}{6EI}$$

$$for\ i = 1 \dots n: \quad M_i = -2EIC_{4i-1} - 6EIC_{4i}x + \frac{qx^2}{2}$$

$$for\ i = 1 \dots n: \quad V_i = -6EIC_{4i} + qx$$

In order to derive the integration coefficients, it is necessary to establish boundary- and interface conditions. The specific conditions depend on whether a model with or without slipping between the UCF and retaining wall is used.

B.1 Beam model without slipping between UCF and retaining wall

Figure B.1 illustrates a non-slipping beam model with n fields, where the length of each field is depicted with L. Figure B.2 illustrates small sections of the beam located at a boundary between the UCF and retaining wall or an interface between two fields. These sections are used to derive the boundary and interface conditions.

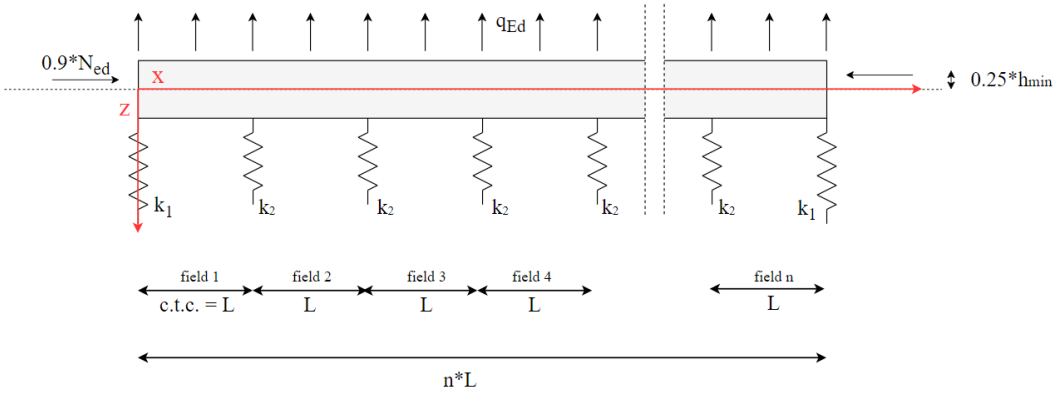

Figure B.1: Beam model for non-slipping UCF

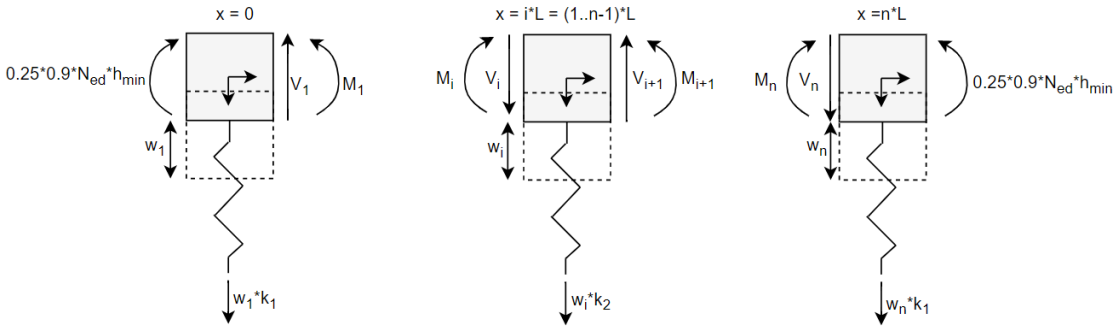

Figure B.2: Sections at boundary or interface

The following boundary and interface conditions are obtained from the sections in figure B.2:

- BC: $M_{x=0} = 0.9 * N_{ed} * 0.25 * h_{min}$
- BC: $M_{x=n*L} = 0.9 * N_{ed} * 0.25 * h_{min}$
- BC: $V_{x=0} = k_1 * w_1$
- BC: $V_{x=n*L} = -k_1 * w_n$
- IC: $for\ i = 1 \ldots . n-1$: $w_i = w_{i+1}$
- IC: $for\ i = 1 \ldots . n-1$: $\varphi_i = \varphi_{i+1}$
- IC: $for\ i = 1 \ldots . n-1$: $M_i = M_{i+1}$
- IC: $for\ i = 1 \ldots . n-1$: $V_i = V_{i+1} - k_2 * w_i$

This results in n*4 boundary/interface conditions, which is sufficient for the determination of all integration coefficients. These coefficients can be obtained by solving a system of equations represented by a matrix and vectors. Once obtained, the integration coefficients can be substituted in the formulas for w_i, φ_i, M_i and V_i to plot the force distribution and displacements. The parametrized matrix and vectors are given on the next page.

4 ∗ n
4 ∗ n
i = 1
i = 2
i = 3
i = n − 1
=
∗

B.2 Beam model with slipping between UCF and retaining wall

The slipping beam model differs from the non-slipping model in that no bending moments are applied to the edges due to the centrically applied normal force. Additionally, the forces caused by the extension of the retaining wall spring are replaced with a maximum attainable friction force between the UCF and the retaining wall. The equations used to describe the force distribution and interface conditions remain the same, but the boundary conditions are different and can be obtained from the sections in figure B.4.

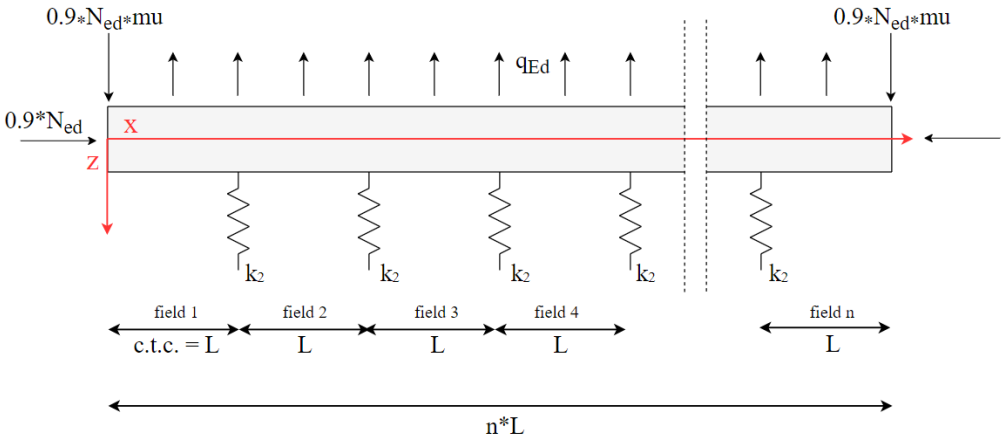

Figure B.3: Beam model for slipping UCF

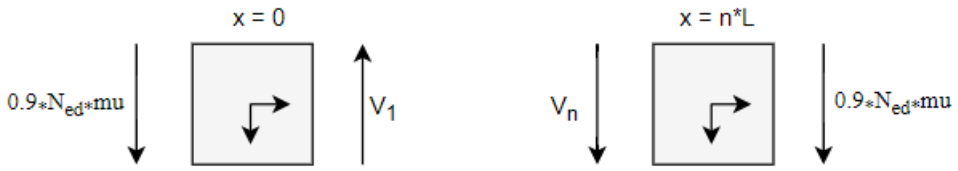

Figure B.4: boundary sections UCF

The following boundary and interface conditions are obtained from the sections in figure B.2:

- BC: $M_{x=0} = 0$
- BC: $M_{x=n*L} = 0$
- BC: $V_{x=0} = 0.9 * N_{Ed} * \mu$
- BC: $V_{x=n*L} = -0.9 * N_{Ed} * \mu$
- IC: $for\ i = 1 \ldots . n-1$: $w_i = w_{i+1}$
- IC: $for\ i = 1 \ldots . n-1$: $\varphi_i = \varphi_{i+1}$
- IC: $for\ i = 1 \ldots . n-1$: $M_i = M_{i+1}$
- IC: $for\ i = 1 \ldots . n-1$: $V_i = V_{i+1} - k_2 * w_i$

This again results in n*4 boundary/interface conditions, which is sufficient for the determination of all integration coefficients. The system of equations expressed as a matrix and vectors is given on the next page. Solving and substituting the integration coefficients gives the force distribution.

Matrix size: 4 ∗ n × 4 ∗ n. Coloured blocks: i = 1, i = 2, i = 3, i = n − 1.

$$
\begin{bmatrix}
0 & 0 & -2EI & 0 & 0 & 0 & 0 & 0 & 0 & 0 & 0 & 0 & \cdots & 0 & 0 & 0 & 0 \\
0 & 0 & 0 & -6EI & 0 & 0 & 0 & 0 & 0 & 0 & 0 & 0 & \cdots & 0 & 0 & 0 & 0 \\
1 & iL & (iL)^2 & (iL)^3 & -1 & -iL & -(iL)^2 & -(iL)^3 & 0 & 0 & 0 & 0 & \cdots & 0 & 0 & 0 & 0 \\
0 & -1 & -2iL & -3(iL)^2 & 0 & 1 & 2iL & 3(iL)^2 & 0 & 0 & 0 & 0 & \cdots & 0 & 0 & 0 & 0 \\
0 & 0 & -2EI & -6EIiL & 0 & 0 & 2EI & 6EIiL & 0 & 0 & 0 & 0 & \cdots & 0 & 0 & 0 & 0 \\
k_2 & k_2iL & k_2(iL)^2 & k_2(iL)^3-6EI & 0 & 0 & 0 & 6EI & 0 & 0 & 0 & 0 & \cdots & 0 & 0 & 0 & 0 \\
0 & 0 & 0 & 0 & 1 & iL & (iL)^2 & (iL)^3 & -1 & -iL & -(iL)^2 & -(iL)^3 & \cdots & 0 & 0 & 0 & 0 \\
0 & 0 & 0 & 0 & 0 & -1 & -2iL & -3(iL)^2 & 0 & 1 & 2iL & 3(iL)^2 & \cdots & 0 & 0 & 0 & 0 \\
0 & 0 & 0 & 0 & 0 & 0 & -2EI & -6EIiL & 0 & 0 & 2EI & 6EIiL & \cdots & 0 & 0 & 0 & 0 \\
0 & 0 & 0 & 0 & k_2 & k_2iL & k_2(iL)^2 & k_2(iL)^3-6EI & 0 & 0 & 0 & 6EI & \cdots & 0 & 0 & 0 & 0 \\
0 & 0 & 0 & 0 & 0 & 0 & 0 & 0 & 1 & iL & (iL)^2 & (iL)^3 & \cdots & 0 & 0 & 0 & 0 \\
0 & 0 & 0 & 0 & 0 & 0 & 0 & 0 & 0 & -1 & -2iL & -3(iL)^2 & \cdots & 0 & 0 & 0 & 0 \\
0 & 0 & 0 & 0 & 0 & 0 & 0 & 0 & 0 & 0 & -2EI & -6EIiL & \cdots & 0 & 0 & 0 & 0 \\
0 & 0 & 0 & 0 & 0 & 0 & 0 & 0 & k_2 & k_2iL & k_2(iL)^2 & k_2(iL)^3-6EI & \cdots & 0 & 0 & 0 & 0 \\
\vdots & \vdots & \vdots & \vdots & \vdots & \vdots & \vdots & \vdots & \vdots & \vdots & \vdots & \vdots & \ddots & \vdots & \vdots & \vdots & \vdots \\
0 & 0 & 0 & 0 & 0 & 0 & 0 & 0 & 0 & 0 & 0 & 0 & \cdots & -1 & -iL & -(iL)^2 & -(iL)^3 \\
0 & 0 & 0 & 0 & 0 & 0 & 0 & 0 & 0 & 0 & 0 & 0 & \cdots & 0 & 1 & 2iL & 3(iL)^2 \\
0 & 0 & 0 & 0 & 0 & 0 & 0 & 0 & 0 & 0 & 0 & 0 & \cdots & 0 & 0 & 2EI & 6EIiL \\
0 & 0 & 0 & 0 & 0 & 0 & 0 & 0 & 0 & 0 & 0 & 0 & \cdots & 0 & 0 & 0 & 6EI \\
0 & 0 & 0 & 0 & 0 & 0 & 0 & 0 & 0 & 0 & 0 & 0 & \cdots & 0 & 0 & -2EI & -6EInL \\
0 & 0 & 0 & 0 & 0 & 0 & 0 & 0 & 0 & 0 & 0 & 0 & \cdots & 0 & 0 & 0 & -6EI
\end{bmatrix}
*
\begin{bmatrix}
C_{4i-3} \\ C_{4i-2} \\ C_{4i-1} \\ C_{4i} \\ C_{4i-3} \\ C_{4i-2} \\ C_{4i-1} \\ C_{4i} \\ C_{4i-3} \\ C_{4i-2} \\ C_{4i-1} \\ C_{4i} \\ C_{4i-3} \\ C_{4i-2} \\ \vdots \\ C_{4i-1} \\ C_{4i} \\ C_{4n-3} \\ C_{4n-2} \\ C_{4n-1} \\ C_{4n}
\end{bmatrix}
=
\begin{bmatrix}
0 \\ 0.9N_{Ed}\mu \\ 0 \\ 0 \\ 0 \\ k_2q(iL)^4/24EI \\ 0 \\ 0 \\ 0 \\ k_2q(iL)^4/24EI \\ 0 \\ 0 \\ 0 \\ k_2q(iL)^4/24EI \\ \vdots \\ 0 \\ 0 \\ 0 \\ k_2q(iL)^4/24EI \\ -q(nL)^2/2 \\ -0.9N_{Ed}\mu - qnL
\end{bmatrix}
$$

Annex C: Materials savings expressed in percentages

This annex includes additional graphs that are supplementary to the ones presented in chapter five of the main report. The latter illustrate potential material savings by calculating the difference in required floor thickness between a UCF and SFUCF, and express the results in meters of floor thickness saved when applying a SFUCF. The data behind the graphs in this annex is the same as for the graphs in chapter five, however material savings are expressed in percentages. The formula used to calculate the reduction is:

$$saved\ concrete\ [\%] = 100 - \frac{100 * h_{min,req,SFUCF}}{h_{min,req,UCF}}$$

Standard values of parameters which occur commonly in practice are used as basis for comparison. To demonstrate how each variable affects the possible material savings, it will be changed within a representable domain. The standard set of parameters is listed below and uses dish anchors as standard connection type:

- c.t.c. = 2.50 m
- p_{head} = 0.00 m
- k_3 = 35000 kN/m²
- p = 0.25 m
- a_r = 0.085 m
- tol_{top} = 0.150 m
- tol_{bottom} = 0.075 m
- $tol_{anchorage}$ = 0.100 m

Results in these graphs are derivatives of the graphs presented in the main report. Therefore discussion on the results can be found in chapter five.

Saved concrete [%] – Changing the c.t.c. distance

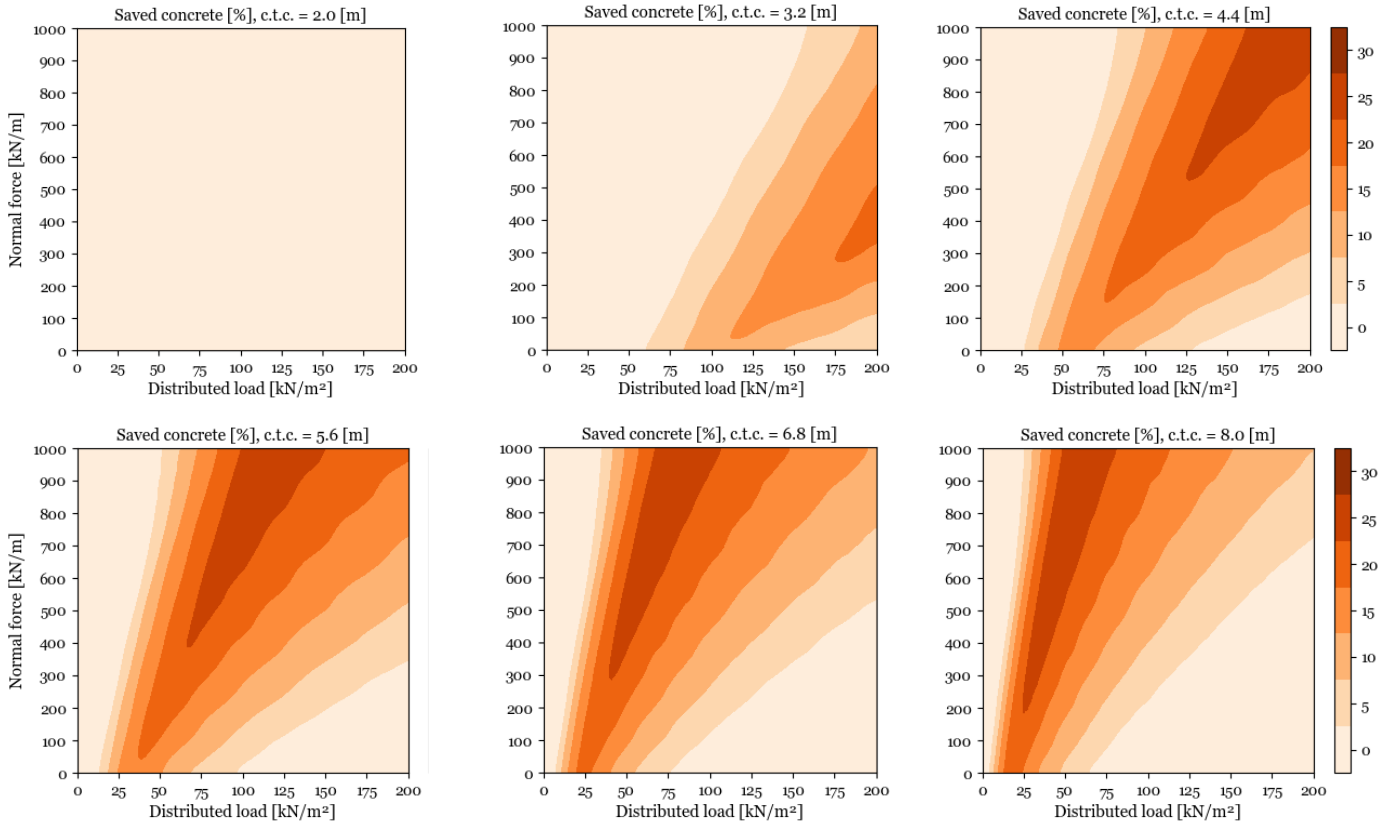

Saved concrete [%] – Changing p_{head}

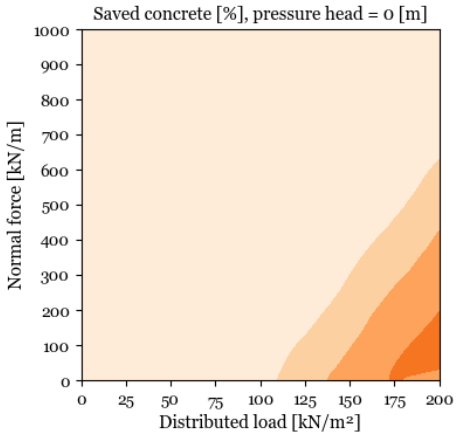

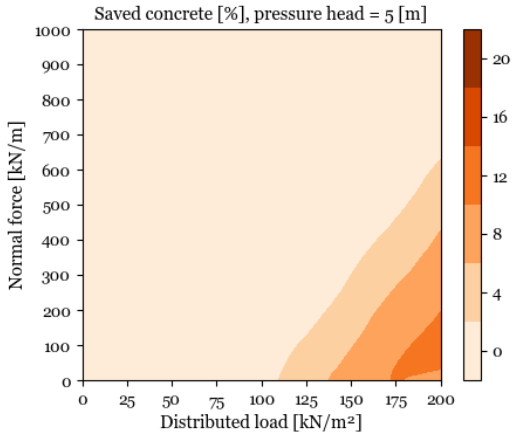

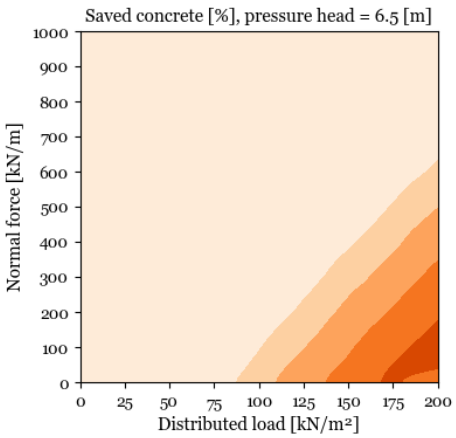

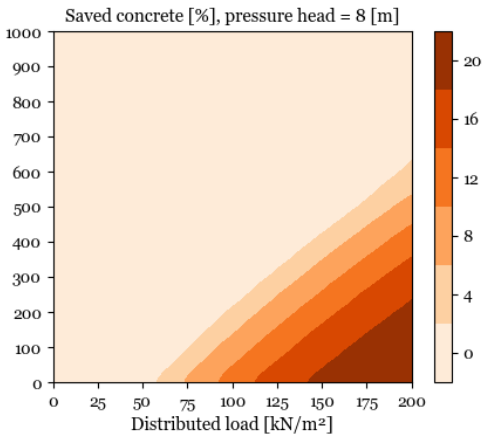

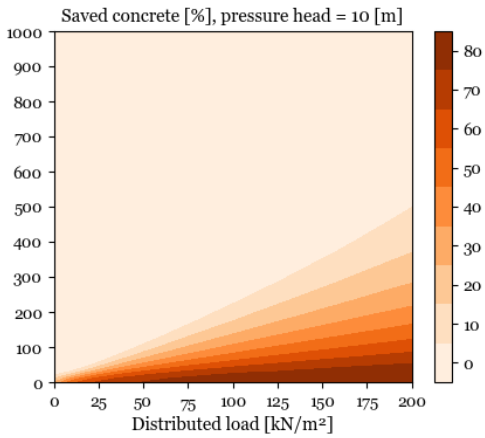

Saved concrete [%] – Changing k_3

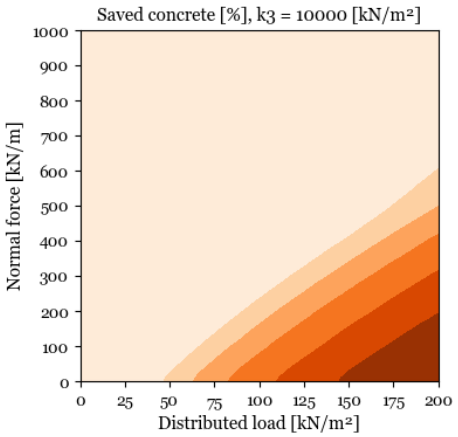

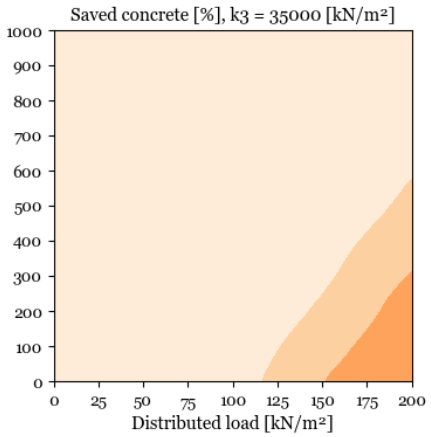

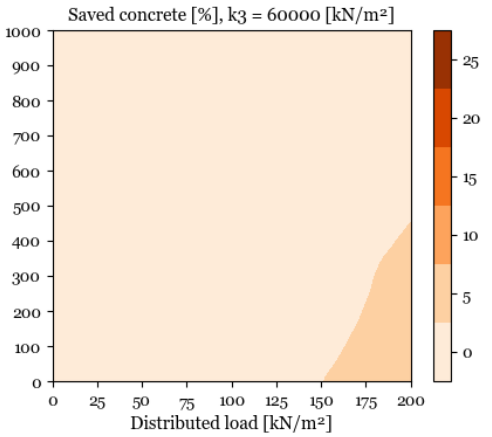

Saved concrete [%] – Changing p

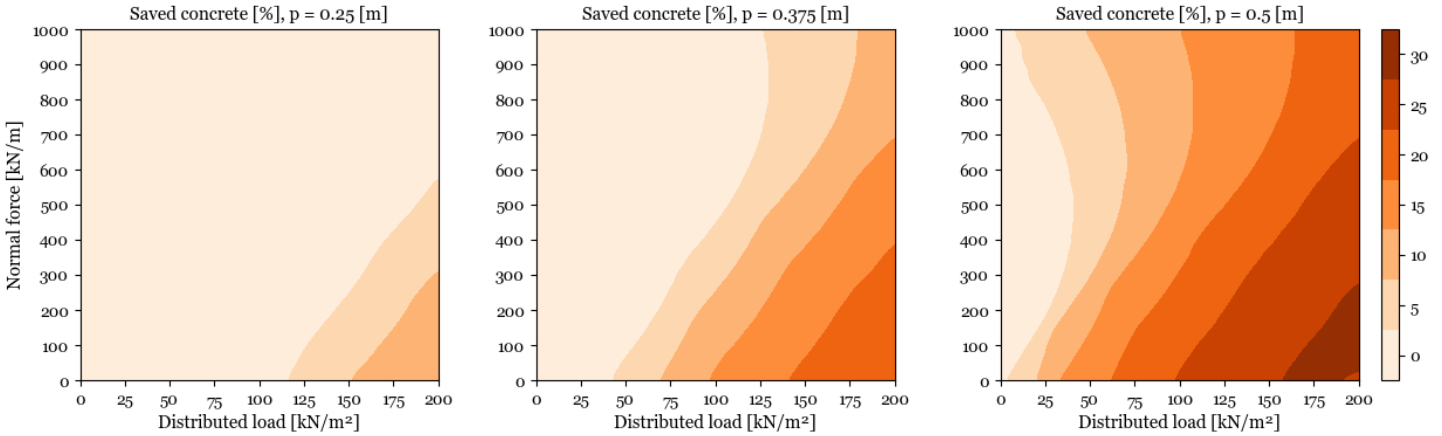

Saved concrete [%] – Changing connection type

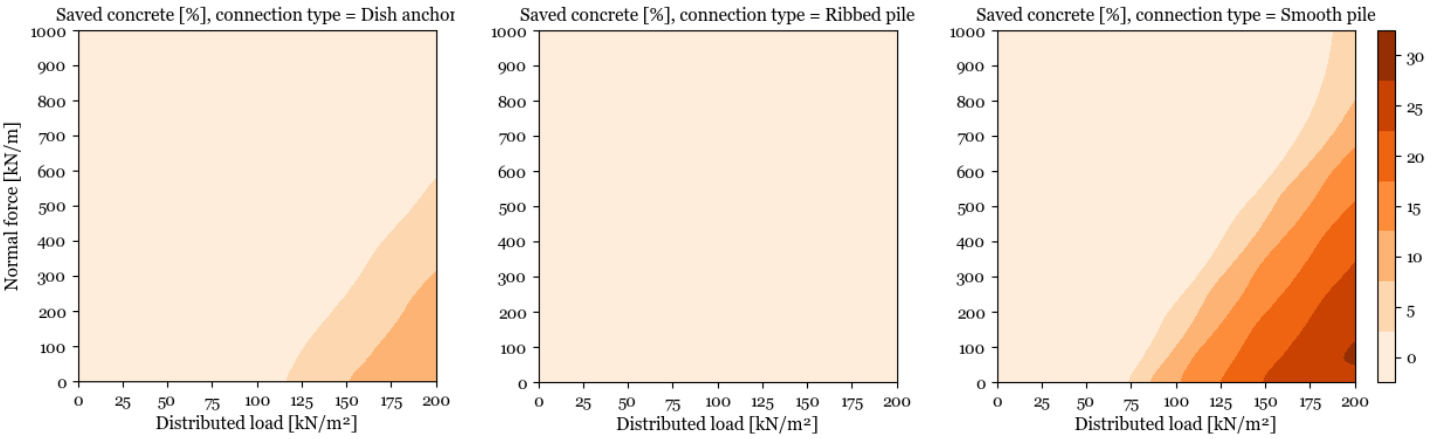

Saved concrete [%] – Changing a_r

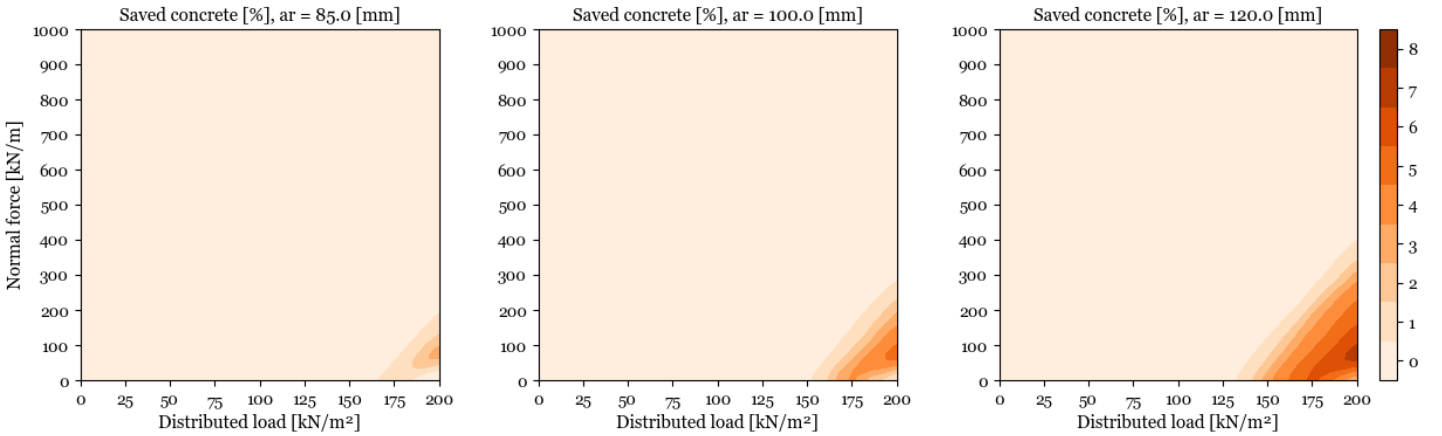

Annex D: Test results Botlekspoortunnel

This Annex contains the results of 4 point bending tests that were performed to calculate post-cracking tensile strength of a concrete mix used at Botklekspoortunnel. These tests are the basis for the post-cracking tensile strength that is used to answer the research question of this thesis.

Four point bending tests

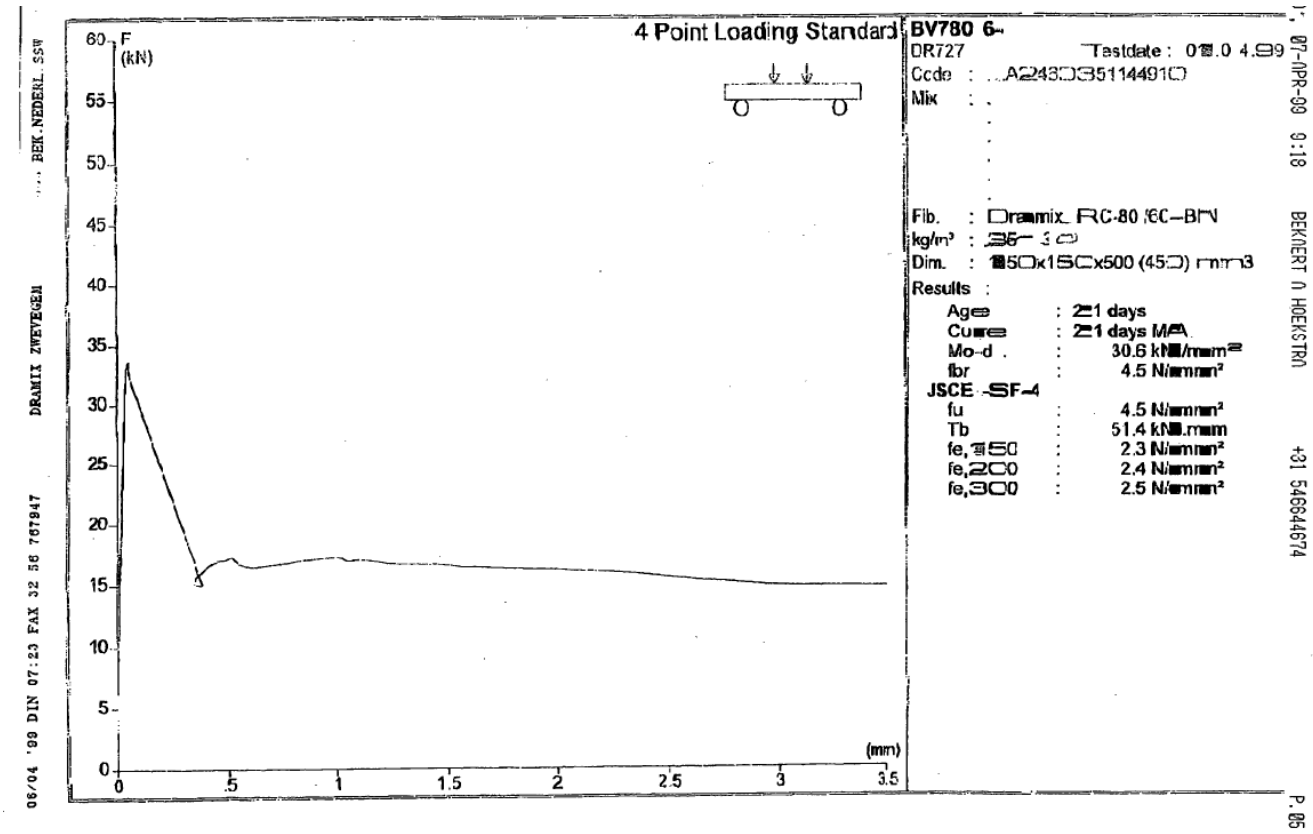

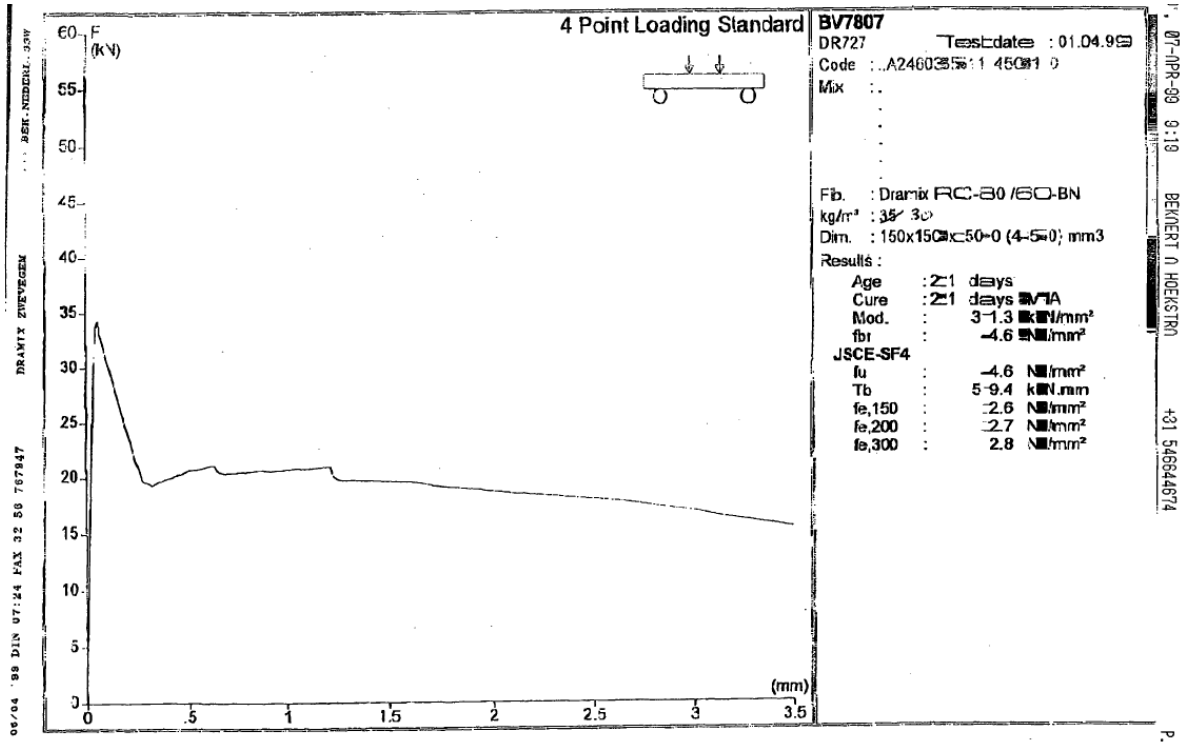
4 Point Loading Standard
BV7807
DR727
Testdate : 01.04.99
Code : ..A24603
Mix : . .
Fib. : Dramix RC-80 /60-BN
kg/m³ : 35 30
Dim. : 150x150x500 (450); mm3
Results :
Age : 21 days
Cure : 21 days
Mod. : 31.3
fbr : 4.6
JSCE-SF4
fu : 4.6
Tb : 59.4 kN.mm
fe,150 : 2.6
fe,200 : 2.7
fe,300 : 2.8
F (kN)
(mm)
07-APR-99 9:19
BEKAERT N HOEKSTRA
+31 56644674
P. 06

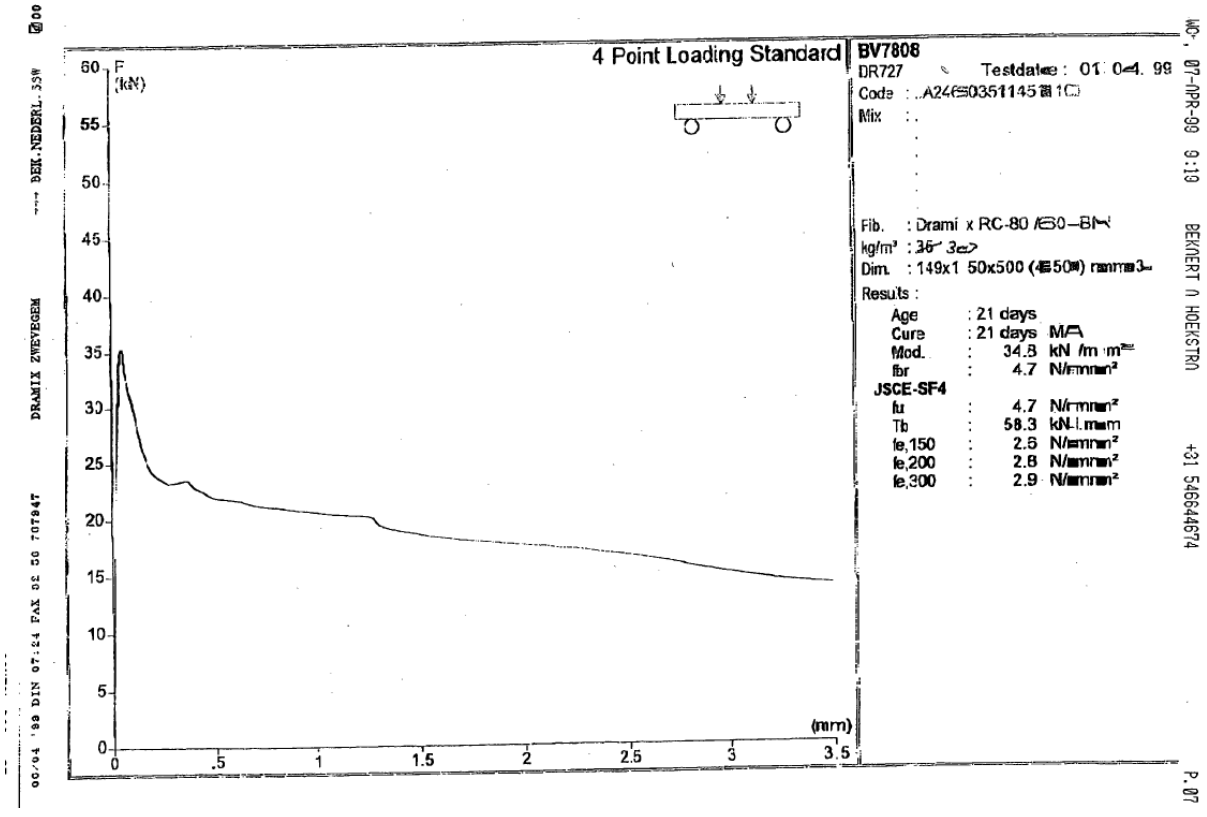
4 Point Loading Standard
BV7808
DR727
Testdate : 01.04.99
Code : ..A24603
Mix : . .
Fib. : Dramix RC-80 /60-BN
kg/m³ : 35 30
Dim. : 149x150x500 (450) mm3
Results :
Age : 21 days
Cure : 21 days
Mod. : 34.8 kN /mm²
fbr : 4.7 N/mm²
JSCE-SF4
fu : 4.7 N/mm²
Tb : 58.3 kN.mm
fe,150 : 2.6 N/mm²
fe,200 : 2.8 N/mm²
fe,300 : 2.9 N/mm²
F (kN)
(mm)
07-APR-99 9:19
BEKAERT N HOEKSTRA
+31 56644674
P. 07

Compressive strength

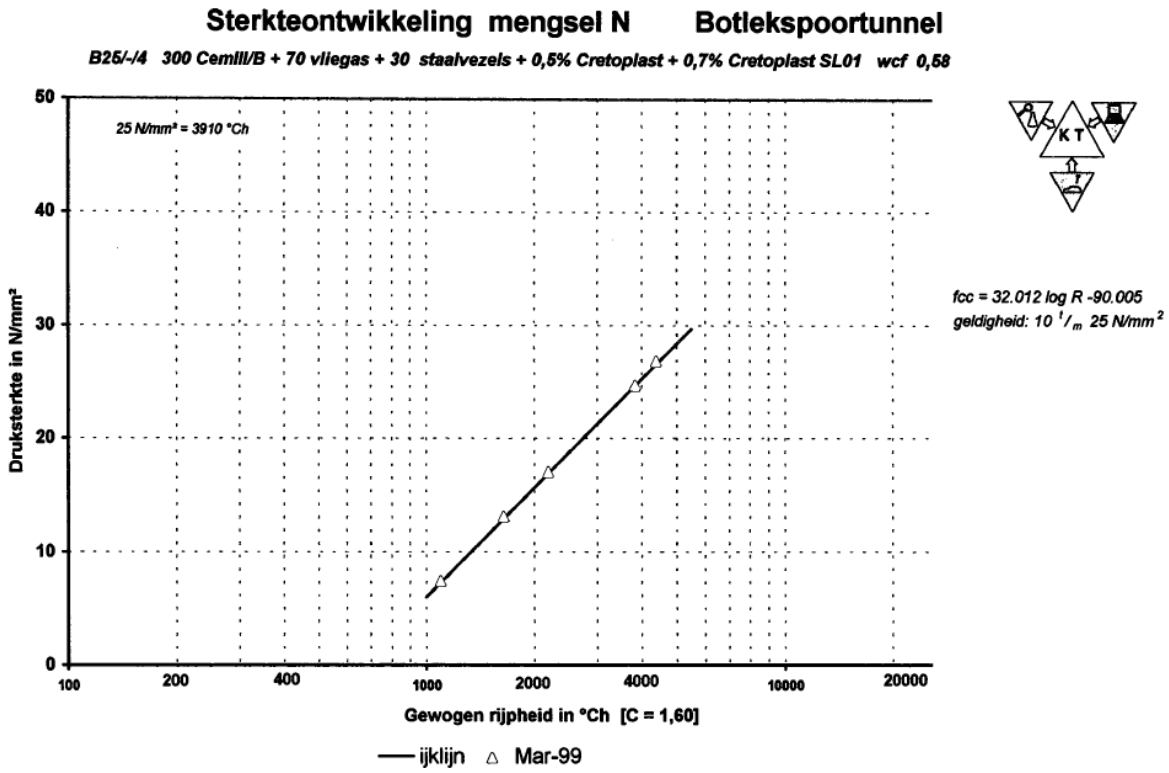

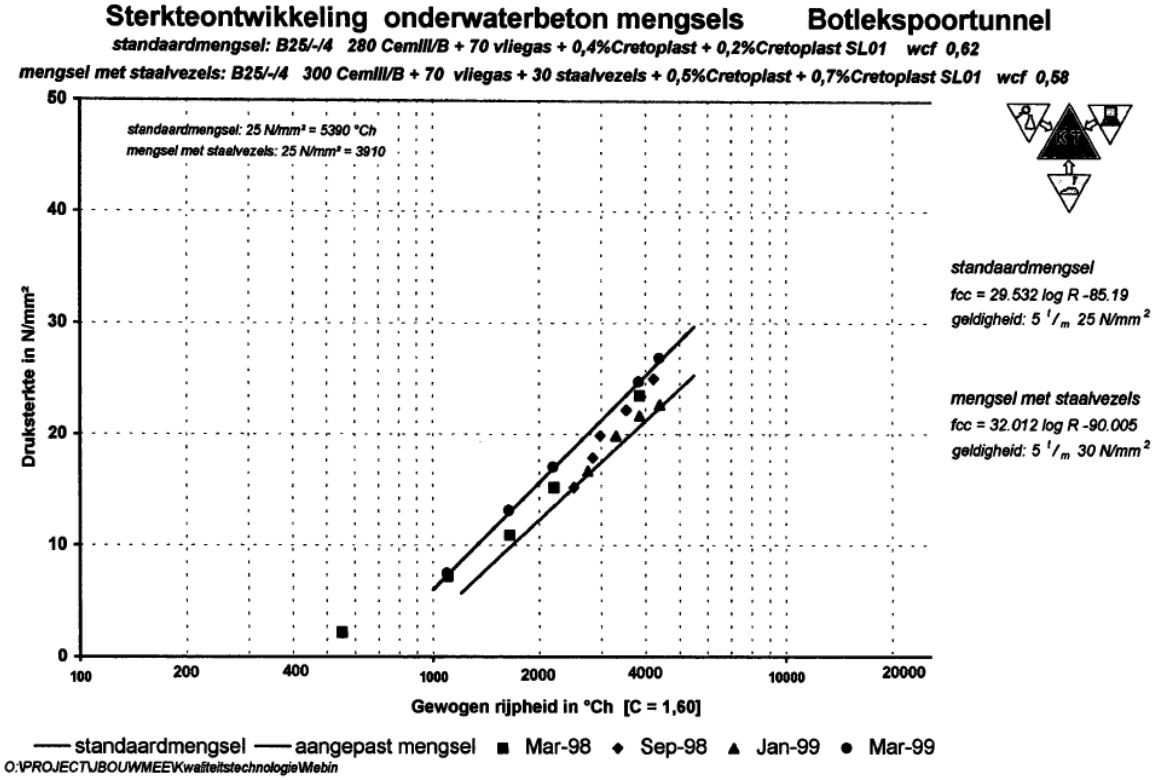

Workability

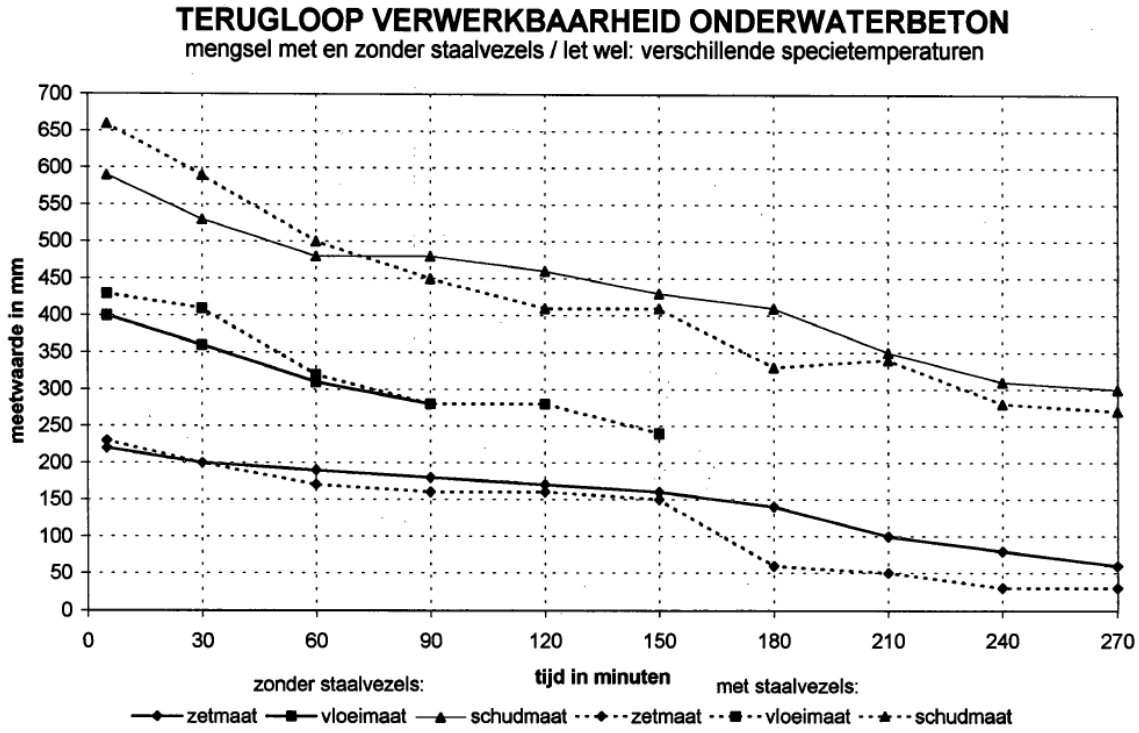

Annex E: Automatically generated calculation report case study

This annex does not contain the supplementary Excel file that should be used as input for the optimization tool because all required input is described in paragraph 7.2.

Price-based optimization UCF

This document presents results of an iterative calculation process to finding the most cost-effective set of parameters for the design of a UCF.

Project: Case study Rotterdamsebaan
Author: Pim van Starrenburg
Date: 01/03/2023

1. Parameters

Table 1: Case-specific parameters (user input)

Parameter	Value	Unit
$length_x$	29.46	[m]
$length_y$	30.67	[m]
top pit	1.5	[m]
top UCF	-15.45	[m]
pressure head	12.95	[m]
N_x	1100	[kN/m]
N_y	1170	[kN/m]
μ_x	0.3	[-]
μ_y	0.3	[-]
f_y	505	[N/mm²]
$k_{1,x}$	60000	[kN/m]
$k_{1,y}$	100000	[kN/m]
k_3	0	[kN/m²]
Consequence class	2	[-]
tol_{bottom}	0.15	[m]
tol_{top}	0.075	[m]
$tol_{anchorage}$	0.1	[m]
estimated pile length	27.5	[m]

Table 2: safety factors for load combinations

Loadtype	γ_{ULS}	γ_{SLS}
Self-weight	0.9	1.0
Water pressure	1.2	1.0
Heave	1.35	1.0
Strutting force	0.9	1.0
Distributed load [kN/m²]	**146.5**	**116.2**

For material prices and iterable connection types with corresponding geometric properties and spring stiffnesses, refer to the supplementary Excel file supplied by the author.

2. Results

2.1: Optimal parameters

Table 3: Iterative Parameters & resulting optimal value

Parameter	Values	Unit	Optimal
h_{nom}	[0.8 0.825 0.85 0.875 0.9 0.925 0.95 0.975 1.0 1.025 1.05 1.075 1.1 1.125 1.15 1.175 1.2 1.225 1.25 1.275 1.3 1.325 1.35 1.375 1.4 1.425 1.45 1.475 1.5]	[m]	**1.025**
s_x	[4 5 6 7 8 9 10 11 12 13 14]	[-]	**13**
s_y	[5 6 7 8 9 10 11 12 13 14 15]	[-]	**9**
Concrete class	['C20/25', 'C25/30', 'C30/37']	[-]	**C30/37**
Connection type	['Dish anchor']	[-]	**Dish anchor**
c	[0.1, 0.2, 0.4, 0.5]	[-]	**-**
a_r	[0.085, 0.09, 0.095, 0.1, 0.105, 0.12]	[m]	**-**
p	[tol_{top} + $tol_{anchorage}$, …, …., h_{min}/2]	[m]	**0.175**
$D_{Smooth\ pile}$	Refer to supplementary Excel-file	[m]	**-**
$B_{Concrete\ ribbed\ pile}$	Refer to supplementary Excel-file	[m]	**-**
$D_{Ribbed\ steel\ pile}$	Refer to supplementary Excel-file	[m]	**-**
$D_{Dish\ anchor}$	Refer to supplementary Excel-file	[m]	**0.0635**
$d_{Dish\ anchor}$	Refer to supplementary Excel-file	[m]	**0.35**
k_2	Refer to supplementary Excel-file	[m]	**50000**

Addition of steel fibres: **No**
Long span check: **Yes**

In case the long span check equals “Yes”, Check A on page 8 may be neglected. In case long span check equals “No”, the results on pages 9-13 may be neglected.

2.2 Overview of construction

Figure 1: Cross-section along short span

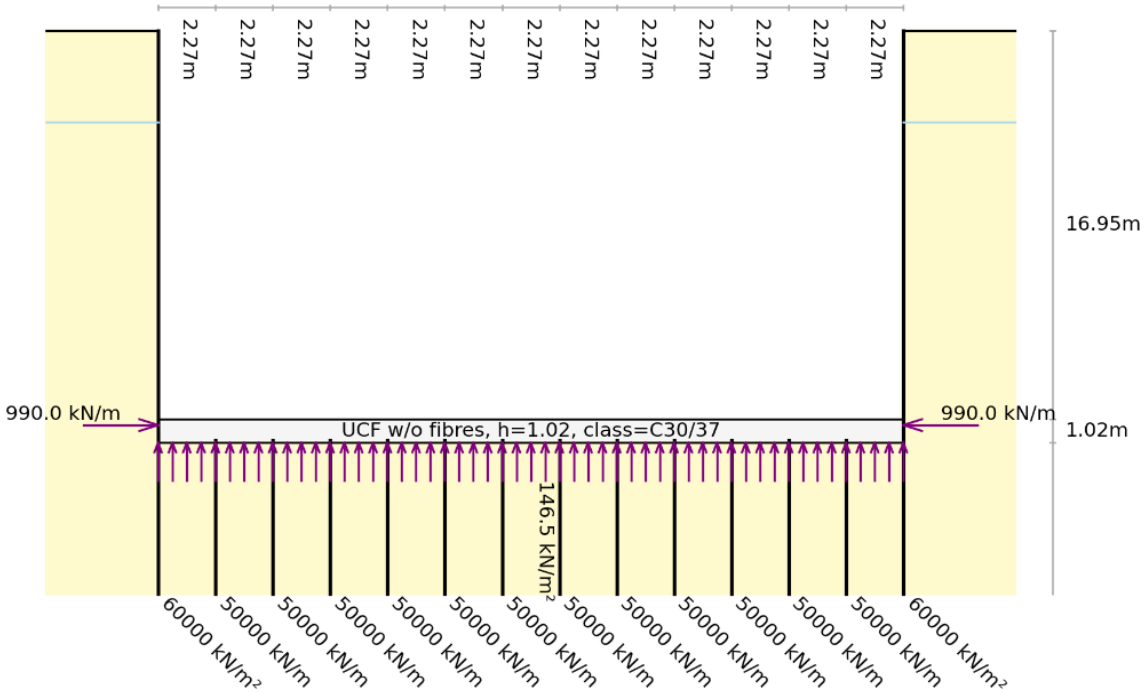

Figure 2: Cross-section along long span

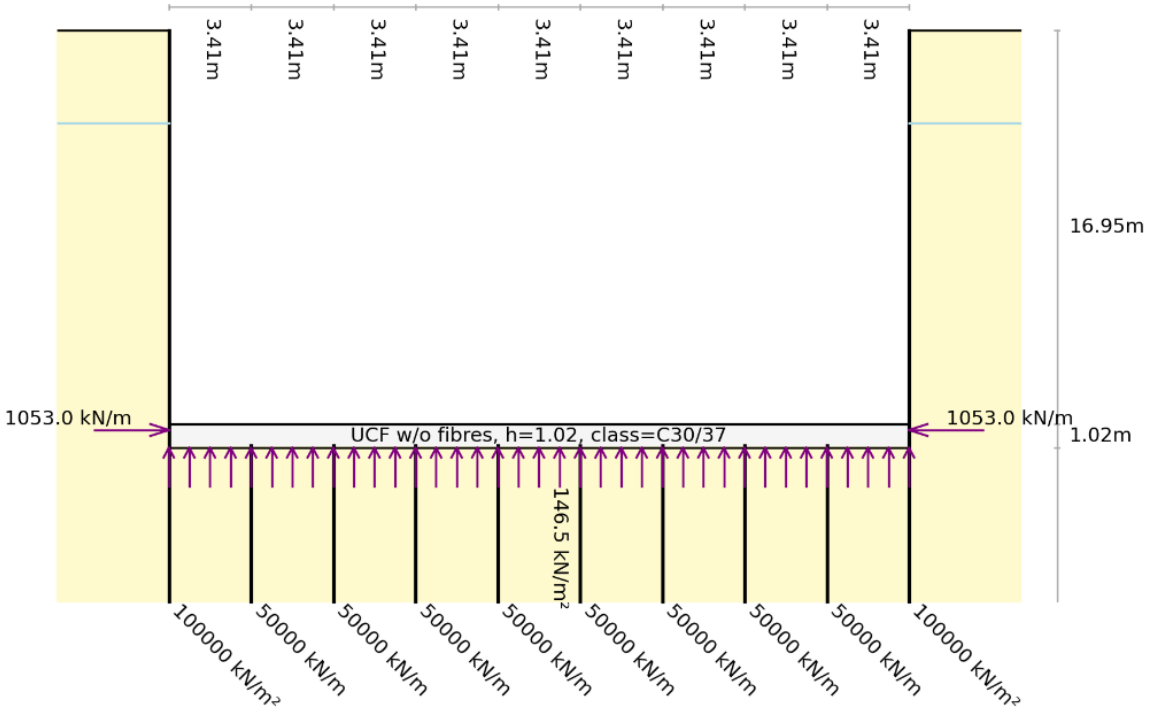

3. Short span, check B

In case p_{head} > 10m, Check B3 may be ignored. Check FB may be ignored if the optimal set of parameters does not include the addition of steel fibres.

Check	Unity Check No Slip	Unity Check Slip
B1	5.4	2.64
B2	0.19	0.19
B3	0.21	0.21
FB	0.13	0.13

Figure 3: Moment distribution no slip

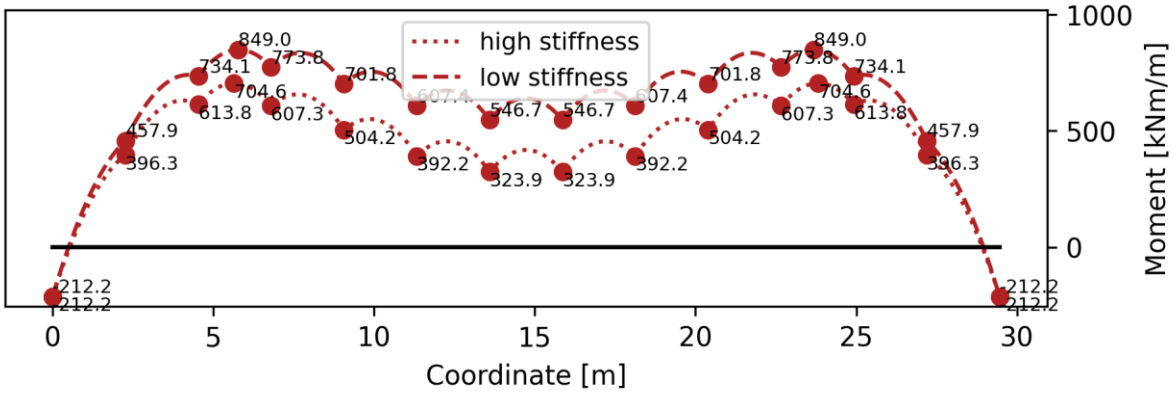

Figure 4: Moment distribution slip

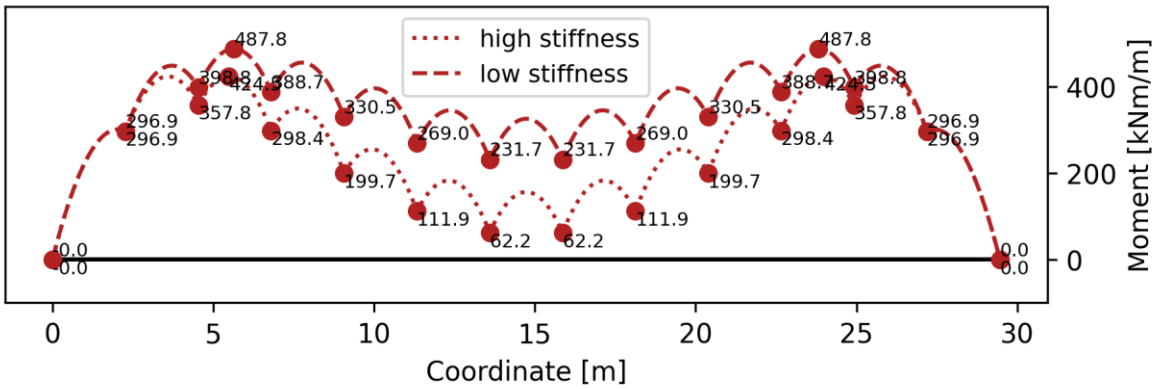

Figure 5: Check B3

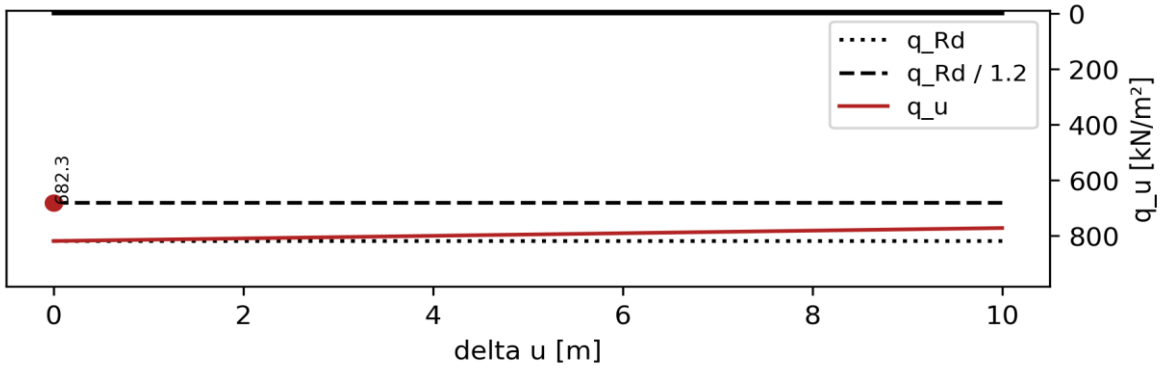

Check B1 No Slip:

h_{min}	=	0.86		[m]
M_{Ed}	=	848.99		[kNm/m]
N_{Ed}	=	990.0		[kN/m]
σ_{Ed}	=	$6 * M_{Ed} / h_{min}^2 - N_{Ed} / h_{min}$	= 5.78	[N/mm²]
UC	=	σ_{Ed} / f_{ctd}	= **5.4**	[-]

Check B2 No Slip

z	=	0.49		[m]
M_{Ed}	=	$q_{ULS} * (length_x / s_x)^2 / 8$	= 94.03	[kNm/m]
M_{Rd}	=	$z * N_{Ed}$	= 485.1	[kN/m]
UC	=	M_{Ed} / M_{Rd}	= **0.19**	[-]

Check B3 No Slip

$q_{u,max}$	=	818.71		[kN/m²]
q_{Rd}	=	$q_{u,max} / 1.2$	= 682.26	[kN/m²]
UC	=	q_{ULS} / q_{Rd}	= **0.21**	[-]

Check FB No Slip

M_{cr}	=	263.81		[kNm]
M_p	=	514.0		[kNm]
q_{Rd}	=	$8*(M_{cr}/1.25 + M_p) / c.t.c.^2$		[kN/m]
UC	=	q_{ULS} / q_{Rd}	= **0.13**	[-]

Check B1 Slip:

h_{min}	=	0.86		[m]
M_{Ed}	=	487.82		[kNm/m]
N_{Ed}	=	990.0		[kN/m]
σ_{Ed}	=	$6 * M_{Ed} / h_{min}^2 - N_{Ed} / h_{min}$	= 2.83	[N/mm²]
UC	=	σ_{Ed} / f_{ctd}	= **2.64**	[-]

Check B2 Slip

z	=	0.49		[m]
M_{Ed}	=	$q_{ULS} * (length_x / s_x)^2 / 8$	= 94.03	[kNm/m]
M_{Rd}	=	$z * N_{Ed}$	= 485.1	[kN/m]
UC	=	M_{Ed} / M_{Rd}	= **0.19**	[-]

Check B3 Slip

$q_{u,max}$	=	818.71		[kN/m²]
q_{Rd}	=	$q_{u,max} / 1.2$	= 682.26	[kN/m²]
UC	=	q_{ULS} / q_{Rd}	= **0.21**	[-]

Check FB Slip

M_{cr}	=	263.81		[kNm]
M_p	=	514.0		[kNm]
q_{Rd}	=	$8*(M_{cr}/1.25 + M_p) / c.t.c.^2$		[kN/m]
UC	=	q_{ULS} / q_{Rd}	= **0.13**	[-]

4. Short span, check C

Check C2 may be ignored in case check C suffices.

Check	Unity Check No Slip	Unity Check Slip
C1	0.76	0.39
C2a	0	0
C2b	0.46	0.46
C2c	0.31	0.31

Figure 6: Shear force distribution no slip

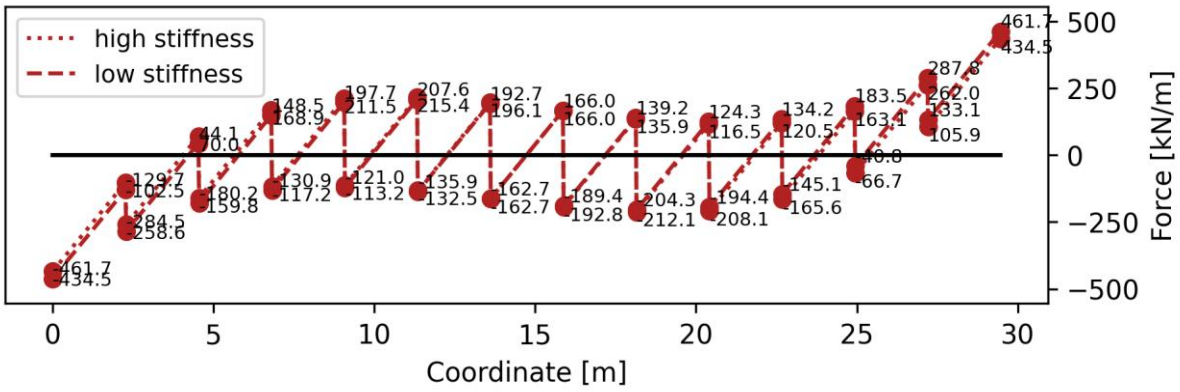

Figure 7: Shear force distribution slip

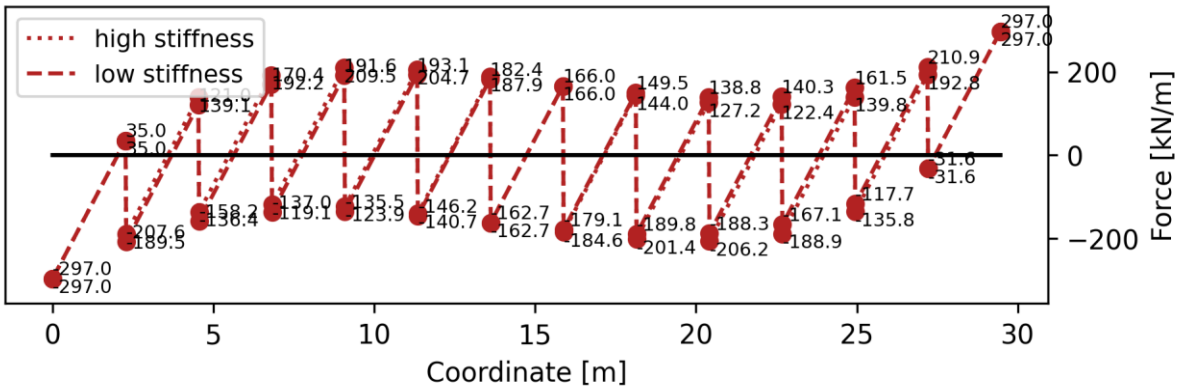

Figure 8: Principal stress

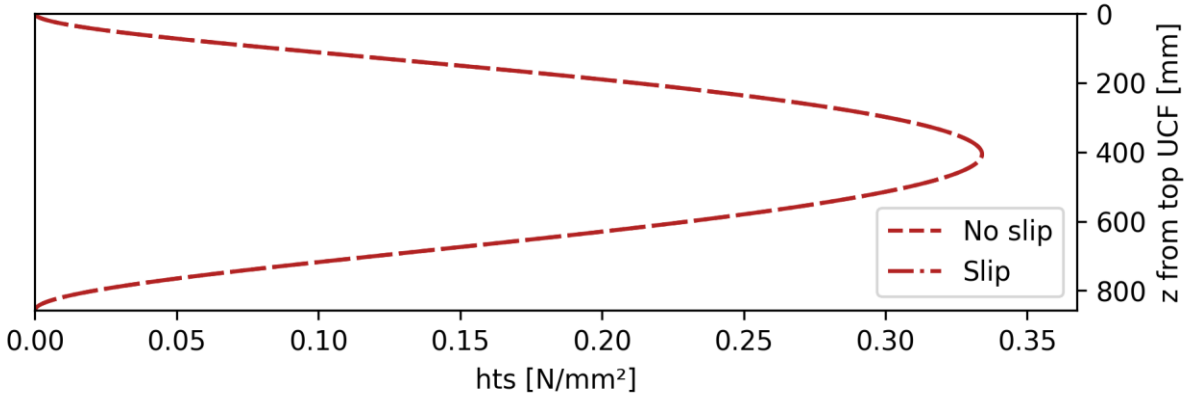

Check C1 No Slip

V_{Ed}	=	338.86		[kN/m]
k	=	$\min(1 + (200 / h_{min})^{0.5}, 2.0)$	= 1.48	[-]
v_{min}	=	$0.035 * k^{1.5} * f_{ck}^{0.5}$	= 0.35	[N/mm²]
σ_{cp}	=	$\min(N_{Ed} / h_{min}, 0.2 * f_{cd,pl})$	= 1.15	[N/mm²]
$V_{Rd,c}$	=	$(v_{min} + 0.15 * \sigma_{cp}) * h_{min}$	= 445.31	[kN/m]
UC	=	$V_{Ed} / V_{Rd,c}$	= **0.76**	[-]

Check C2a No Slip

M_{Ed}	=	38.68		[kNm/m]
σ_{Ed}	=	$6 * \lvert M_{Ed}\rvert / h_{min}^2 - N_{Ed} / h_{min}$	= -0.84	[N/mm²]
UC	=	$\sigma_{Ed} / f_{ctd,pl}$	= **0**	[-]

Check C2b No Slip

V_{Ed}	=	401.93		[kN/m]
A_{cc}	=	$\min(h_{min}/2 + N_{Ed}*h_{min}^2/(12*\lvert M_{Ed}\rvert), h_{min}) * 1000$	= 857294.9	[mm²]
τ_{cp}	=	$1.5 * V_{Ed} / A_{cc}$	= 0.7	[N/mm²]
σ_{cp}	=	$N_{Ed} * A_{cc}$	= -1.15	[N/mm²]
f_{cvd}	=	$(f_{ctd,pl}^2 + \sigma_{cp} * f_{ctd,pl})^{0.5}$	= 1.54	[N/mm²]
UC	=	τ_{cp} / f_{cvd}	= **0.46**	[-]

Check C2c No Slip

$\sigma_{1,max}$	=	0.33		[N/mm²]
UC	=	$\sigma_{1,max} / f_{ctd,pl}$	= **0.31**	[-]

Check C1 Slip

V_{Ed}	=	174.18		[kN/m]
k	=	$\min(1 + (200 / h_{min})^{0.5}, 2.0)$	= 1.48	[-]
v_{min}	=	$0.035 * k^{1.5} * f_{ck}^{0.5}$	= 0.35	[N/mm²]
σ_{cp}	=	$\min(N_{Ed} / h_{min}, 0.2 * f_{cd,pl})$	= 1.15	[N/mm²]
$V_{Rd,c}$	=	$(v_{min} + 0.15 * \sigma_{cp}) * h_{min}$	= 445.31	[kN/m]
UC	=	$V_{Ed} / V_{Rd,c}$	= **0.39**	[-]

Check C2a Slip

M_{Ed}	=	38.68		[kNm/m]
σ_{Ed}	=	$6 * \lvert M_{Ed}\rvert / h_{min}^2 - N_{Ed} / h_{min}$	= -0.84	[N/mm²]
UC	=	$\sigma_{Ed} / f_{ctd,pl}$	= **0**	[-]

Check C2b Slip

V_{Ed}	=	401.93		[kN/m]
A_{cc}	=	$\min(h_{min}/2 + N_{Ed}*h_{min}^2/(12*\lvert M_{Ed}\rvert), h_{min}) * 1000$	= 857294.9	[mm²]
τ_{cp}	=	$1.5 * V_{Ed} / A_{cc}$	= 0.7	[N/mm²]
σ_{cp}	=	$N_{Ed} * A_{cc}$	= -1.15	[N/mm²]
f_{cvd}	=	$(f_{ctd,pl}^2 + \sigma_{cp} * f_{ctd,pl})^{0.5}$	= 1.54	[N/mm²]
UC	=	τ_{cp} / f_{cvd}	= **0.46**	[-]

Check C2c Slip

$\sigma_{1,max}$	=	0.33		[N/mm²]
UC	=	$\sigma_{1,max} / f_{ctd,pl}$	= **0.31**	[-]

5. Connection tensile element

Check	Connection type	Unity Check
G	Dish anchor	0.98

6. Short span, SLS Displacements

Figure 9: Displacement No Slip

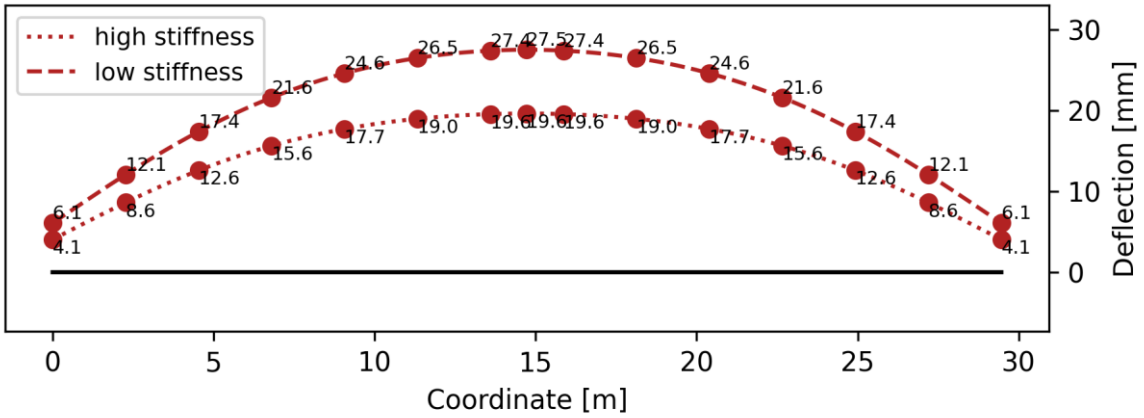

Figure 10: Displacement Slip

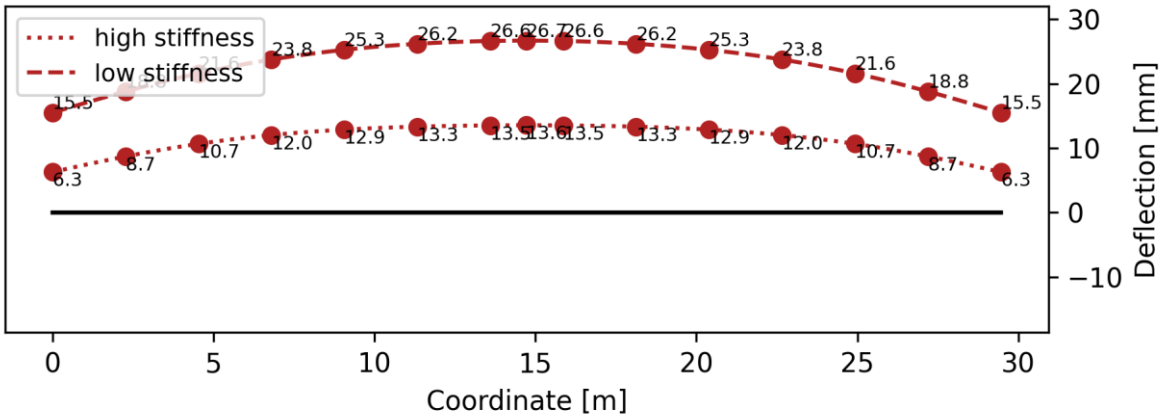

,

7. Long span, check A

This check may be ignored in case longspancheck equals “Yes”

Check	Unity Check
A	1.03

8. Long span, check B

In case p_{head} > 10m, Check B3 may be ignored. Check FB may be ignored if the optimal set of parameters does not include the addition of steel fibres.

Check	Unity Check No Slip	Unity Check Slip
B1	6.02	2.12
B2	0.42	0.42
B3	0.46	0.46
FB	0.28	0.28

Figure 11: Moment distribution no slip

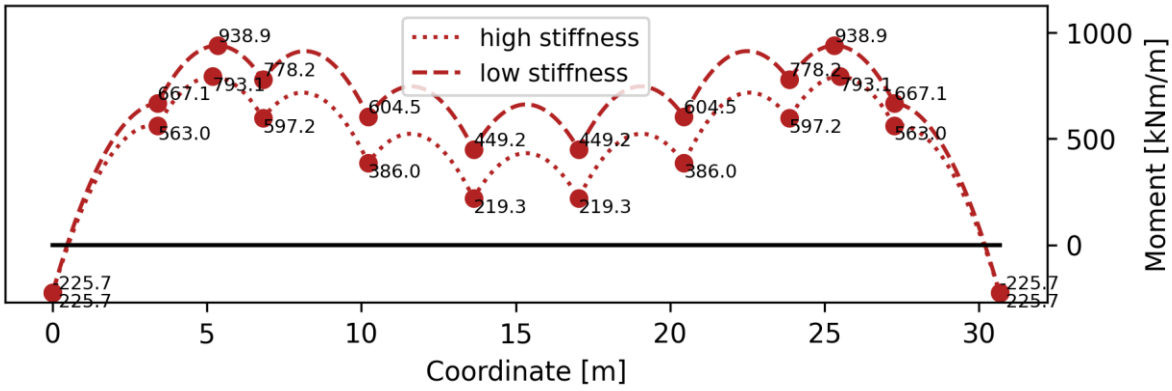

Figure 12: Moment distribution slip

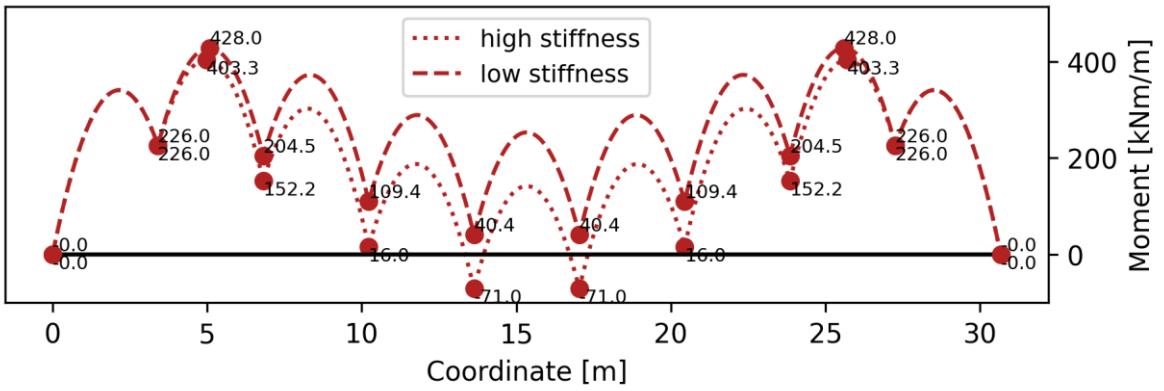

Figure 13: Check B3

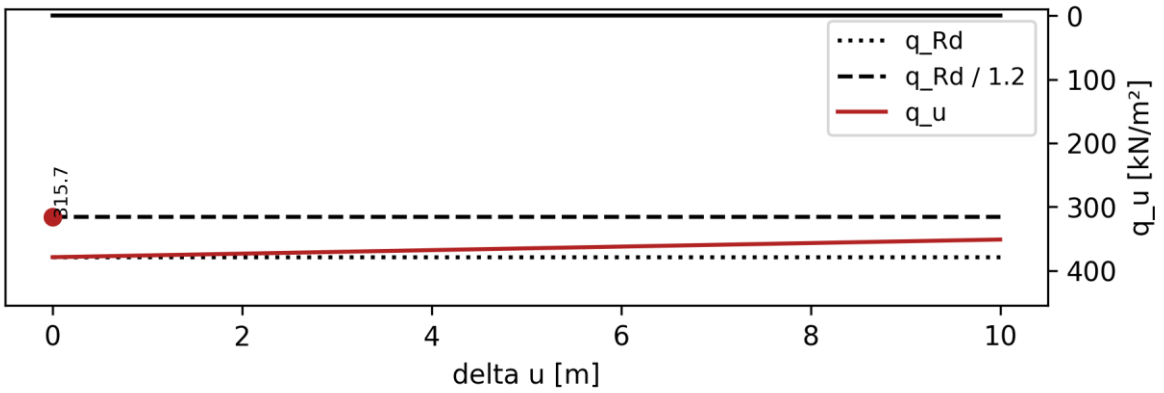

Check B1 No Slip:

h_{min}	=	0.86		[m]
M_{Ed}	=	938.9		[kNm/m]
N_{Ed}	=	1053.0		[kN/m]
σ_{Ed}	=	$6 * M_{Ed} / h_{min}^2 - N_{Ed} / h_{min}$	= 6.44	[N/mm²]
UC	=	σ_{Ed} / f_{ctd}	= **6.02**	[-]

Check B2 No Slip

z	=	0.49		[m]
M_{Ed}	=	$q_{ULS} * (length_y / s_y)^2 / 8$	= 212.64	[kNm/m]
M_{Rd}	=	$z * N_{Ed}$	= 508.6	[kN/m]
UC	=	M_{Ed} / M_{Rd}	= **0.42**	[-]

Check B3 No Slip

$q_{u,max}$	=	378.82		[kN/m²]
q_{Rd}	=	$q_{u,max} / 1.2$	= 315.68	[kN/m²]
UC	=	q_{ULS} / q_{Rd}	= **0.46**	[-]

Check FB No Slip

M_{cr}	=	272.81		[kNm]
M_p	=	534.0		[kNm]
q_{Rd}	=	$8*(M_{cr}/1.25 + M_p) / c.t.c.^2$		[kN/m]
UC	=	q_{ULS} / q_{Rd}	= **0.28**	[-]

Check B1 Slip:

h_{min}	=	0.86		[m]
M_{Ed}	=	428.0		[kNm/m]
N_{Ed}	=	1053.0		[kN/m]
σ_{Ed}	=	$6 * M_{Ed} / h_{min}^2 - N_{Ed} / h_{min}$	= 2.27	[N/mm²]
UC	=	σ_{Ed} / f_{ctd}	= **2.12**	[-]

Check B2 Slip

z	=	0.48		[m]
M_{Ed}	=	$q_{ULS} * (length_y / s_y)^2 / 8$	= 212.64	[kNm/m]
M_{Rd}	=	$z * N_{Ed}$	= 508.6	[kN/m]
UC	=	M_{Ed} / M_{Rd}	= **0.42**	[-]

Check B3 Slip

$q_{u,max}$	=	378.82		[kN/m²]
q_{Rd}	=	$q_{u,max} / 1.2$	= 315.68	[kN/m²]
UC	=	q_{ULS} / q_{Rd}	= **0.46**	[-]

Check FB Slip

M_{cr}	=	272.81		[kNm]
M_p	=	534.0		[kNm]
q_{Rd}	=	$8*(M_{cr}/1.25 + M_p) / c.t.c.^2$		[kN/m]
UC	=	q_{ULS} / q_{Rd}	= **0.28**	[-]

9. Long span, check C

Check	Unity Check No Slip	Unity Check Slip
C1	0.85	0.42
C2a	0	0
C2b	0.5	0.5
C2c	0.36	0.36

Figure 14: Shear force distribution no slip

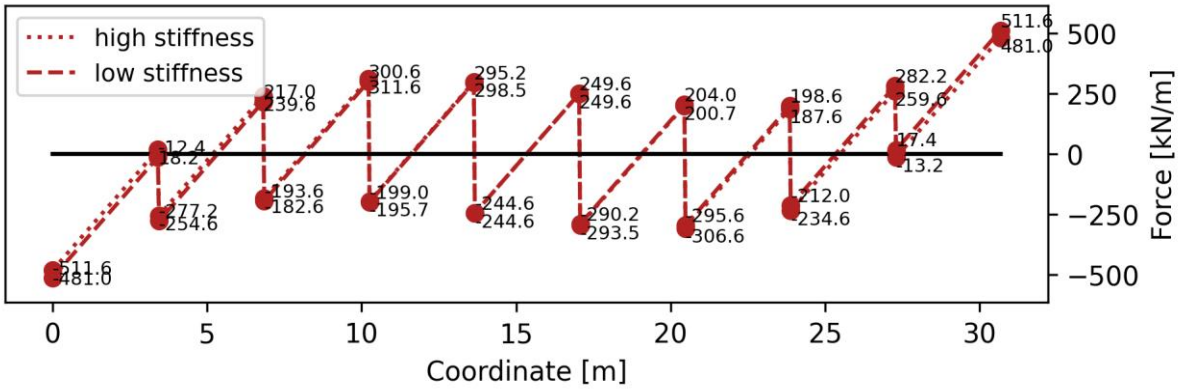

Figure 15: Shear force distribution slip

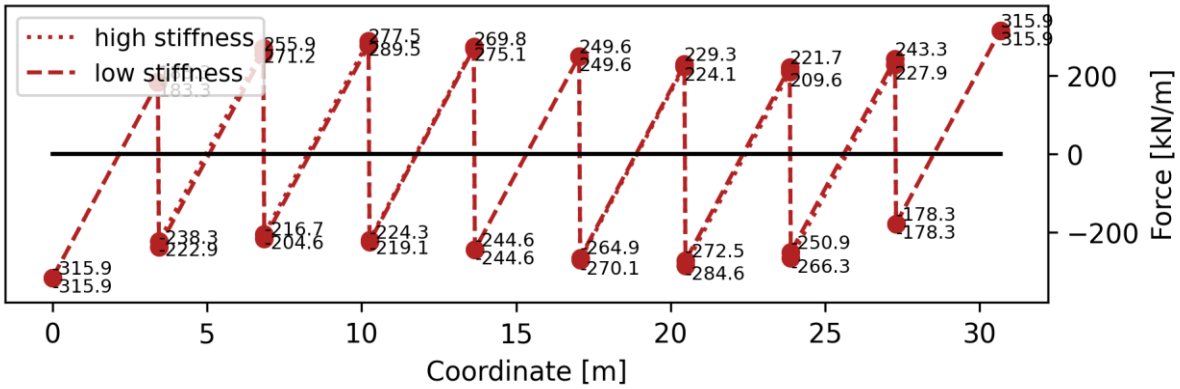

Figure 16: Principal stress

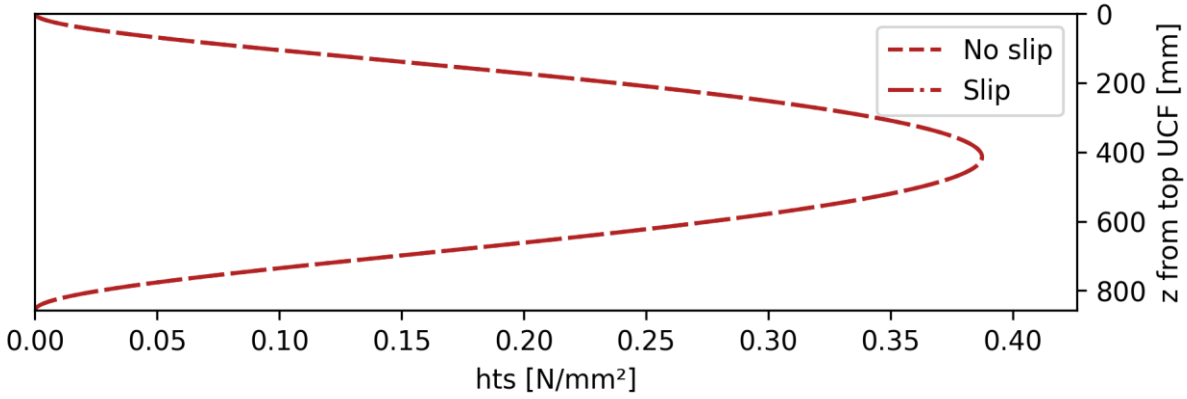

Check C1 No Slip

V_{Ed}	=	386.78		[kN/m]
k	=	$\min(1 + (200 / h_{min})^{0.5}, 2.0)$	= 1.48	[-]
v_{min}	=	$0.035 * k^{1.5} * f_{ck}^{0.5}$	= 0.35	[N/mm²]
σ_{cp}	=	$\min(N_{Ed} / h_{min}, 0.2 * f_{cd,pl})$	= 1.23	[N/mm²]
$V_{Rd,c}$	=	$(v_{min} + 0.15 * \sigma_{cp}) * h_{min}$	= 454.76	[kN/m]
UC	=	$V_{Ed} / V_{Rd,c}$	= **0.85**	[-]

Check C2a No Slip

M_{Ed}	=	26.96		[kNm/m]
σ_{Ed}	=	$6 * \lvert M_{Ed}\rvert / h_{min}^2 - N_{Ed} / h_{min}$	= -1.01	[N/mm²]
UC	=	$\sigma_{Ed} / f_{ctd,pl}$	= **0**	[-]

Check C2b No Slip

V_{Ed}	=	451.67		[kN/m]
A_{cc}	=	$\min(h_{min}/2 + N_{Ed}*h_{min}^2/(12*\lvert M_{Ed}\rvert), h_{min}) * 1000$	= 857294.9	[mm²]
τ_{cp}	=	$1.5 * V_{Ed} / A_{cc}$	= 0.79	[N/mm²]
σ_{cp}	=	$N_{Ed} * A_{cc}$	= -1.23	[N/mm²]
f_{cvd}	=	$(f_{ctd,pl}^2 + \sigma_{cp} * f_{ctd,pl})^{0.5}$	= 1.57	[N/mm²]
UC	=	τ_{cp} / f_{cvd}	= **0.5**	[-]

Check C2c No Slip

$\sigma_{1,max}$	=	0.39		[N/mm²]
UC	=	$\sigma_{1,max} / f_{ctd,pl}$	= **0.36**	[-]

Check C1 Slip

V_{Ed}	=	191.11		[kN/m]
k	=	$\min(1 + (200 / h_{min})^{0.5}, 2.0)$	= 1.48	[-]
v_{min}	=	$0.035 * k^{1.5} * f_{ck}^{0.5}$	= 0.35	[N/mm²]
σ_{cp}	=	$\min(N_{Ed} / h_{min}, 0.2 * f_{cd,pl})$	= 1.23	[N/mm²]
$V_{Rd,c}$	=	$(v_{min} + 0.15 * \sigma_{cp}) * h_{min}$	= 454.76	[kN/m]
UC	=	$V_{Ed} / V_{Rd,c}$	= **0.42**	[-]

Check C2a Slip

M_{Ed}	=	26.96		[kNm/m]
σ_{Ed}	=	$6 * \lvert M_{Ed}\rvert / h_{min}^2 - N_{Ed} / h_{min}$	= -1.01	[N/mm²]
UC	=	$\sigma_{Ed} / f_{ctd,pl}$	= **0**	[-]

Check C2b Slip

V_{Ed}	=	451.67		[kN/m]
A_{cc}	=	$\min(h_{min}/2 + N_{Ed}*h_{min}^2/(12*\lvert M_{Ed}\rvert), h_{min}) * 1000$	= 857294.9	[mm²]
τ_{cp}	=	$1.5 * V_{Ed} / A_{cc}$	= 0.79	[N/mm²]
σ_{cp}	=	$N_{Ed} * A_{cc}$	= -1.23	[N/mm²]
f_{cvd}	=	$(f_{ctd,pl}^2 + \sigma_{cp} * f_{ctd,pl})^{0.5}$	= 1.57	[N/mm²]
UC	=	τ_{cp} / f_{cvd}	= **0.5**	[-]

Check C2c Slip

$\sigma_{1,max}$	=	0.39		[N/mm²]
UC	=	$\sigma_{1,max} / f_{ctd,pl}$	= **0.36**	[-]

10. Connection tensile element

Check	Connection type	Unity Check
G	Dish anchor	0.99

11. Long span, SLS Displacements

Figure 17: Displacement No Slip

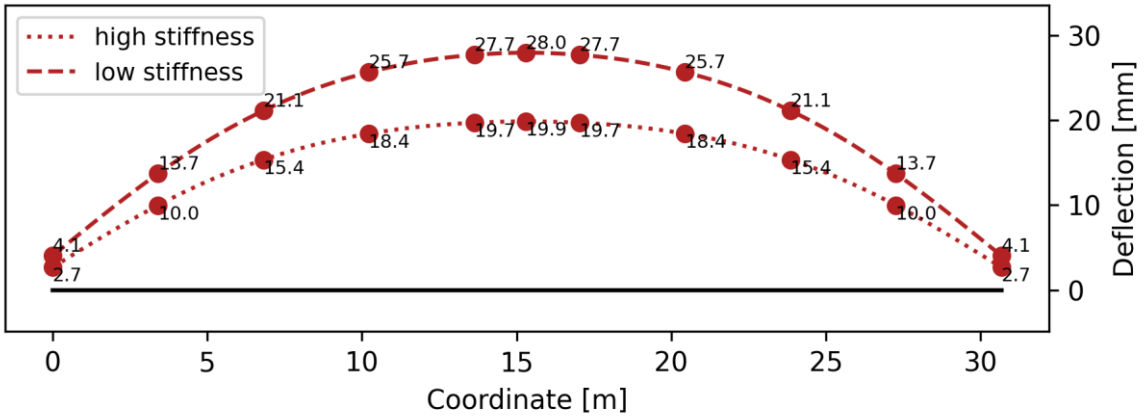

Figure 18: Displacement Slip